Design, Operation and Assessment of Process Systems Integrating Demand-Side Management Through Mathematical Optimization

By

Yu Liu

Dissertation

Submitted in partial satisfaction of the requirements for the degree of

Doctor of Philosophy

in

Chemical Engineering

in the

Office of Graduate Studies

of the

University of California

Davis

Approved:

Ahmet Palazoglu, Chair

Nael H. El-Farra

Yueyue Fan

Committee in Charge

2021

To my dear parents.

Contents

List of Figures

List of Tables

Abstract

Design, Operation and Assessment of Process Systems Integrating Demand-Side Management Through Mathematical Optimization

With the increasing penetration of intermittent energy resources such as solar and wind power, the issue of instantaneous mismatch between power generation and power demand has become increasingly severe and difficult to deal with. Adapting to such an energy paradigm, electricity markets have become more and more volatile, jeopardizing the stability of the power grid and potentially causing significant damage to the network. One solution to address such a challenge is to adopt Demand Response (DR) policies, where the consumers of electricity will modify or reduce their electricity usage from their normal consumption patterns responding to the changes in the electricity price or incentives offered. As one of the largest electricity consumers, the process industry could potentially benefit from demand response operation, such as lowering the production capacity when the electricity price is high and raising it when the electricity price is lower. However, such flexible process operation usually depends on two main factors: fast response to the price or incentive signals and large capacity allowing flexible operation, both of which will depend on the underlying process design. While process operation under a volatile electricity market has attracted a lot of attention from researchers, the design of DR-enabled chemical processes has received limited scrutiny.

Motivated by above considerations, this dissertation focuses on developing a process design and analysis framework to integrate process design and process operation, with the consideration of DR. The first part of the dissertation will focus on developing the framework to design process networks, allowing varied operating levels, as well as enabling optimal process flow sheet reconfiguration under different DR scenarios. The second part of the dissertation will focus on developing the framework and proposing new metrics to evaluate and quantify the ability and potential of the process to participate in DR programs (i.e., DR-particibility).

Acknowledgments

First and foremost, I would like to thank my advisors, Professor Ahmet Palazoglu and Professor Nael El-Farra, who have provided me invaluable support and mentorship in the past few years, particularly for last one and half years when I encountered one of my hardest time through the life. I am grateful all the supports and helps from both of them. It was my great honor to join the team and I truly appreciate all the efforts and insights they have contributed in my work.

Besides my advisors, I would also like to thank to my thesis committee, Professor Yueyue Fan for her valuable guidance and fruitful collaboration. I also want to thank the members served in my qualifying exam committee, Dr. Roland Faller, Dr. Greg Miller, Dr. Coleman Kronawitter and Dr. Spyros Tseregounis for the time they have committed as well as the the helpful feedback throughtout the process.

I also owe my special thanks to my friends and peers in the research group: Gustavo, James, Amr, Da, Shriram and Mats for all the helps throughout this journey; and especially to Gustavo: it was my great honor to work with you as office-mates and all the meaninful discussion over the research topics.

I have some amazing cohort and friends for the past few years, Chenghan, Pinghui, Yi, Cai, Yihan, Mary and Weidi. I will truly miss each and every one of you for all of those relaxing weekend plans. The leisure life in Davis would not be such an enjoyable memory without you.

Finally, there aren't words to express my gratitude to my unconditionally supportive family, my father and my mother. I won't be here today without all the love and understanding you've given to me. You mean all to me, and this disseration is dedicated to you.

Chapter 1

Introduction

1.1 Motivation

With the increasing penetration of renewable energy resources such as solar and wind energy into the power grid, the issue of instantaneous mismatch between power generation and power demand has become increasingly severe and difficult to deal with. In California, for instance, where state lawmakers recently re-affirmed the goal of 100% carbon-free retail electricity by 2045 [2], this issue has become the focus of ongoing debate. As the diminishing solar power coincides with the peaking electricity demand during the early evening hours, a 3-hour ramp of 13,000 MW were required on the generation side during a typical spring day in the year 2020 [3]. This challenge in the California grid system could be seen in Figure 1.1, where the net load is defined as the total electricity generated minus the energy generated from solar and wind resources. As one can clearly note, during the daytime, the net load will go down as the majority of the electricity will come from solar; however, when the evening arrives and the solar power starts to diminish, there is a steep increase in the requirement of the net load. Meanwhile, the energy requirement also peaks around this time. Such a steep ramp threatens the stability of the power grid and causes electricity over-generation, which usually results in a negative price of power in the spot market. Also, a steeper ramp might trigger frequent curtailment from the renewable resources. With more and more solar power becoming available in the grid, the risk of over-generation will keep growing and thus pose a significant challenge to the grid

operators.

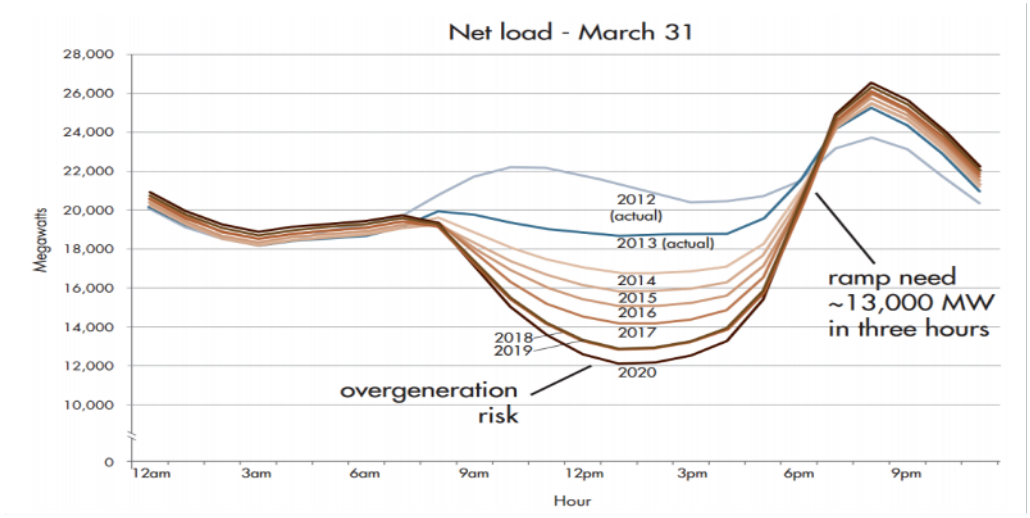

Figure 1.1. The "Duck Curve" in the California grid system

1.2 Background on electricity markets

In a power grid, electrical energy is generated by power generating resources, sent through high-voltage transmission lines and then converted to lower voltage, and then distributed to consumers. In a regulated environment, generation, transmission, and distribution are managed by one entity, which is referred to as a vertically integrated utility; this utility holds the monopoly for the supply of electricity. Since the 1990s, the electricity markets in the United States have become deregulated, resulting in a variety of regulations and market designs overseen by the Federal Energy Regulatory Commission (FERC). Different parts of the power grid system are owned and operated by different participants, and electricity markets provide a platform for a variety of trading and competition activities among those participants. As shown in Figure 1.2, there are generally several participants in the electricity market: the power generators who own the power generation resources such as solar panels or traditional firepower plants, the transmission line owners who own the transmission cables and transformers, the distributors, the retailers who purchase the electricity in bulk from the wholesale market and resell it to the end customers and large/small electricity consumers. Before the deregulation, from the power generation to the consumer, this relationship was essentially a vertical line and the whole process was

owned by a single party. In a deregulated market, for example, a small-end electricity customer with household solar panels installed could potentially become both a seller of the electricity as well as a customer (consumer). Depending on the market structure and the deregulation level, the roles of the market participants could be very different and complicated. Thus, to guarantee the operation of the grid and to maintain its reliability, typically, a grid operator, commonly referred to as the Independent System Operator (ISO), manages the transmission network and monitors the wholesale market. The electricity market could be roughly divided into two different markets: a wholesale market and a retail market. In general, small electricity consumers belong to the retail market and for large electricity consumers such as the chemical process industries, the electricity is usually purchased from the wholesale market.

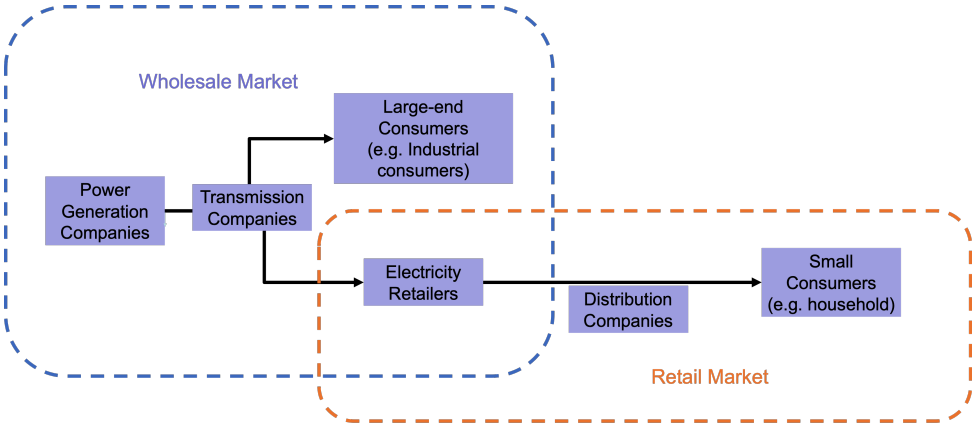

Figure 1.2. Participants in deregulated electricity markets

1.3 Background on demand response and demand-side management

To mitigate the increasing challenges in the renewable energy penetration, there are generally two different approaches. The first one is to invest in a large battery system to store the electricity and utilize the stored electricity when needed. However, the cheap and easily achievable battery is only recently becoming available to the market, and thus the purchase price for the battery is often high. It is estimated that the utility-scale battery cost is around $625/kWh [4], which is still significantly higher than the average price

purchased through the market. Another approach is to implement a Demand Response (DR) strategy. As defined by the FERC [5], DR refers to "changes in electric usage by demand-side resources from their normal consumption patterns responding to economic incentives and dynamic pricing structures at times of high wholesale market prices or when system reliability is jeopardized." Demand-side management plays an important role in coordinating energy generation and consumption in the smart grid, where DR is expected to reduce net peak power demand in the US by about 5% (or about 50GW) over the next ten years [6].

DR has become increasingly important as a strategy for balancing the power supply and demand under an ambitious renewable portfolio standard, keeping the electric grid stable and efficient; deferring upgrades to generation, transmission and distribution systems; and providing other economic benefits to customers. Energy-intensive industries could participate in the electricity market through different DR mechanisms, providing stability to the grid system as well as lowering their operating costs ([7]). Generally, it is well-recognized that participation in the DR market requires that the specific energy-intensive process have sufficient operational flexibility, and that the process dynamics should also be fast enough to respond to the rapidly changing electricity price trends. One of the current bottlenecks for residential and commercial applications in terms of their ability to participate in the DR market is the lack of advanced control equipment; yet for large-end industrial electricity users, the cost of advanced metering to facilitate DR participation does not appear to be a significant barrier ([8]); rather, DR design is a critical consideration when decisions for investments are made.

As defined in [9] Demand-side management (DSM) "encompasses systematic activities at the interplay between system operator and electricity consumer aiming at changing the amount and/or timing of the consumer's use of electricity in order to increase grid performance and consumer benefits. DSM activities on the system operator side involve the assessment of the need for load adjustment and the creation of financial incentives for the consumer, while the consumer reacts to these financial incentives and performs the actual physical load adjustment operations". There are two main DSM categories: the

energy efficiency (EE) and the aforementioned DR.

DR services can be usually categorized as either dispatchable or non-dispatchable types [10]. Dispatchable DR refers to the electricity usage profile adjustment responding to the DR events, while the non-dispatchable DR refers to the load profile adjustment responding to the price signals. While in different ISOs, the detailed mechanism or the payment of the participation of the DR services can be different, the general idea of dispatchable DR is usually incentive-driven while the non-dispatchable DR is price-driven [11]. In dispatchable DR, the electricity consumer agrees to participate in certain services to a certain degree, then, when there is an event, the grid operator will order the electricity consumer to perform a specific activity, such as decreasing the energy usage. Such a DR service, from the electricity consumer's perspective, is "dispatched" to the grid operator. While such successfully implemented DR services will have an incentive, failing to do so might incur penalties. Thus, the capability to participate in the dispatchable services requires careful examination. On the other hand, non-dispatchable DR is a price-driven process. Usually, the electricity consumer will follow the electricity price variation to determine the potential operating levels. As when to lower the load consumption or when to increase, the decision is still made by the electricity consumer. Thus, in general, a judicious choice of the DR activity can offer significant economic benefits to the process industries.

1.4 DSM in the process industry

Although DR is a promising approach to increase demand flexibility, the potential peak reduction from DR programs in the US was only 6.6% of the peak demand in 2015 [5]. The reason for this is that electricity is a resource whose value for consumers is much higher than its price. In the industrial category, chemical processes are promising contributors due to several factors [12]. Firstly, process plants are usually equipped with advanced meters for control and monitoring purposes that could facilitate the implementation of DR. Moreover, chemical processes can easily incorporate excess capacity to store excess product. The economic potential of DR operation or DSM in energy intensive industries

has been widely recognized through a number of recent studies focusing on various applications such as air separation [13–15], chlor-alkali production [16, 17], cement and pulping [18], steel production [13], aluminum smelting [19], and oil refining [20]. Its impact on the electricity power infrastructure such as combined heat and power plants has also been studied [21], in addition to studies on concentrated solar power plants [22–24]. A significant majority of the earlier work in this area formulated the problem using mixed-integer linear programming (MILP) models, where the optimal process scheduling sequence that minimizes the total operating cost under time-varying electricity prices is determined. In [13] MILP models were developed to account for different operating modes and the mode transitions that lead to the most cost-effective scheduling policy. Later studies focused on the integration of the scheduling problem with process dynamics. Tong et al. [25] introduced a decomposition scheme to perform process scheduling while optimizing the controller parameters that can manage the scheduling sequence under time-varying electricity prices. Kelley et al. [15] proposed an MILP scheduling model to account for the process dynamics using a low-order model. In addition to the studies focusing on operational strategies, several other studies have focused on electricity contract procurement or price bidding strategies. For example, Zhang et al. [26] considered the production scheduling and electricity procurement simultaneously and incorporated the conditional value-at-risk in the model to study the optimal scheduling problem in the presence of electricity contracts. Additionally, other DR participation mechanisms have also been investigated including reserve market [27], and interruptible load problems [28].

The above-mentioned studies supporting DR capabilities for process systems have all been in the area of the production scheduling and capacity planning; very few attempts have been made to solve the *process design* problem with the explicit goal of DSM. As an example, Pattison and Baldea [29] developed a pseudo-transient steady-state model to study the optimal design of air separation units operated at different capacities under varying electricity prices. Cao et al. [30] investigated the design limitations of a cryogenic nitrogen plant under product demand and electricity price fluctuations using a two-tier model, where operating points were decided using a dynamic model and the implementa-

tion was addressed via dynamic optimization. In both of these studies, a framework was proposed to incorporate process dynamics into the process flow sheet, but the focus was on the equipment design and the flow sheet was assumed to be fixed. As the design of a plant or a process would usually have significant impact on its operation, we argue that in an environment of varying energy prices and resources, as well as product demand, a fixed plant structure (flow sheet) might be disadvantaged in the sense that it could only respond to such variations through dynamic shifting of operational levels.

Recently, the operation of a process with direct participation in the short-term market (e.g., Five-Minute Ahead Market) has gained significant attention among researchers (see, for example, [24, 31, 32] for frequency control). Participation in the short-term market requires the fast response from the processes to the price signals. Otashu et al. [33] performed a first-principle optimization-based simulation on a chlor-alkali plant, and noticed that the open-loop control of the electrolyzers will cause violation of the safety requirements, yet there will be economics benefits for such operation. Further investigations are required to explore the closed-loop operation. Also, model-based bidding strategies for industrial processes have been investigated (e.g., see [34]). While the above works have investigated the participation of a fixed plant into the time-varying electricity market, the flexibility potential on the demand side from the design perspective have not been addressed. Teichgraeber et al. [35] explored the capacity design of a chlor-alkali plant under the real-time electricity market (RTM). While the integration of control towards a short-term market have gained interest, none of the current studies directly addressed the impact of process design or process dynamics (and the associated costs) on the ability of the process to participate in DR services.

Incorporating DR objectives directly into the design and operation of chemical processes needs to take account of the plant capacity design as well as the intrinsic process dynamics, which usually introduces significant nonlinearities into the modeling. Furthermore, the design stage is usually at a different time scale compared to the DR operational decisions, which in general is in hours or even minutes, and thus a multi-scale model is usually required, often leading to an intractable model, where the impact of design on the

DR capability is difficult to quantify.

1.5 Objectives and organization of the dissertation

Motivated by the points highlighted in the previous section, the broad objectives of this dissertation are:

- To address demand-side management considerations explicitly in the process design problem.
- To develop a flexible framework for process design, integrating process network reconfiguration under demand-side management.
- To develop a model-based analytical framework for evaluating the cost-effectiveness of process design alternatives regarding their ability to participate (i.e., participibility) in Demand Response (DR) services.

The rest of the dissertation is divided in two parts. In the first part, Chapter 2.3 and Chapter 3, we focus on the flexible design of process networks. The objective is to evaluate the design of a reconfigurable process network that could satisfy the DR requirements. We implement a mathematical modeling and optimization approach to evaluate two different power-intensive process networks focusing on flexible design. The second part of the dissertation, including Chapter 4 and Chapter 5, will focus on the development of a metric and analysis framework to quantify the process DR particibility, which is defined as the ability of a process to participate in the DR markets by taking advantage of the integration of design and the operational levels.

More specifically, the presentation of the material is organized as follows:

Chapter 2 introduces the superstructure optimization and offers a detailed model of the work-heat exchange network. The work-heat exchange network will then be studied to demonstrate the concept of the reconfigurable process design under different electricity price scenarios in a heuristic way.

Chapter 3 presents the flexible design network problem formulation using stochastic programming and the solution strategy using the progressive hedging algorithm, followed

by a case study involving a pump network system. A mathematical model that enables process network reconfiguration under demand-side management is introduced.

Chapter 4 explores a model-based analytical framework that integrates the design, operation and process control levels to evaluate the cost-effectiveness of process design alternatives regarding their ability to participate in DR services through the use of supply curves.

Chapter 5 proposes the innovative usage of levelized cost of electricity (LCOE) as the quantification metric to evaluate the benefits of a process design to participate in different time-scale electricity markets. The original concept of the LCOE for the energy systems is extended in this work to treat chemical processes, usually regarded as power consumers, as energy storage units similar to batteries.

Finally, limitations of the current study and possibilities for future research are presented in Chapter 6.

Chapter 2

Optimal Configuration of Work-Heat Exchanger Networks (WHEN) in the Presence of Demand Response Objectives

In this chapter, we propose a process network design case study incorporating the reconfiguration of the equipment under different electricity price profile scenarios. Motivated by an earlier study on the reconfiguration of Heat Exchanger Networks (HENs) under varying electricity profiles [36], in this work, a case study is carried out using a work-heat exchanger network (WHEN), which, compared to the original HEN, will directly incorporate the electricity intensive equipment in the pressure manipulating units. We first demonstrate the process synthesis and superstructure-based optimization in Section 2.2, followed by a review of the literature on the WHEN and its application in Section 2.3. We then describe the problem in Section 2.4 and state the modeling equations in Section 2.5. The model will then be studied using different electricity scenarios and a heuristic design that allows for reconfigurability during DR events using a superstructure formulation that conceptualizes a DR-enabled process design is presented. The results first appeared in [37]

2.1 Motivation

While recent studies on DR have created a new research direction (see 1.4), the above-mentioned studies supporting DR capabilities for process systems have all been in the area of production scheduling and capacity planning. Very few attempts have been made to solve the *process design* problem with the explicit goal of DSM. As an example, Pattison and Baldea [29] developed a pseudo-transient steady-state model to study the optimal design of air separation units operated at different capacities under varying electricity prices. They discovered that the capacity of the air separation unit should be a dominant factor to allow extra flexibility in the process design. Later, Cao et al. [30] investigated the design limitations of a cryogenic nitrogen plant under product demand and electricity price fluctuations using a two-tier model, where operating points were decided using a dynamic model and the implementation was addressed via dynamic optimization. In both of these studies a framework was proposed to incorporate process dynamics into the process flow sheet, but the focus was on the equipment design, and the flow sheet was assumed to be fixed. As the design (configuration) of a plant or a process would usually have significant impact on its operation, we argue that in an environment of varying energy prices and resources, as well as product demand, a fixed plant structure (flow sheet) might be disadvantaged in the sense that it could only respond to such variations through dynamic shifting of operational levels. The key question is: can one design a process network where, in addition to allowing variable operational levels, the optimal flow sheet may vary in time and would be accessible through the reconfiguration of process equipment in real-time?

In an earlier work in our group [36], we first raised the issue of potentially reconfiguring the process flow sheet responding to varying electricity prices and the availability of renewable energy resources during the day. The proactive reconfiguration of a process flow sheet was demonstrated using a HEN example and shown to be economically beneficial. Yet, in that study, the reconfigurable HEN network flow sheets were assumed to exist, and only the real-time reconfiguration among these was attempted. The study mainly focused on the operational aspect of the reconfiguration, while the design part is mostly

not discussed. Meanwhile, the study assumed that the HEN is driven by electricity (e.g., assuming heaters and coolers are electrical equipment), which is generally not realistic in practice.

Motivated by above studies, in this work, we explore the process network design paradigm where besides the operational level change, the flow sheet could also be available for reconfiguration. The study will differ from the earlier work by Wang et al.[36] in following aspects: (i) the design will be directly considered, and (ii) the analysis is extended to consider a truly electricity-intensive process.

2.2 Process synthesis approaches

Process synthesis is the assembly and interconnection of process units into a network, which involves both physical and chemical transformations to convert raw material and energy inputs into the products with the goal of optimizing economic, environmental and/or social objectives [38]. There are mainly two approaches used to address the process synthesis problem: (1) hierarchical decomposition approach and (2) optimization-based modeling approach. The hierarchical approach is represented by Douglas's five-level decision approach [39], where the economic short-cut evaluations are performed at different levels to reduce the total number of design alternatives. Usually, such an approach can generate a near-optimal process design, but it is mainly heuristic and usually ignores the interconnections between different decision levels, and thus, cannot guarantee the final design to be the best possible one.

With the growth of computing power and advances in the mathematical programming algorithms, optimization-based approaches were developed to incorporate the interaction between different decision layers. Usually, an optimization-based approach involves these steps: (1) a set of the process alternatives will be postulated, and such process alternatives are represented as *superstructure*; (2) the mathematical model will then be formulated; (3) lastly, the best process flow sheet will be determined by solving the mathematical model. In general, the best process flow sheet solution has to be incorporated in the superstructure because configurations that are not as part of the search space will not be found. After the

superstructure is proposed, the mathematical model will be proposed. Process synthesis problems typically would be modeled as a discrete/continuous mathematical model solved through a mixed-integer nonlinear program (MINLP) as follows:

$$\begin{aligned} \text{minimize} \quad & Z = f(x, y) \\ \text{subject to} \quad & h(x, y) = 0, \\ & g(x, y) \leq 0, \\ & X \in \mathbb{X}, y \in \{0, 1\}, \end{aligned}$$

where the objective function $f(x, y)$ subject to the constraints defined by the equalities $h(x, y)$ (typically mass and energy balance) and inequalities $g(x, y)$, typically the safety and product requirements or the equipment capacity constraints. The continuous variables x usually specify the state values such as flow rate, temperature and size of equipment, while the binary variables y correspond to the selection of the process units. As physical models and constraints in processes typically are nonlinear in nature, the resulting model results in the MINLP problem.

In general, due to the mixed-integer decision variables and the highly nonlinear physical constraints displayed in the superstructure optimization, the resulting model formulation, in most cases, could be difficult to solve and computationally intractable. A myriad of optimization algorithms has therefore been developed in the Process System Engineering community, including the outer-approximation approach for the MINLP problem to obtain the local optimum [40], a global solver like the Branch-and-Reduce Optimization Navigator (BARON) [41] and the Algorithms for continuous/integer global optimization of nonlinear equations (ANTIGONE) [42].

2.3 Work-Heat Exchanger Networks (WHENs)

As mentioned earlier, the HEN reconfiguration study under demand response is not realistic when considering the interaction with the electricity market, and one of the extension of the original work is to consider the so-called work exchanger networks (WENs). Both HEN and WEN process synthesis based on mathematical modeling have been explored before. For HEN, since the heuristic pinch analysis proposed by Linnhoff and Flower [43],

the heat integration has led to an enormous number of successful applications. Yee and Grossmann [44] later proposed the simultaneous superstructure-based HEN model. Since then, the work in mathematical modeling of the HEN has witnessed a wide application. A thorough review on the development of the HEN synthesis could be referred to Furman and Sahindis [45].

The WEN, based on the idea of work exchange between high-pressure and low-pressure streams, on the other hand, received less attention than the HEN, which is quite surprising as work, in general, is much more expensive than heat and pressure manipulation and typically involves the purchase of electricity. Wechsung et al. [46] combined the pinch analysis and exergy analysis to maximize the exergy efficiency by integrating both heat and power for the process. Yet, they did not consider the work exchange between different pressure streams. This might be partially due to the equipment limitations at that time. Razib et al. [47] first introduced the idea of single-shaft-turbine-compressor (SSTC) to enable the work exchange of such process streams and developed the mathematical model for WEN optimization. An SSTC is similar to a steam turbine running a compressor via a common shaft. The turbine generates the power to turn the shaft that drives the compressor. The only difference is that an SSTC derives its energy by depressurizing a high-pressure process stream instead of a high-pressure stream. The SSTC unit has, in fact, already been explored in liquefied natural gas (LNG) industry in Qatar [47].

Since then, the synthesis and optimization of WHEN became a focus of research. Onishi et al. [48] extended the work of Razib et al. [47] by incorporating a HEN into the WEN model and thus presented a WHEN model. However, their formulation employed a number of big-M constraints and the equipment cost correlations in their model that are also highly nonlinear. Huang et al. [49] then addressed the issues in Onishi et al. [48] and developed a simpler version of the WHEN synthesis framework.

2.4 Problem statement

In this work, we consider a set of high-pressure streams and low-pressure streams, all of which are gaseous with known mass flows, heat capacities as well as supply states and

target states. The goal is to synthesize the minimum cost (including both capital cost and operating cost) network under different electricity prices utilizing different types of heat exchangers and different type of pressure manipulating equipment such as valves, compressors, turbines, motors, generators and SSTC. Utilities such as steam, cooling water and electricity are available. After obtaining the minimum cost network under different electricity prices, we then explore the synthesis of a reconfigurable network.

2.5 Problem formulation

The development of the WHEN combines the WEN with heat integration. The model is then formulated as a mixed-integer nonlinear programming (MINLP) problem. A sample WHEN framwork is demonstrated in Figure 2.1. It combines a HEN model and a WEN model. The WEN superstructure contains compression and expansion, in which the work exchange occurs between the high-pressure streams and low-pressure streams.

The modeling of both networks, WEN and HEN, requires two separate models which are then connected by additional stream constraints. In this work, we implemented the WEN model presented by Huang et al. [49] and the HEN model from Yee et al. [44]. A sample WHEN process flow sheet could be seen in Figure 2.1, where low-pressure and high-pressure streams will enter the HEN first and then the WEN, while the no-pressure change streams will enter the HEN only. HEN will only change the temperature and WEN will be exclusively for work integration. Thus, the pressure will not be changed in the HEN; yet in WEN, the temperature of the gaseous streams will be changed accordingly.

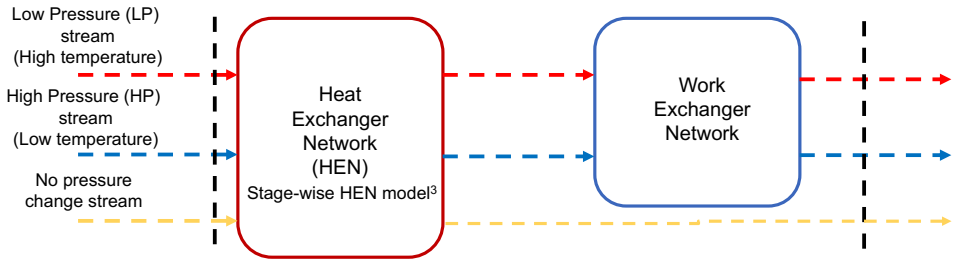

Figure 2.1. WHEN process sample flow sheet

2.5.1 Modeling assumptions

We make the following assumptions:

- The process is at steady-state.
- Gas streams are assumed to be ideal gas and remain above the corresponding dew points.
- All pressure manipulating equipment are single stage and centrifugal with provided known efficiency. Compression and expansion processes are assumed to be adiabatic and reversible.
- The expansion via valves is assumed to be adiabatic but irreversible with known Joule-Thomson coefficients.
- The heat capacities of streams are known and assumed to be constant.
- The gaseous streams undergoing expansion are always below their inversion temperatures.
- The process operating conditions do not warrant special equipment design considerations that would make the cost correlations inappropriate.
- The film heat transfer coefficient of each stream is a known to be a constant.
- The pressure drops, and heat losses are negligible for all heat exchangers.
- The purchase cost of mixers and splitters are negligible. The equipment degradation by flexible operation is also neglected.
- In the HEN, countercurrent heat exchangers are used and isothermal mixing of streams is assumed.
- There is only one type of (hot or cold) utility at the outlet of the superstructure.

2.5.2 WEN model formulation

The WEN model is formulated as a MINLP problem and responsible for work integration only. Following the binary decisions for selecting equipment, the equations for calculating flow rates, temperatures and pressures, as well as an energy balance of the SSTC unit are presented.

2.5.2.1 Sets and stages

The goal of WHEN synthesis is to find the optimal network configuration for a specific number of streams whose states have to be changed in a given process. While liquid and gaseous streams are considered in the HEN, in the WEN just gaseous streams are allowed, resulting in two sets.

$$PC = \{s | s\ is\ gaseous\ \cup\ PIN_s \neq POUT_s\}, \tag{2.1}$$

$$NPC = \{s | PIN_s = POUT_s\}, \tag{2.2}$$

and $s \in S$ where S defines the union of streams. PC denotes the pressure-changed streams while NPC denotes the no-pressure-changed streams. PIN_s and $POUT_s$, therefore, denote the inlet pressure and outlet pressure of the stream $s \in S$. Furthermore, PC can be divided into high-pressure streams, HP, and low-pressure streams, LP; NPC can be divided into cold no-pressure-changed streams, $NPCS$, and hot no-pressure-changed streams, $NPHS$, given as:

$$PC = HP \cup LP, \tag{2.3}$$

$$HP = \{s | PIN_s > POUT_s\}, \tag{2.4}$$

$$LP = \{s | PIN_s < POUT_s\}, \tag{2.5}$$

$$NPCS = \{s | PIN_s = POUT_s \cup TIN_s < TOUT_s\}, \tag{2.6}$$

$$NPHS = \{s | PIN_s = POUT_s \cup TIN_s > TOUT_s\}, \tag{2.7}$$

with TIN_s and $TOUT_s$ specifying inlet temperature and outlet temperature of streams s. Since an arbitrary number of stages $k \in K$ is allowed in both networks, we assign 3 as the default maximum stage, while K could be specified accordingly.

2.5.2.2 WEN equipment selection

The pressure manipulating equipment is chosen by binary variables (0, 1) where a value of 0 means that the equipment is not chosen and 1 implies it is used in the specific stage of the WEN. While for increasing pressure just compressors can be selected, expansion could

be achieved by using turbines and/or valves. For changing the state of process streams, at least one stage has to be used. Hence, no bypass is allowed in the first WEN stage.

$$y_{s,k} = 0, s \in PC, k = 1, \tag{2.8}$$

Here $y_{s,k}$ denotes the binary variable for bypass for stream s at stage k. If a bypass is selected at a stage, the following stage should be bypassed as well, thus,

$$y_{s,k-1} \leq y_{s,k}, s \in PC, 3 \leq k \leq K_s. \tag{2.9}$$

Also, if there is no bypass, at least one of the pressure manipulating equipment has to be used and thus,

$$u_{s,k} + v_{s,k} + x_{s,k} + y_{s,k} \geq 1, s \in PC, 1 \leq k \leq K_s, \tag{2.10}$$

where $u_{s,k}$, $v_{s,k}$ and $x_{s,k}$ describe binary variables for whether using a utility turbine/compressor, valve or SSTC turbine/compressor or not for stream s at stage k. Also, at any given stage only one equipment could be selected and one should avoid a partial bypass, since a partial bypass will result in mixing two different pressure streams, therefore,

$$u_{s,k} + v_{s,k} + y_{s,k} \leq 1, s \in PC, 1 \leq k \leq K_s, \tag{2.11}$$

$$x_{s,k} + y_{s,k} \leq 1, s \in PC, 2 \leq k \leq K_s, \tag{2.12}$$

As one might notice, Eqs. 2.11 and 2.12 avoid the partial bypass, but do not prevent the split of the stream going to two different pressure manipulating units.

For leveling the work exchanged on SSTC axes, a helper motor or generator can be installed. While the motor is chosen if the workload of the SSTC turbine is lower than the SSTC compressor load, the opposite is true in case a generator is required.

$$g + h \leq 1, \tag{2.13}$$

where g and h are the binary variables for utilizing generator and helper motor. Finally, if a generator is used, then at least one SSTC turbine has to be installed; meanwhile, if

the helper motor is chosen, a SSTC compressor is required.

$$g + h \leq \sum_{s \in HP} \sum_{k=1}^{K_s} x_{s,k}, \tag{2.14}$$

$$g + h \leq \sum_{s \in LP} \sum_{k=1}^{K_s} x_{s,k}. \tag{2.15}$$

2.5.2.3 Mass balance

The assumption that heat capacities of all process streams are known and constant simplifies the calculation of the flow rates. The flow balance of the inlet is given as,

$$F_s = y_{s,k} \cdot F_s + FU_{s,k} + FV_{s,k} + FE_{s,k},\ s \in PC,\ 1 \leq k \leq K_s, \tag{2.16}$$

where F_s is the total heat capacity flow rate for stream s, $y_{s,k} \cdot F_s$ is the stream bypass and $FU_{s,k}$, $FV_{s,k}$ and $FE_{s,k}$ specify the heat capacity flow rate to pass through utility compressor/turbine, valve and SSTC unit for stream s at stage k.

Meanwhile, one would want to avoid using small equipment and therefore a set of minimum flow rate constraints are applied as follows:

$$F_s^{min} \cdot u_{s,k} \leq FU_{s,k} \leq F_s \cdot u_{s,k}, s \in PC, 1 \leq k \leq K_s, \tag{2.17}$$

$$F_s^{min} \cdot v_{s,k} \leq FV_{s,k} \leq F_s \cdot v_{s,k}, s \in PC, 1 \leq k \leq K_s, \tag{2.18}$$

$$F_s^{min} \cdot x_{s,k} \leq FE_{s,k} \leq F_s \cdot x_{s,k}, s \in PC, 1 \leq k \leq K_s. \tag{2.19}$$

2.5.2.4 Stream temperature and pressure

Given the initial and target states of all process streams, their temperature and pressure values have to be adjusted by using appropriate equipment. For describing the behavior of these units, the following equations are used. While the initial pressure of the inlet stream is the same as the inlet into the first WEN stage, since it is assumed to have no pressure drop in the HEN, the outlet pressure of the last stage equals the target pressure.

$$P_{s,0} = PIN_s, \tag{2.20}$$

$$P_{s,K_s} = POUT_s, \tag{2.21}$$

where $P_{s,0}$ and P_{s,K_s} are inlet stream pressure and outlet target stream pressure, respectively.

The stream pressure is also expected to change monotonically. While the pressure of the HP stream is decreased and therefore is equal to or lower than the subsequent stage, the pressure of the LP stream should be increased. This set of constraints are given as follows:

$$P_{s,k} + \Delta P_s^{min} \cdot (1 - y_{s,k}) \leq P_{s,k-1}, s \in HP, 1 \leq k \leq K_s, \tag{2.22}$$

$$P_{s,k} + PIN_s \cdot (1 - y_{s,k}) \geq P_{s,k-1}, s \in HP, 1 \leq k \leq K_s, \tag{2.23}$$

$$P_{s,k} - \Delta P_s^{min} \cdot (1 - y_{s,k}) \geq P_{s,k-1}, s \in LP, 1 \leq k \leq K_s, \tag{2.24}$$

$$P_{s,k} - POUT_s \cdot (1 - y_{s,k}) \leq P_{s,k-1}, s \in LP, 1 \leq k \leq K_s, \tag{2.25}$$

where ΔP_s^{min} denotes the minimum requirement of the change in pressure manipulation for stream s.

Furthermore, the pressure of the process streams within the WEN is bounded by the initial and target pressures, given as:

$$min[PIN_s, POUT_s] \leq P_{s,k} \leq max[PIN_s, POUT_s], s \in PC, 1 \leq k \leq K_s. \tag{2.26}$$

The temperature of the process streams are changed by flowing through the WEN equipment with different units calculated as such. In general, when a compressor is used, the temperature will increase and when a turbine is used, the stream temperature will decrease. These temperature changes will depend on the efficiency of the pressure manipulating units and heat capacity ratios.

$$TM_{s,k} = TI_{s,k} \cdot (1 + \eta_s \cdot [(\frac{P_{s,k}}{P_{s,k-1}})^{\frac{r_s - 1}{r_s}} - 1]), s \in HP, 1 \leq k \leq K_s, \tag{2.27}$$

where $TM_{s,k}$ denotes the outlet temperature of a utility mover for stream s at stage k while $TI_{s,k}$ denotes the inlet temperature, η is the utility mover efficiency and r_s is the heat capacity ratio for stream s. Similarly, the temperature change for the LP can be defined as follows:

$$TM_{s,k} = TI_{s,k} \cdot (1 + 1/\eta_s \cdot [(\frac{P_{s,k}}{P_{s,k-1}})^{\frac{r_s - 1}{r_s}} - 1]), s \in LP, 1 \leq k \leq K_s, \tag{2.28}$$

If a valve is used, the temperature change will be calculated based on the Joule-Thomson coefficient [50], as follows:

$$TV_{s,k} = TI_{s,k} + \mu_s \cdot [P_{s,k} - P_{s,k-1}], s \in HP, 1 \leq k \leq K_s, \tag{2.29}$$

where μ_s is the Joule-Thomson coefficient. Based on the assumption, the mixing of different substreams is allowed and assumed to be isothermal, therefore, the outlet temperature for HP will be given as:

$$TO_{s,0} = TIN_s, \tag{2.30}$$

$$F \cdot TO_{s,k} = y_{s,k} \cdot F_s \cdot TI_{s,k} + TM_{s,k} \cdot (FU_{s,k} + FE_{s,k}) + TV_{s,k} \cdot FV_{s,k}, s \in HP, 1 \leq k \leq K_s \tag{2.31}$$

and the outlet temperature for the LP streams is calculated similar to the Eq. 2.28:

$$TO_{s,k} = TI_{s,k} \cdot (1 + 1/\eta_s \cdot [(\frac{P_{s,k}}{P_{s,k-1}})^{\frac{r_s-1}{r_s}} - 1]), s \in LP, 1 \leq k \leq K_s. \tag{2.32}$$

2.5.2.5 SSTC energy balance

SSTC is the unit performing the work exchange, and the energy balance on the SSTC units is achieved by using the inlet and outlet temperatures of the streams in WEN:

$$\sum_{s \in HP} \sum_{k=1}^{K_s} FE_{s,k} \cdot (TI_{s,k} - TM_{s,k}) + WH = \sum_{s \in LP} \sum_{k=1}^{K_s} FE_{s,k} \cdot (TO_{s,k} - TI_{s,k}) + WG, \tag{2.33}$$

where WG and WH are the capacity for the generator and the helper motor, respectively. The power generated by $s \in PC$ via the SSTC turbine at stage k is defined as $FE_{s,k} \cdot (TI_{s,k} - TM_{s,k})$. Also, the bound of the capacity of the ancillary equipment is given as:

$$WG \leq g \cdot WG^U, \tag{2.34}$$

$$WH \leq h \cdot WH^U, \tag{2.35}$$

where WG^U and WH^U are the upper bounds for the generator and the helper motor, respectively.

2.5.3 HEN model formulation

As the model assumption neglects the pressure drop in the HEN model, the below HEN model focuses on the stream temperatures only. The HEN model mostly follows the one proposed in [44], and will be provided here with minor changes.

2.5.3.1 Sets and stages

In the HEN, similarly, different sets and stages are used. While the number of cold streams ($c \in CS$) is defined as ($NPCS + K_s \cdot HP$), hot streams, $h \in HS$ with number of, $NPHS + K_s \cdot LP$ are considered. Similar to the WEN, HEN will also have stages where $n \in ST$. This stage can also be arbitrary, the assumption of using counter-current heat exchanger implies that hot and cold stream inlets are at the first and last stages, respectively.

2.5.3.2 Overall heat balance

$$(TIN_h - TOUT_h)F_h = \sum_{c \in CS} \sum_{n=1}^{st} q_{h,c,n} + qcu_h, \qquad h \in HS,, \tag{2.36}$$

$$(TOUT_c - TIN_c)F_c = \sum_{h \in HS} \sum_{n=1}^{st} q_{h,c,n} + qhu_c, \qquad h \in CS,, \tag{2.37}$$

where $TIN_h, TOUT_h, TIN_c$ and $TOUT_c$ specify the inlet, outlet temperatures of the hot stream and inlet, outlet temperatures of the cold stream, respectively. F_h and F_c specify the heat capacity flow rate for the hot stream and the cold stream. $q_{h,c,n}$ is the heat exchanged in the heat exchanger at stage n between stream h and c. qcu_h and qhu_c are heat exchanged in the cooling utility and heating utility, respectively.

2.5.3.3 Stage-wise heat balance

Besides the overall heat balance, the heat balance around each HEN stage is achieved.

$$(t_{h,n} - t_{h,n+1}) \cdot F_h = \sum_{c \in CS} q_{h,c,n}, n \in ST, h \in HS, \tag{2.38}$$

$$(t_{c,n} - t_{c,n+1}) \cdot F_c = \sum_{h \in HS} q_{h,c,n}, n \in ST, h \in HS, \tag{2.39}$$

where t denotes the temperature for stream at stage n.

2.5.3.4 Temperature constraints

The initial temperatures are assigned since they are known and assumed to be constant.

$$TIN_h = t_{h,1}, h \in HS, \tag{2.40}$$

$$TIN_c = t_{c,N+1}, x \in CS \tag{2.41}$$

where $t_{h,1}$ and $t_{c,N+1}$ are known parameters. The change of temperature is monotonous; therefore, the temperature feasibility constraints are given as

$$t_{h,n} \leq t_{h,n+1}, n \in ST, h \in HS, \tag{2.42}$$

$$t_{s,n} \leq t_{c,n+1}, n \in ST, c \in CS, \tag{2.43}$$

$$TOUT_h \leq t_{h,n+1}, h \in HS, \tag{2.44}$$

$$TOUT_c \geq t_{c,1}, c \in CS. \tag{2.45}$$

Besides the heat transferred by process streams, heating and cooling utilities can be placed at the end of a HEN stage. Their loads are calculated by the following:

$$(t_{h,N+1} - TOUT_h) \cdot F_h = qcu_h, h \in HS, \tag{2.46}$$

$$(TOUT_c - t_{c,1}) \cdot F_c = qhu_c, c \in CS. \tag{2.47}$$

2.5.3.5 Selection of HEN units

The selection of the HEN units, including the process heat exchangers as well as cooling and heating utility heat exchangers could be achieved by introducing the logical constraints as follows:

$$q_{h,c,n} - \Omega \cdot z_{h,c,n} \leq 0, h \in HS, c \in CS, n \in ST, \tag{2.48}$$

$$qhu_c - \Omega \cdot zhu_c \leq 0, c \in CS, \tag{2.49}$$

$$qcu_h - \Omega \cdot zcu_h \leq 0, h \in HS, \tag{2.50}$$

where $z_{h,c,n}$, zhu_c and zcu_h denotes the binary variable whether the equipment is selected as a heat exchanger, heating utility and cooling utility, respectively. As cooling and heating utility will only be used at the end stage of each stream, the variables do not have a stage index.

2.5.3.6 Approach temperature

For calculating the areas of installed heat exchangers, temperature approaches have to be introduced. By coupling these variables with binaries, they, and thus the areas, are

activated and deactivated, respectively.

$$dt_{h,c,n} \leq t_{h,n} - t_{c,n} + \Gamma \cdot (1 - z_{h,c,n}), n \in ST, h \in HS, c \in CS, \tag{2.51}$$

$$dt_{h,c,n+1} \leq t_{h,n+1} - t + c, n + 1 + \Gamma \cdot (1 - z_{h,c,n}), n \in ST, h \in HS, c \in CS, \tag{2.52}$$

$$dthu_c \leq TOUT_{HU} - t_{c,1} + \Gamma \cdot (1 - zhu_c), c \in CS, \tag{2.53}$$

$$dtcu_h \leq t_{h,N+1} - TOUT_{CU} + \Gamma \cdot (1 - zcu_h), h \in HS, \tag{2.54}$$

where, $dt_{h,c,n}$, $dthu_c$ and $dtcu_h$ specify the approach temperatures in the heat exchanger, the heating utility and the cooling utility; Γ defines the upper limit temperature difference. This set of constraints could be explained as when the equipment is used, such that the binary variable is 1, the approach temperature will be bounded; however, if the binary variable is 0, Γ, which will be a large variable will deactivate the constraint. This is a big-M formulation. In the end, as a lower bound, the minimum exchanger approach temperature (EMAT) can be set to avoid infinite exchanger areas, thus:

$$dt_{h,c,n} \geq EMAT. \tag{2.55}$$

2.5.4 Connection between HEN and WEN

So far, HEN and WEN processes are modeled separately, and thus they have to be connected properly by additional equations shown in this section. Since the pressure is changed in the WEN but not in the HEN, temperatures are used for achieving this. Based on the description in the process, the process streams are first sent to the first stage of the HEN, where heat could be exchanged, followed by the first stage of the WEN. The outlet temperature of the first WEN stage is assumed to be equal to the inlet. Thus, the outlet of the WEN stream will be the inlet stream to the next stage HEN; while the outlet of the HEN will be the inlet stream to the WEN at the same stage.

$$THIN_h = TO_{s,k}, \qquad h \in HS, s \in LP, k < K, \tag{2.56}$$

$$THOUT_h = TI_{s,k}, \qquad h \in HS, s \in LP, k \geq 1, \tag{2.57}$$

$$TCIN_c = TO_{s,k}, \qquad c \in CS, s \in HP, k < K, \tag{2.58}$$

$$TCOUT_c = TI_{s,k}, \qquad c \in CS, s \in CS, k \geq 1, \tag{2.59}$$

where $THIN$, $THOUT$, $TCIN$ and $TCOUT$ specify the inlet, outlet temperatures of the hot stream and inlet, outlet temperatures of the cold stream, respectively.

2.5.5 Objective function

The goal of WHEN synthesis is the minimization of total annualized cost (TAC). While capital cost (CAPEX) and operational cost (OPEX) increase TAC, revenues generated by selling excess electricity back to the grid can be subtracted from TAC.

2.5.5.1 Capital cost

To calculate the CAPEX, fixed capital cost of the equipment as well as cost coefficients depending on flow rates and work loads for considering different sizes are used. The overall capital cost for the WHEN is given as follows:

$$\begin{aligned} CAPEX = {} & CF_G \cdot g + C_G \cdot WG + CF_H \cdot h + C_H \cdot WH \\ & + \sum_{s \in PC} CC_s + \sum_{s \in HP} \sum_{k=1}^{K_s} [CF_S^V \cdot v_{s,k} + C_S^V \cdot FV_{s,k}] \\ & + \sum_{s \in PC} \sum_{k=1}^{K_s} [CF_s^U \cdot u_{s,k} + C_s^U \cdot FU_{s,k} + CF_s^E \cdot x_{s,k} + C_s^V \cdot FE_{s,k}] \\ & + \sum_{h,c,n} [CF_{h,c} \cdot z_{h,c,n} + C_{h,c}[q_{h,c,n} U_{h,c} / [dt_{h,c,n} dt_{h,c,n+1} (dt_{h,c,n} dt_{h,c,n+1})/2]^{1/3}]^{\beta_{h,c}}] \\ & + \sum_{h \in HS} [CF_{h,CU} \cdot zcu_h \\ & + C_{h,CU}[qcu_h U_{h,CU}] / [dtcu_h (TOUT_h - TIN_{CU})(dtcu_h + (TOUT_h - TIN_{CU}))/2]^{1/3}]^{\beta_{h,CU}} \\ & + \sum_{c \in CS} [CF_{c,HU} \cdot zhu_c \\ & + C_{c,HU}[qhu_c U_{c,HU}] / [dthu_c (TIN_{HU} - TOUT_c)(dthu_c + (TIN_{HU} - TOUT_c))/2]^{1/3}]^{\beta_{c,HU}} \end{aligned} \tag{2.60}$$

where $U_{h,c}$ defines the overall heat transfer coefficient, and it is a parameter. As noted, the equipment costs for the pressure manipulating equipment are linear and could be expressed as fixed cost plus the cost coefficient times the size of the equipment; the equipment cost for the heat exchanger is based on the Chen [51]. CF_G, C_G, are fixed cost and cost coefficient for the generator; CF_H, C_H are fixed cost and cost coefficient

for the helper motor; CC_s are fixed cost for WEN final heater and cooler; CF_s^V, C_s^V are fixed cost and cost coefficient for valve; CF_S^U, C_s^U are fixed cost and cost coefficient for utility turbine; CF_s^U, C_s^U are fixed cost and cost coefficient for utility turbine/compressor; CF_s^E, C_s^E are fixed cost and cost coefficient for SSTC unit.

Also, the cost for the final heater and cooler installed in the WEN are calculated as:

$$CC_s \geq CF_S^{HU} + C_s^{HU} \cdot (TOUT_s, TO_{s,K_s}), \tag{2.61}$$

$$CC_s \geq CF_S^{CU} + C_s^{CU} \cdot (TO_{s,K_s} - TOUT_s) \tag{2.62}$$

2.5.5.2 Operating cost

The total operating cost includes the energy cost of heating and cooling, as well as the electricity for driving helper motor and utility compressor:

$$OPEX = CO_H \cdot WH + \sum_{s \in PC} UC_s + \sum_{s \in LP} \sum_{k=1}^{K_s} CO_U \cdot FU_{s,k} \cdot (TO_{s,k} - TI_{s,k}) + \sum_{h \in HP} CO_{CU} \cdot qcu_h + \sum_{c \in CP} CO_{HU} \cdot qhu_c, \tag{2.63}$$

where CO_H and CO_U are the appropriate unit costs for the helper ,motor and utility compressors respectively, and CO_{HU}, CO_{CU} are the unit cost for hot, colld utility. UC_s is the operating cost of the final heater/cooler. It is also noted that

$$UC_s \geq CO_{HU} \cdot F_s \cdot (TOUT_s - TO_{s,K_s}), \tag{2.64}$$

$$UC_s \geq CO_{HU} \cdot F_s \cdot (TO_{s,K_s} - TOUT_s). \tag{2.65}$$

As the turbines might be used in the network, electricity could be generated from steam and then sold back to the grid. We define the revenue as:

$$REV = CE \cdot [WG + \sum_{s \in HP} \sum_{k=1}^{K_s} FU_{s,k}(TI_{s,k} - TM_{s,k})] \tag{2.66}$$

where CE is the electricity cost parameter. The above equation describes the work generated by the end generator (WG), as well as the utility mover at stage k.

2.5.5.3 Annualized cost

As the objective function, the minimization of TAC is used. Therefore, an annualized factor is introduced and the operating time per year has to be set.

$$TAC = f \cdot CAPEX + t \cdot (OPEX - REV), \tag{2.67}$$

where f is the annualized factor for the capital cost and t is the operating hour per year.

2.6 Case study

The above model is cast as a non-convex MINLP model, and therefore, obtaining a global optimum is challenging and not the focus of this study. As observed and reported by Onishi et al. [48] and Huang and Karimi [49], the global MINLP solver such as BARON does not provide a satisfactory performance. We obtained the solution by using the DICOPT solver in GAMS.

Table 2.1. Stream data for case study

Stream	TIN[K]	TOUT[K]	PIN[MPa]	POUT[MPa]	F[kW/K]	H[kW/(m^2K)]
HP	103.45	242.3	10	0.1	2.47	0.1
LP	288.15	104.75	7	10	4.10	0.1
NPCS	221.12	244.2	-	-	5.70	0.1
HP	383.15	383.15	1-	-	-	1

Other parameters include $EMAT = 5(K)$, $\mu_s = 1.961(K/MPa)$, $\eta_1 = 0.7$, $\eta_2 = 1.0$, $r_1 = 1.51$ and $r_2 = 1.352$.

2.6.1 Scenarios

To test the WHEN model formulation and confirm the scenario assumptions, the data of Example 3 in Huang and Karimi [49] are used for evaluating a LNG process. This case study deals with the work and heat integration between two gaseous and one liquid process streams, where the stream data can be seen in Table 2.1. For the liquefaction of natural gas (NG), the feed stream has to be compressed and thus is considered as a low-pressure (LP) stream in the WEN, while it is regarded as a hot stream in the HEN

Table 2.2. Cost parameters in the case study

Process unit	Fixed cost(k$)	Cost coefficient	Energy cost (k$/kWh)
Utility turbine	200	1	electricity price
Utility compressor	250	1	electricity price
SSTC turbine	40	1	-
SSTC compressor	50	1	-
Generator	2	1	electricity price
Helper motor	2	1	electricity price
Valve	2	1	-
Heat exchanger	3	0.03	-
Heater	3	0.03	0.035
Cooler	3	0.03	0.001
Operating time t = 8000h per year			

since it is more energy efficient to compress cold streams. In contrast, the liquid nitrogen used to cool down NG is supposed to be a high-pressure (HP) and cold stream. Liquid CO_2, a side-stream of the LNG process, is considered to be a no-pressure-change stream (NPCS) to be heated, and is not involved in the WEN. All process data are taken from Huang and Karimi [49]. This study focuses on a varying electricity price structure to demonstrate how DR objectives can be met. Furthermore, since selling electricity back to the grid is allowed and would generate a revenue, the electricity selling price is assumed to be 50% of the purchase price. For evaluating off-, mid-, and on-peak scenarios, three different electricity price levels are assumed, with off-peak price at \$0.07/kWh, mid-peak at \$0.15/kWh and on-peak at \$0.30/kWh. The equipment cost parameters are shown in Table 2.2.

2.6.2 Results of scenarios

First, the MINLP problem is solved using the fixed electricity price for different price profile. As a result, the optimal configurations for the different periods are obtained

as shown in Table 2.3. While an off-peak electricity price leads to the use of a valve for expanding HP, a utility turbine is chosen for higher prices. Since the utility turbine is assumed to be much more expensive than a valve, its use has to be economically compensated by the generated revenue, which is the case when the electricity selling price is high.

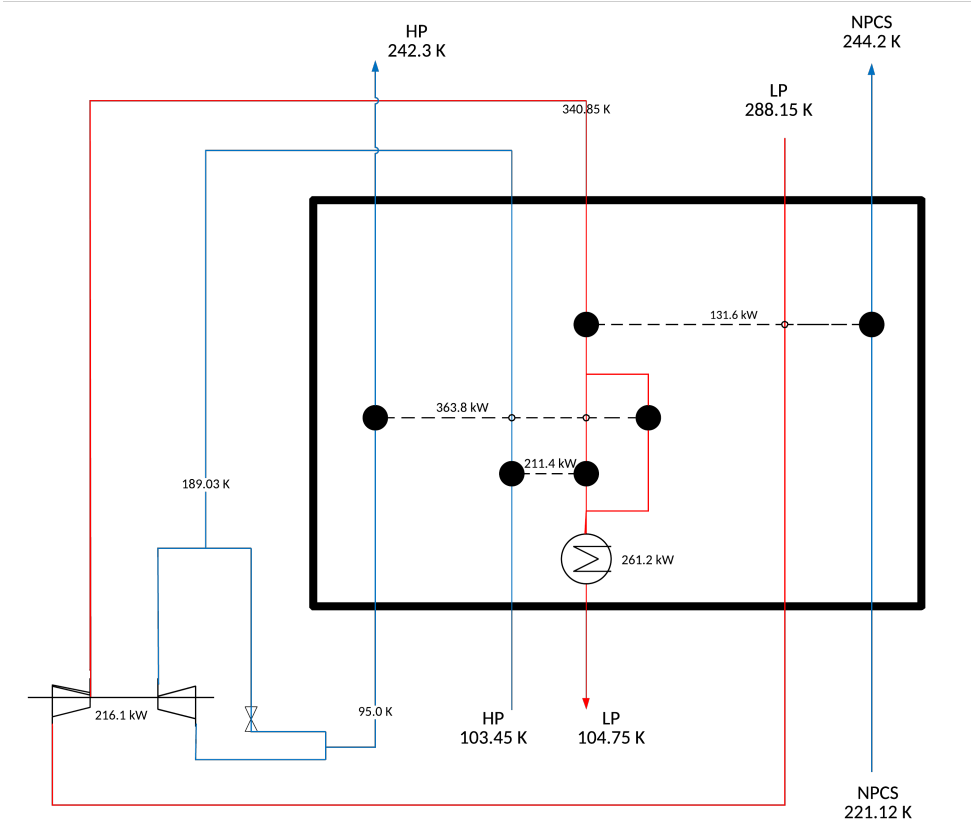

Figure 2.2. WHEN superstructure for off-peak scenario

2.6.2.1 Off-peak

The resulting flow sheet for the off-peak scenario is shown in Figure 2.2. The assumption of having a low electricity price of \$0.07/kWh results in a WHEN superstructure with TAC of \$118,699 which is the highest of the base cases since a valve is used and no electricity is sold back to the grid. In contrast to the other scenarios, no heater and just one cooler are used within the HEN. Instead, the overall heat exchanged between the process streams is around 706.8 kW and thus larger than in the mid- (688.0 kW) and

on-peak (635.3 kW) scenarios. Another key difference with the other cases is the parallel use of a SSTC turbine and a valve in the first stage of the WEN. While higher electricity prices favor a lower workload on the SSTC axis and no use of a valve, at low prices the cost of a utility turbine is too high to be used. Due to the very low cost for a valve, this unit is more appropriate in economic terms during the off-peak hours.

Table 2.3. Stream loads for the optimal deterministic configurations

Equipment	Streams, stage	Load[kW]		
		Off-peak	Mid-peak	On-peak
SSTC turbine	HP1, s1	216.1	71.2	-
	HP1, s2	-	-	71.2
SSTC compressor	LP1, s1	216.1	71.2	71.2
Valve	HP1, s1	0	-	-
Utility turbine	HP1, s1	-	-	621.9
	HP1, s2	-	621.9	-
Heat exchanger	LP1,HP1,s1	-	338.1	238.0
	LP1, HP1, s2	-	46.6	80.9
	LP1, HP2, s1	-	-	353.0
	LP1, HP3, s1	-	288.9	-
	LP3, HP1, s2	211.4	-	-
	LP3, HP2, s2	363.8	-	-
	LP3, HP4, s1	131.6	-	-
Heater	HP1	-	190.2	364.2
	HP2	-	179.4	-
	HP4	-	131.6	131.6
Cooler	LP1	-	118.3	120.0
	LP2	-	-	31.3
	LP3	261.2	31.3	-

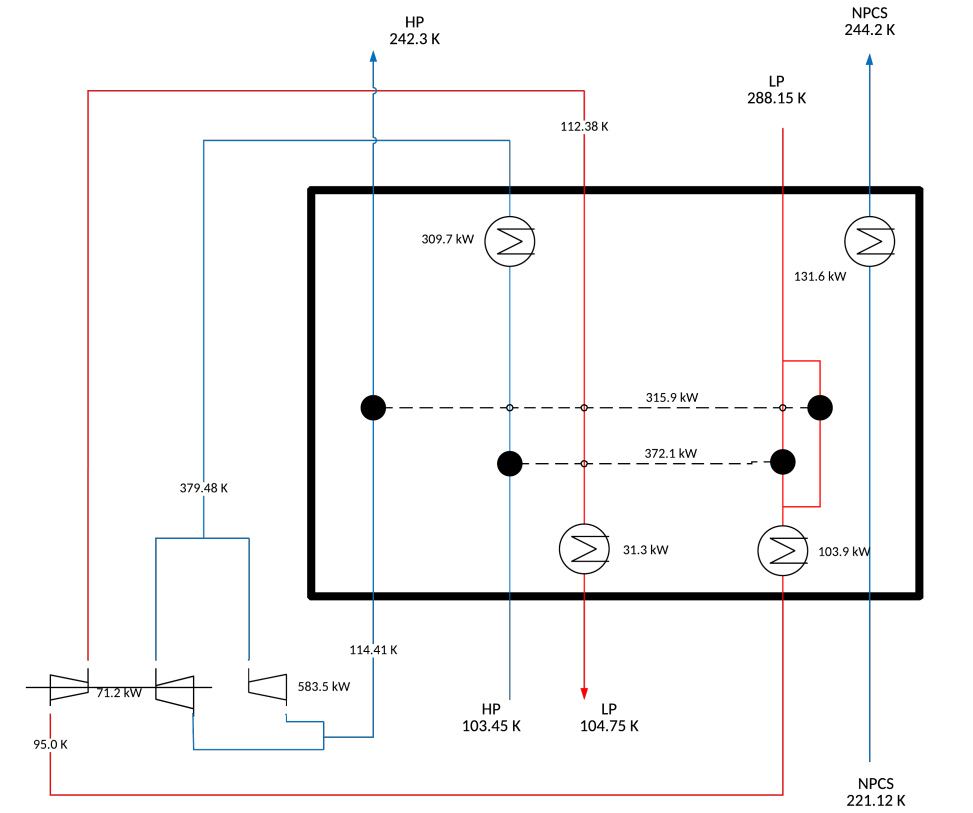

Figure 2.3. WHEN superstructure for mid-peak scenario

2.6.2.2 Mid-peak

The resulting flow sheet for the off-peak scenario is shown in Figure 2.3. In contrast to the off-peak scenario, in the mid-peak case a utility turbine is used instead of a valve. As a result, excess work is converted to electricity, which can be sold and a revenue is generated. Therefore, the TAC is slightly decreased to \$114,610. Beside the replacement of the valve by a utility turbine in the first stage of the WEN, the difference in temperatures and the workload of the SSTC axis are main aspects to be noted. As illustrated in the modeling section, the energy recoverable in a turbine is increasing with higher temperatures. Hence, the inlet temperature of the utility turbine is 190.45 K higher compared to the inlet temperature of the valve in the off-peak scenario, while the outlet temperature is just 19.41 K higher. As a result, since the utility turbine has more than an eight-fold flow rate of the SSTC turbine, its workload is much higher and the surplus electricity generated

can be sold back to the grid. Though the equipment cost of this unit is the highest of the installed equipment, the generated revenue justifies its use.

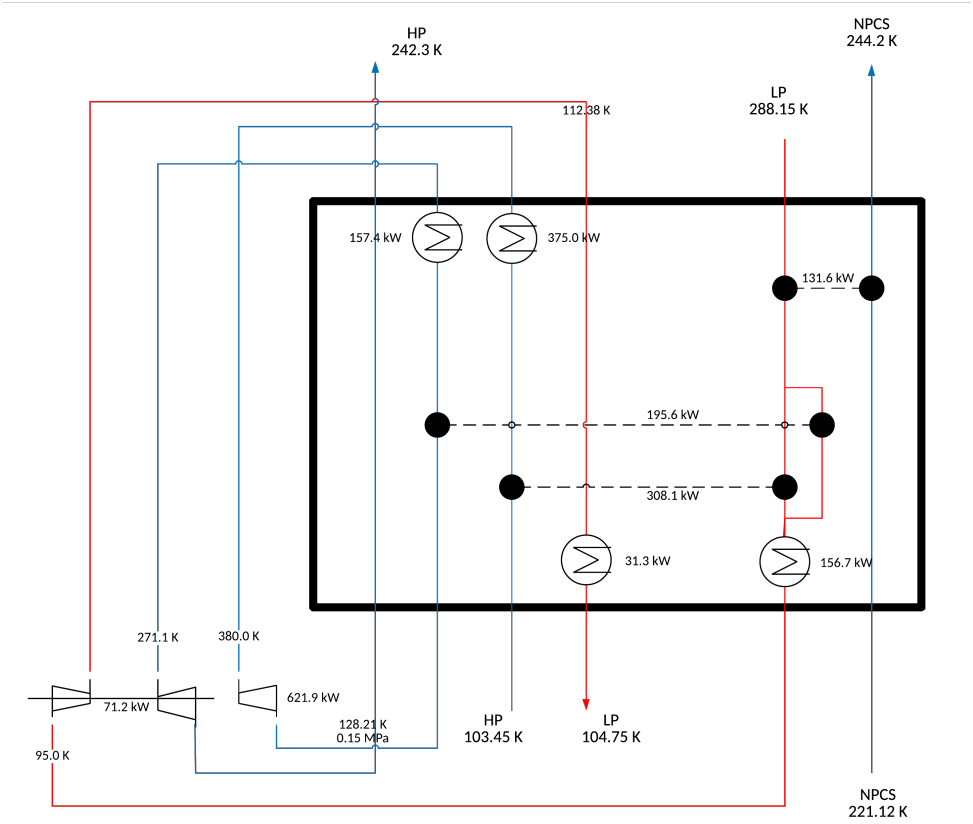

Figure 2.4. WHEN superstructure for on-peak scenario

2.6.2.3 On-peak

The resulting flow sheet for the off-peak scenario is shown in Figure 2.4. Similar to the mid-peak scenario, during on-peak hours, a utility turbine for generating a revenue is used. Since the electricity selling price is \$0.15/kWh, the TAC is decreased to a negative value of \$-251,169 while this result has to be considered carefully due to the assumption of having this price for the entire operating time of 8,000 hours per year. The main adjustment between the mid- and on-peak scenarios is the arrangement of SSTC and utility turbine, as well as their workload. Although the configurations for mid- and on-peak processes look similar (Figure 2.4), their loads and process stream connections are slightly different. Specifically, in the WEN, the utility and SSTC turbine are in reverse order, and in the

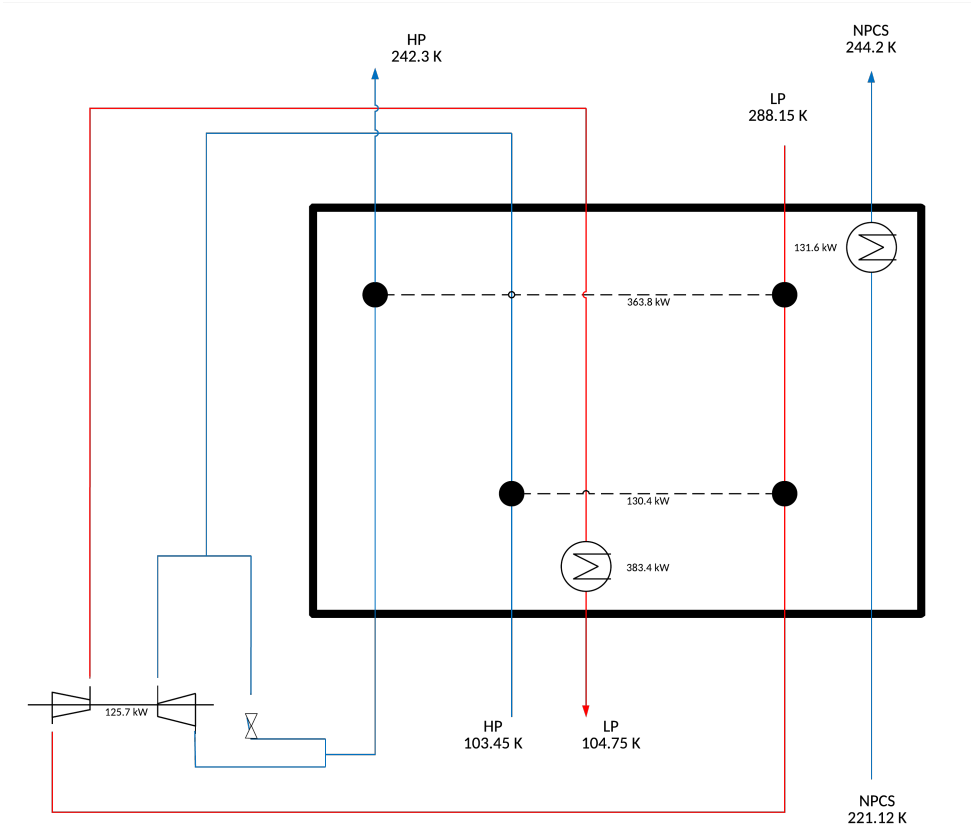

Figure 2.5. WHEN supra-structure for off-peak scenario

HEN, the number of heaters is higher in the mid-peak scenario. Due to the doubled electricity purchase and selling price, a WHEN superstructure with a two-stage WEN is favored, where the entire mass flow of the HP stream is expanded in the utility turbine and the SSTC turbine subsequently. For generating a high revenue, see Table 4.5, the target pressure of the HP stream is almost reached in the outlet of the first WEN stage, while the workload of the SSTC axis remains the same and the overall load of the heat exchanger within the HEN is adjusted slightly compared with the mid-peak scenario.

Equipment		0:00	1:00	2:00	3:00	4:00	5:00	6:00	7:00	8:00	9:00	10:00	11:00	12:00	13:00	14:00	15:00	16:00	17:00	18:00	19:00	20:00	21:00	22:00	23:00
SSTC Turbine	HP1, s1																								
SSTC Compressor	LP1, s1																								
Valve	HP1, s1																								
Utility Turbine	HP1, s1																								
Heat Exchanger	LP1, HP1, s1																								
Heat Exchanger	LP1, HP1, s2																								
Heat Exchanger	LP1, HP2, s3																								
Heater	HP1																								
Heater	NPCS																								
Cooler	LP1																								
Cooler	LP2																								

Figure 2.6. Gantt chart for equipment commitment in the *suprastructure*

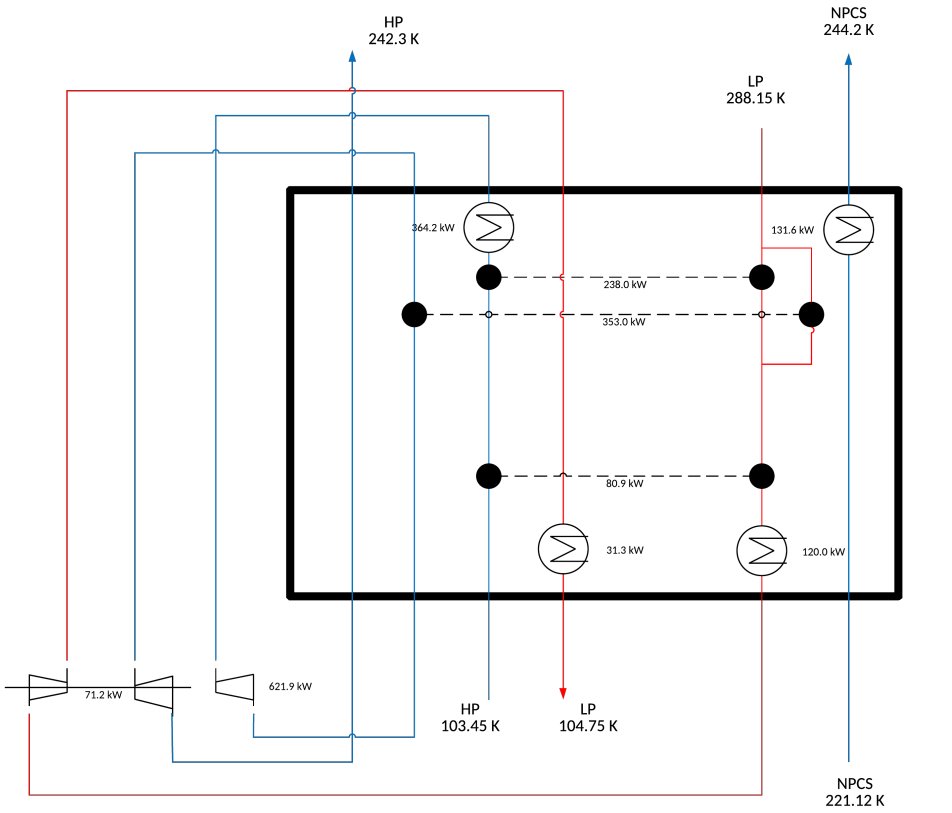

Figure 2.7. WHEN suprastructure for on-peak scenario

2.6.3 Reconfigurable WHEN structure with heuristic rule

The deterministic optimization results under different electricity prices result in three different fixed flow sheets with no equipment reconfiguration. We next explore two different reconfigurable designs that allow the changing of the equipment.

The first design is generated through committing to the purchase of all equipment under all three configurations and allow for the reconfiguration of the flow sheet among these available equipment, switching configurations as electricity price changes. From the CAPEX standpoint, this is the worst-case scenario. We will refer to this as the WHEN superstructure.

The second design is synthesized in a way that modifies each optimal configuration in an ad-hoc fashion so that the modified configurations have more common equipment. When all such equipment are combined, one still has a reconfigurable flow sheet but much

Table 2.4. Stream loads for the WHEN suprastructure

Equipment	Streams, stage	Load[kW]		
		Off-peak	Mid-peak	On-peak
SSTC turbine	HP1, s1	125.7	71.2	71.2
SSTC compressor	LP1, s1	125.7	71.2	71.2
Valve	HP1, s1	0	-	-
Utility turbine	HP1, s1	-	584.4	584.4
Heat exchanger	LP1,HP1,s1	-	356.2	356.2
	LP1, HP1, s2	130.4	21.8	21.8
	LP1, HP2, s1	363.8	315.5	315.5
Heater	HP1	-	305.1	305.1
	HP4	131.6	131.6	131.6
Cooler	LP1	-	98.4	98.4
	LP2	383.4	31.3	31.3

less capital commitment than the WHEN superstructure. This comes at the expense of likely increased OPEX during the realization of various electricity price levels. We will refer to this as the WHEN *suprastructure*.

The WHEN *suprastructure* is achieved by fixing the HEN equipment, while the binary variables of the WEN remain as decision variables. This scenario was used since a single WEN configuration under a varying electricity price showed high TAC, so one HEN was assumed to lower the cost. The configuration generated could be seen in Figure 2.5 and 2.7 and the detailed stream results are shown in Table 2.4. And the Gantt Chart for the equipment commitment is demonstrated in Figure 2.6. Though a slight decrease in the cost was achieved, it could be different for other electricity price profiles due to the heuristic nature of this approach. Furthermore, although only the HEN equipment was fixed under different electricity prices, the WEN configuration is almost the same in mid- and on-peak periods.

Table 2.5. Daily cost of all configurations

Cost [$/d]	Off-Peak	Mid-peak	On-peak	WHEN superstructure	Reconfigurable synthesis
CAPEX	350	1040	1041	1066	1037
OPEX	6	347	347	295	269
Revenue	0	1069	1063	887	836
Total	356	318	325	474	470

2.6.4 Comparison of all flow sheets

To compare the different design including the non-reconfigurable design obtained in the deterministic optimization, we perform the simulation by fixing the equipment variables and calculate the nonlinear programming problem and related cost. The daily electricity price profile followed the time of use (TOU) electricity price structure, and the following distribution was assumed: \$0.07/kWh for 11 h/d (midnight to 11 am), \$0.15/kWh for 7 h/d (11 am to 6 pm) and \$0.30/kWh for 6 h/d (6 pm to midnight).

The results of the above calculation are summarized in Table 2.5. As one might note, all the costs are converted to a daily basis from the annualized cost since the operating cost is for a 24-hr period. The OPEX cost for off-peak, mid-peak and on-peak configurations are obtained by assuming the optimal configuration for a specific price is operated for the whole day. Thus, the cost in Table 2.5 is different from the TAC obtained through solving the deterministic optimization problem. One can see that when using a single configuration for the entire day, the mid-peak configuration has the lowest cost, while the WHEN suprastructure is slightly cheaper compared to the WHEN superstructure. Although the CAPEX and OPEX for the off-peak configuration are the lowest, the total cost is higher than the mid-peak and on-peak configurations since no revenue is generated due to the low electricity selling price.

Also, in contrast to the results obtained before, the on-peak configuration does not have the lowest total cost since instead of assuming an electricity selling price of \$0.15/kWh for the entire time the profile was applied. It can be observed that the CAPEX and

OPEX of the mid-peak scenario are slightly lower compared with the on-peak, resulting in marginally lower average cost of the WHEN per day. Furthermore, since during off-peak just a single cooler and a valve is used its OPEX are very low in comparison with the other configurations and no revenue is generated.

2.7 Conclusions

In this chapter, the concept of a reconfigurable design for process flow sheets under varying electricity profiles was introduced and demonstrated using a WHEN case study. The preliminary results show that different electricity purchasing and selling prices highly influence the WHEN configuration, while the use of the single mid-peak configuration for the entire time yields the lowest TAC. We note that the current results are ad hoc solutions, and no global optima is presumed to be obtained, meaning that under other assumptions, the WHEN superstructure could have a lower TAC. Further research needs to be conducted, focusing on other electricity price profiles, cost data and scenarios using a broader variety of process streams. While the MINLP problem of work-heat integration between two gaseous and one liquid process streams is a relatively simple example, a higher number of streams would result in more complex models, which are difficult to solve. More importantly, a rigorous solution of the optimal network reconfiguration needs to be formulated.

The simultaneous synthesis of work and heat exchanger networks is a comparatively new research field, where no example for applying demand response objectives had been found in literature. Therefore, this work is considered as a novel approach for evaluating this superstructure under fluctuating electricity prices. Though different options for increasing the capacity of technologies capable for DR are already a focus of research, the synthesis of WHEN can be considered as a promising alternative. Since the case study considers LNG production, for the natural gas industry, the results show the potential for decreasing its power demand, though all processes using pressure manipulating equipment are assumed to benefit from implementing WHEN. However, due to the high-growth rate in LNG production and the increase in its capacity in many countries, this sector is

assumed to be more open to innovative technologies since they are easier to realize in the planning process of new plants.

The case study showed the economic benefits of a WHEN superstructure using at least one utility turbine, while the revenue depends on the electricity price. Since many scenarios have been tested and the mid-peak configuration mostly showed the best performance, this superstructure is favorable, but further research is required. Additional case studies evaluating a larger variation of electricity prices and assuming different cost parameters could lead to a better understanding of WHEN under DR objectives, while the model could be adjusted as well. Beside the use of more accurate cost functions, temperature approaches in the HEN and bounds on equipment, constant parameters like the Joule-Thomson coefficients and heat capacities of process streams could be replaced by equations for considering their dependence on state. Furthermore, the overall system response to transitions, as well as the dynamic performance, have not been analyzed in this work due to the complexity of these aspects. While for the assumed discrete electricity prices three configurations have been obtained and during these periods, i.e., mechanical stress was neglected, sudden price changes occurring in shorter periods most likely have a negative impact on the operability and durability of the equipment.

Due to the simplified model formulation in terms of using cost parameters instead of nonlinear equations, case studies with a larger number of process streams can be evaluated. Instead of using a more accurate but complex model, where obtaining feasible solutions could be challenging, the system presented seems to be eligible for further evaluations. Beside other critical price fluctuations, the electricity selling price is a parameter to be varied, while a smaller step-size of increasing the purchasing price could provide information about the point where using a utility turbine is favored for generating revenue.

Chapter 3

A Flexible Design Framework for Process Systems Under Demand Side Management

In Chapter 2, a deterministic MINLP superstructure optimization problem was formulated to study the design under various electricity scenarios and a heuristic process synthesis with process network reconfiguration is presented. However, the resulting WHEN model is highly nonlinear and sensitive to the initial guess, making it difficult to model it from the DSM perspective. Meanwhile, the model used a bottom-up approach to synthesize the reconfigurable flow sheet and the sequential approach, while demonstrating the concept, is not desirable for rigorous optimization. In this chapter, we explore the flexible design problem using a pump network, another electricity-intensive process in various industries, as the case study. The resulting design problem is formulated as a stochastic programming problem, in which the uncertainties associated with electricity pricing and production requirements are represented by a set of discrete scenarios with corresponding probabilities. The problem is solved using Progressive Hedging [52], a heuristic algorithm for coping with the computational complexity that arise when numerous scenarios is considered. We first provide a problem overview and pump network design background, followed by a preliminary discussion on stochastic programming. Modeling details are then presented, followed by the results and discussion. The results in this chapter first appeared in [53].

3.1 Problem overview

The minimization of energy consumption costs as well as the total cost of the pump systems have attracted significant interest in industries with high-energy consumption using such equipment. Process pumps are considered to be intensive consumers of electrical power and widely used in almost all industrial processes, accounting for nearly 20% of the world's electrical energy demand and range from 25 to 50% of the energy usage in certain industrial operations [54]. In addition, pumps are considered to be one of the most promising DR providers in agricultural irrigation applications [55, 56], as well as in wastewater treatment facilities [57]. The design of a network of centrifugal pumps was first introduced in [58]. The objective was to select the optimal pump network, where pumps are connected in either series or parallel configurations, and also determine the optimal pump operation conditions. This problem formulation took advantage of the superstructure optimization framework (see 2.2), where the total head (pressure rise) and total flow rate requirements were specified while the total cost including both capital and operating costs were minimized. The model was presented as a deterministic mixed-integer nonlinear non-convex programming problem. A noteworthy result from that study was the articulation of different optimal pump configurations under different pressure and total flow rate conditions. The original model solved the deterministic problem locally. Later, Adjiman et al. [59] updated this model with a tighter relaxation for the purpose of obtaining a deterministic global optimum. Recently, Li et al. [60] reformulated the problem to reduce the non-convexity by replacing the original integer variables with pure binary variables and developed a stochastic programming problem where the uncertainty originated from the physical parameters. Furthermore, they applied the piecewise Mccormick relaxation and outer linearization to approximate the original nonlinear non-convex constraints with a mixed-integer linear programming problem. The model was then solved where the first-stage variables were pure binary and the recourse variables (second-stage decision) were all continuous variables.

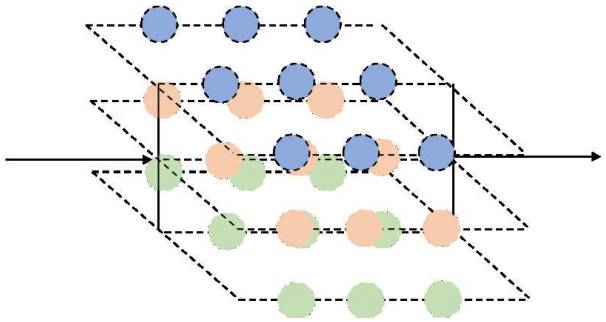

Figure 3.1. The superstructure for a pump network including three different pump types.

3.2 Stochastic programming

Two major approaches generally used when modeling the uncertainty under the DSM are stochastic programming [61] and robust optimization [62]. In stochastic programming, the uncertainty is represented by discrete scenarios given known distribution and decision are made at different stages. Under the standard two-stage stochastic programming paradigm, the decision variables in the optimization problem under uncertainty are divided into two sets. The first-stage decision variables are those decided before the actual realization of the uncertain parameters. The second-stage variables, or recourse variables, are determined once the uncertain events coming to be presented. Due to the uncertainty, the cost for the second-stage is also a random variable. Thus, the objective of the two-stage model is to choose the first-stage variables such that the sum of the first stage cost and the expected value of the second stage cost is minimized (maximized). In the robust optimization, however, the uncertain parameters are specified as a set in which any point is a possible realization of the uncertainty. It is usually formulated for the entire uncertainty set and find the best solution for the worst case scenarios.

Generally, a two-stage stochastic programming problem can be modeled using an extensive formulation as follows:

$$\begin{aligned} \text{minimize} \quad & \sum f(X) + \mathbb{E}_{h \in S}\{Q(X, Y_h, \theta_h)\} \\ \text{subject to} \quad & F(X, h) \leq 0, \\ & G(X, Y, h) \leq 0, \\ & X \in \mathbb{R}^n, Y_h \in \mathbb{R}^m, \end{aligned}$$

where X is the first-stage decision which is made *before* the realization of uncertain information, and Y_h denotes the second-stage decision which is made *after* the realization of the uncertain parameters. Here, $h \in S$ denotes the set of uncertain scenarios and $\theta \in \Theta$ is the set of uncertain parameters. The uncertain scenarios θ_h are usually provided with certain probability distributions, and in practice are presented as a set of discrete scenarios with their associated probabilities. The function $F(X, h)$ describes the constraints that involve only the first-stage decision variables, and the function $G(X, Y, h)$ describes the constraints that involve both the first-stage and second-stage decisions. The objective is to minimize the first-stage cost $f(X)$ and the expectation of the second-stage cost $\mathbb{E}_{h \in S}\{Q(X, Y_h, h)\}$, or $\sum_{h \in S} w_h Q(X, Y_h, h)$ after the discretization, where w_h is the probability related to the scenario h.

3.3 Problem formulation

3.3.1 Assumptions

We present here a stochastic mixed-integer nonlinear programming problem with mixed-integer recourse variables inspired by the model proposed by Li et al. [60]. The problem presented here, however, includes additional variables and constraints to enable the reconfigurability of the network. As noted earlier, the problem will be cast as a two-stage stochastic programming problem. The first-stage design variables will be the existence of the pumps and the network configuration, while the second-stage variables include:

- Scenario-based operating (integer) decision on the pump
- Scenario-based operating (continuous) condition: flow fraction, pump flow rate, pressure rise, and rotational speed.

It should be noted that one approximation is made in the two-stage framework described here. The design decisions are made once in the beginning, and we assume that the second-stage operation is at steady-state. Otherwise, if one were particularly interested in capturing the dynamics of the process or the evolution of the uncertain information over time, it might be more natural to adopt a multi-stage stochastic programming framework,

but this would significantly increase the computational challenge of the problem, and is left to a future study.

We assume that electricity is purchased from the grid and thus subject to market fluctuations. In addition, the total flow rate and the pressure rise requirements may vary in time, thus yielding another source of uncertainty in the operation. It is further assumed that the probability distributions for these uncertain parameters are available, either based on historical data or postulation by engineers. The superstructure of the pump network is depicted in Figure 3.1, where a maximum of 3 parallel pump types (layers) are considered. The objective is to minimize the total cost of the pump network design as well as the expected operating cost, while meeting uncertain production requirements in the presence of uncertain electricity prices.

Based on the above assumptions, the pump network problem is formulated as follows:

3.3.2 Pump performance

The pump performance constraints are described via pump curves. In the original model [58], the pump power curve $P_{i,h}$ and the total head curve $\Delta p_{i,h}$ were both obtained through regression and adjusted through the following relations,

$$P_{i,h} - \alpha_i(\frac{\omega_{i,h}}{\omega_{max}})^3 - \beta_i(\frac{\omega_{i,h}}{\omega_{max}})^2\dot{\nu}_{i,h} - \gamma_i(\frac{\omega_{i,h}}{\omega_{max}})\dot{\nu}_{i,h}^2 = 0, \forall i \in I, \forall h \in S, \tag{3.1}$$

$$\Delta p_{i,h} - a_i(\frac{\omega_{i,h}}{\omega_{max}})^2 - b_i(\frac{\omega_{i,h}}{\omega_{max}})\dot{\nu}_{i,h} - c_i(\frac{\omega_{i,h}}{\omega_{max}})\dot{\nu}_{i,h}^2 = 0, \forall i \in I, \forall h \in S, \tag{3.2}$$

Here, the index i denotes the layer (type) of the pump, and I is defined as the set of all types of pump, while the index $h \in S$ denotes the scenarios associated with each realization of the uncertain parameters, and $\alpha_i, \beta_i, \gamma_i, a_i, b_i$ and c_i are all regression parameters. It is worth pointing out that in [60], the parameters a_i, b_i and c_i were considered as uncertain parameters given that they were estimated through regression techniques and thus were subject to uncertainty. In contrast, these parameters are considered as known in the current work, since our focus is on the uncertainty related to demand. It is possible, however, to generalize the formulation described here to include uncertainty in these parameters. As can be seen from the above relations, both the power curve and the total

head curve are related to the rotational speed $\omega_{i,h}$ and the flow rate $\dot{\nu}_{i,h}$.

3.3.3 Design configuration constraints

These constraints determine the first-stage design, and are updated based on the model in Li et al. [60] to incorporate the integer recourse variables for considering the reconfiguration options. In the model proposed in [60], all integer variables were converted to binary variables to reduce non-convexity in both the objective function and the constraints. This approach is adopted here as well. The number of parallel lines in each pump layer i is $\sum_{j=1}^{2} 2^{j-1} y_{j,i}^{npd}$, while the number of pumps in each line is given as $\sum_{k=1}^{2} 2^{k-1} y_{k,i}^{nsd}$, where $y_{j,i}^{npd}$ and $y_{k,i}^{nsd}$ are binary variables. An additional binary variable $y_{j,k,i}$ is introduced such that $y_{j,k,i} = y_{j,i}^{npd} y_{k,i}^{nsd}$. The expression that involves the multiplication of two binary variables is linearized as,

$$y_{j,k,i} \leq y_{j,i}^{npd}, \forall i \in I, \forall j, k, \tag{3.3}$$

$$y_{j,k,i} \leq y_{k,i}^{nsd}, \forall i \in I, \forall j, k, \tag{3.4}$$

$$y_{j,k,i} \geq y_{j,i}^{npd} + y_{k,i}^{nsd} - 1, \forall i \in I, \forall j, k, \tag{3.5}$$

3.3.4 Reconfiguration constraints

The design configuration constraints define the first-stage design of the network. From the modeling perspective, the reconfiguration constraints are captured using the integer recourse variables.

While the first-stage design should be the same across all the scenarios, the second-stage pump configuration could be different, allowing flexibility responding to various uncertain outcomes. Variables $y_{j,i,h}^{np}$ and $y_{k,i,h}^{ns}$ represent the recourse binary variables, where $\sum_{j=1}^{2} 2^{j-1} y_{j,i,h}^{np}$ denotes the total number of pumps that are operated in parallel and $\sum_{k=1}^{2} 2^{k-1} y_{k,i,h}^{ns}$ denotes the total number of pumps that are operated in series under scenario h. The constraints on the reconfiguration process are given as follows:

$$\sum_{j=1}^{2} 2^{j-1} y_{j,i,h}^{np} \leq \sum_{j=1}^{2} 2^{j-1} y_{j,i}^{npd}, \forall i \in I, \forall j, \forall h \in S, , \tag{3.6}$$

$$\sum_{k=1}^{2} 2^{k-1} y_{k,i,h}^{ns} \leq \sum_{k=1}^{2} 2^{k-1} y_{k,i}^{nsd}, \forall i \in I, \forall k, \forall h \in S, \tag{3.7}$$

where the total number of pumps that are operated in parallel and the total number of pumps that are operated in series under scenario h should not be larger than those for the first-stage design: $\sum_{j=1}^{2} 2^{j-1} y_{j,i}^{npd}$ and $\sum_{k=1}^{2} 2^{k-1} y_{k,i}^{nsd}$, respectively, allowing the process reconfiguration depending on different scenarios. The above constraints define the connection between the first-stage design variables and the integer recourse variables and should be obeyed across all the scenarios.

The variables $z_{i,h}$ decide whether certain pump types are turned on or off; and the relation between $z_{i,h}$ and the binary variables $y_{j,i,h}^{np}$ and $y_{k,i,h}^{ns}$ are given by,

$$\sum_{j=1}^{2} 2^{j-1} y_{j,i,h}^{np} \leq 3 z_{i,h}, \forall i \in I, \forall j, \forall h \in S, \tag{3.8}$$

$$\sum_{j=1}^{2} 2^{j-1} y_{j,i,h}^{np} \geq z_{i,h}, \forall i \in I, \forall j, \forall h \in S, \tag{3.9}$$

$$\sum_{k=1}^{2} 2^{k-1} y_{k,i,h}^{ns} \leq 3 z_{i,h}, \forall i \in I, \forall k, \forall h \in S, \tag{3.10}$$

$$\sum_{k=1}^{2} 2^{k-1} y_{k,i,h}^{ns} \geq z_{i,h}, \forall i \in I, \forall k, \forall h \in S, \tag{3.11}$$

$$\sum_{i=1}^{3} z_{i,h} \geq 1, \forall i \in I, \forall h \in S. \tag{3.12}$$

Again, it should be emphasized that the reconfiguration and design constraints are the key distinctions from the stochastic model given in [60].

3.3.5 Operating constraints

The operating constraints include all the continuous variables, including the fractional flow going to the pumps of type (layer) i, $x_{i,h}$, as the fractions should add up to 1,

$$\sum_{i=1}^{3} x_{i,h} = 1, \forall i \in I, \forall h \in S. \tag{3.13}$$

Other continuous variables include the power, $P_{i,h}$, the pressure rise, $\Delta p_{i,h}$, and the flow rate of type i pumps, $\dot{\nu}_{i,h}$, under scenario h. Since the integer variables are reformulated

using binary variables, $P^y_{j,k,i,h}, \Delta p^y_{k,i,h}$ and $\dot{\nu}^y_{j,i,h}$ are introduced such that:

$$P^y_{j,k,i,h} = P_{i,h} y_{j,k,i}, \forall i \in I, \forall j,k, \forall h \in S, \tag{3.14}$$

$$\Delta p^y_{k,i,h} = \Delta p_{i,h} y^{ns}_{k,i,h}, \forall i \in I, \forall k, \forall h \in S, \tag{3.15}$$

$$\dot{\nu}^y_{j,i,h} = \dot{\nu}_{i,h} y^{np}_{j,i,j}, \forall i \in I, \forall j, \forall h \in S. \tag{3.16}$$

Equations 3.14-3.16 have bilinear terms including the multiplication of a continuous variable and a binary variable, and could be reformulated as a set of linear constraints:

$$0 \leq P^y_{j,k,i,h} \leq P^{max}_i y_{j,k,i}, \forall i \in I, \forall j,k, \forall h \in S, \tag{3.17}$$

$$P_{i,h} - P^{max}_i (1 - y_{j,k,i}) \leq P^y_{j,k,i,h} \leq P_{i,h}, \forall i \in I, \forall j,k, \forall h \in S, \tag{3.18}$$

$$0 \leq \dot{\nu}^y_{j,i,h} \leq V_{tot} y^{np}_{j,i,h}, \forall i \in I, \forall j, \forall h \in S, \tag{3.19}$$

$$\dot{\nu}_{i,h} - V_{tot,h}(1 - y^{np}_{j,i,h}) \leq \dot{\nu}^y_{j,i,h} \leq \dot{\nu}_{i,h}, \forall i \in I, \forall j, \forall h \in S \tag{3.20}$$

$$0 \leq \Delta p^y_{k,i,h} \leq \Delta P_{tot} y^{ns}_{k,i,h}, \forall i \in I, \forall k, \forall h \in S \tag{3.21}$$

$$\Delta p_{i,h} - \Delta P_{tot}(1 - y^{ns}_{k,i,h}) \leq \Delta p^y_{k,i,h} \leq \Delta p_{i,h}, \forall i \in I, \forall k, \forall h \in S. \tag{3.22}$$

The constraints on flow going through each pump layer are then described as follows:

$$\sum_{j=1}^{2} 2^{j-1} \dot{\nu}^y_{j,i,h} - x_{i,h} V_{tot,h} = 1, \forall i \in I, \forall j, \forall h \in S, \tag{3.23}$$

where the fraction of the total flow requirement $V_{tot,h}$ for the scenario h in each layer i should be equal to the sum of the flows in the lines of layer i. The constraints on pressure rise are given as

$$\Delta P_{tot,h} z_i - \sum_{k=1}^{2} 2^{k-1} \Delta p^y_{k,i,h} = 0, \forall i \in I, \forall k, \forall h \in S, \tag{3.24}$$

where the total pressure rise requirement for scenario h, $\Delta P_{tot,h}$, should be equal to the sum of the pressure rise after each pump. Finally, the bounds for all the continuous

variables are defined as: $\forall i \in I, \forall h \in S$,

$$0 \leq x_{i,h} \leq 1, x_{i,h} \leq z_i, \tag{3.25}$$

$$0 \leq \dot{\nu}_{i,h} \leq V_{tot}, \dot{\nu}_{i,h} \leq z_i V_{tot,h}, \tag{3.26}$$

$$0 \leq \omega_{i,h} \leq \omega_{max}, \omega_{i,h} \leq z_i \omega_{max}, \tag{3.27}$$

$$0 \leq P_{i,h} \leq P_i^{max}, P_{i,h} \leq z_i P_i^{max}, \tag{3.28}$$

$$0 \leq \Delta p_{i,h} \leq \Delta P_{tot,h}, \Delta p_{i,h} \leq z_i \Delta P_{tot,h}, . \tag{3.29}$$

3.3.6 Objective function

The objective function includes the first-stage design cost, which is basically the capital cost of the different pumps, as well as the expected value of the second-stage operational cost, which is represented by:

$$\sum_{i=1}^{3} C_i^{fix} \sum_{j=1}^{2} \sum_{k=1}^{2} 2^{j+k-2} y_{j,k,i} + \sum_{h=1}^{s} w_h \sum_{i=1}^{3} C_{i,h} \sum_{j=1}^{2} \sum_{k=1}^{2} 2^{j+k-2} P_{j,k,i,h}^{y}, \tag{3.30}$$

where C_i^{fix} is the annualized fixed capital cost of the pump i and $C_{i,h}$ is the annual operating cost factor under scenario h. It should be noted that the above formulation does not include the cost associated with the reconfiguration of the pumps. The transitions between different configurations take place through re-routing of the flows, which in turn is achieved through the closing and opening of valves in a prescribed sequence. For fast processes, as assumed in this work, the transition would be relatively fast, thus not requiring further consideration. However, if the transition between different configurations becomes too frequent, then the equipment wear could be a significant issue. In this case, one could consider adding a penalty or a constraint to prevent excessive transitions (see, for example, our earlier work in [36]). Based on the previous assumptions, the objective function is linear since all the integer variables are converted to binary variables. The flexible pump network design problem is then cast as a two-stage stochastic programming problem with pure binary first-stage variables, mixed-integer second-stage variables and

non-convex constraints. The problem formulation is summarized as follows:

minimize	*Objective* Eq.(3.30)
subject to	Pump performance Eqs.(3.1), (3.2)
	Design Constraints Eqs.(3.3) − (3.5)
	Reconfiguration Eqs.(3.6) − (3.12)
	Operating Constraints/bounds Eqs.(3.13), (3.17) − (3.29).

3.4 Solution method

Stochastic programming problems are notorious for their formidable computational challenges that arise due to the scale of the problem. To deal with these challenges, the solution methods for stochastic programming problems generally try to exploit the special structure of the problem using decomposition methods. In the current problem formulation, the equality constraints involving the quadratic and cubic terms in the pump performance constraints (Eqs. (3.1) and (3.2)) add a non-convex element to the problem. To the best of our knowledge, there is no existing systematic solution method to handle this class of problems. Li et al. [60] developed the Non-convex Generalized Benders Decomposition (NGBD) algorithm to solve the separable stochastic mixed-integer programming problem. However, as pointed out earlier, the developed algorithm focuses on solving a model with pure first-stage binary variables and only continuous recourse variables. This algorithm is not appropriate for the integer recourse variables in our case.

More recently, Li and Grossmann [63] developed an algorithm to rigorously solve the stochastic mixed-integer convex programming problem with both mixed-integer first-stage variables as well as mixed-integer recourse variables. The ongoing research in the stochastic programming community notwithstanding, our aim in the current work is not to develop a new numerical algorithm, but to demonstrate the concept of a reconfigurable network design. To this end, we simply leverage existing solution techniques.

A popular heuristic algorithm for solving stochastic programming problems is Progressive Hedging (PH) [52], which is guaranteed to converge to a global optimum for convex stochastic programming problems with continuous variables. The PH method

decomposes a stochastic problem across scenarios by partitioning the original problem into manageable scenario sub-problems. For the stochastic mixed-integer programming problem, Gade et al. [64] have shown that PH can also obtain a lower bound solution, which is similar to solving the Lagrangean sub-problems. One of the advantages of the PH algorithm is that, different from the Benders decomposition-based solution methods (e.g., NGBD and improved Benders decomposition in [60]), PH, based on the augmented Lagrangean decomposition, does not require the decomposed problem to be convex. Thus, it can always serve as a high-quality heuristic solution method for stochastic mixed-integer programming problems.

The reconfigurable pump network design problem is now cast as follows:

$$
\begin{aligned}
\text{minimize} \quad & \sum_{h \in S} w_h (c^T X_h + g_h^T Y_h) \\
\text{subject to} \quad & F(X, h) \leq 0, \\
& G(X, Y, h) \leq 0, \\
& X_h - \hat{X} = 0, \ \text{(Non-anticipativity)} \\
& \hat{X}, X \in \mathbb{Z}^n, \\
& Y_h \in \mathbb{Z}^p \times \mathbb{R}^{m-p},
\end{aligned}
$$

where X_h denotes the design vector for the first-stage design under scenario h, and Y_h denotes the recourse variables, including both integer and continuous variables, under scenario h. This form is also referred to as the *scenario formulation* since X_h implies that for different scenarios h, the first-stage decision could be different. However, as this implication usually violates the fact that first design stage should not depend on different scenarios, a constraint, called the non-anticipativity constraint, is added to ensure that all the scenario-dependent decisions X_h will be equal to each other. The term $\hat{X}$ is defined as the aggregated term, and the non-anticipativity constraints state that the first-stage decision should not depend on the scenarios. The PH method is motivated by the augmented Lagrangean decomposition method, where the non-anticipativity constraints are dualized and the quadratic terms with a penalty factor ρ are added to the original objective function in each sub-problem. The scenario formulation then allows the solution

method to decompose the problem by scenarios. The associated PH algorithm is provided in Algorithm 3.1. In the initialization step, or iteration 0, all the individual scenario problems are solved to obtain X_h. During the iterative process, an aggregation of X_h, $\hat{X}$ is computed. The dual parameter, λ, is then updated using the penalty factor ρ. Next, the decomposition of the PH is performed with an objective function including the original objective function, a perturbation with the dual parameters and a quadratic term that quantifies the deviation of the scenario solution X_h from the aggregation $\hat{X}$. When $\hat{X}$ obtained through all the scenarios agree with each other, the algorithm is terminated.

Algorithm 3.1 Progressive Hedging Algorithm

$k \leftarrow 0$, $\lambda^k \leftarrow 0, \epsilon_{ph}$

for all $h \in S$ **do**

$X_h^k, Y_h^k = \mathbf{argmin}_{x,y}(c^T X_h + g_h^T Y_h)$

end for

while Not convergent **do**

$k \Leftarrow k + 1$

$\hat{X}^{k-1} = \sum_{h \in S} w_h X_h^{k-1}$

$\lambda^k = \lambda^{k-1} + \rho(X_h^{k-1} - \hat{X}^{k-1})$

for all $h \in S$ **do**

$X_h^k, Y_h^k = \mathbf{argmin}_{X,Y}(f_h(X_h, Y_h) + \lambda_h^k X_h + \frac{\rho}{2}||X_h - \hat{X}_h^{k-1}||)$

end for

if $\sum_{h \in S} w_h ||X_h^k - \hat{X}_h^k|| \leq \epsilon_{ph}$ **then**

Stop Iteration, convergent

end if

end while

When PH is applied to a stochastic mixed-integer problem, it has been observed that first-stage integer variables often would undergo a so-called variable oscillation and convergence is difficult to obtain. Such cyclic behavior generally implies a poor choice of the penalty factor ρ [65], which is generally set as a constant. The performance of the PH algorithm is generally sensitive to the value of the penalty factor. There are several

heuristics available for choosing the proper ρ value, but none of these approaches have been proven to be universally better than others. Many numerical studies on different choices of the penalty factor have shown that different ρ values would lead to different convergence rates or even final objective function values [66]. Different ρ selection approaches are also available. One such approach is to set ρ to be constant for all the first-stage decision variables, which usually uses a constant value that is proportional to the first-stage cost. Another approach is the variable-dependent ρ strategy, which is described by Watson et al. [65], where after the initialization, the penalty factor is calculated based on the scenario solution,

$$\rho(l) = \frac{c(l)}{X^{max} - X^{min} + 1}, \tag{3.31}$$

where $X^{max} = \max_{h \in S} X_h^{(0)}$ and $X^{min} = \min_{h \in S} X_h^{(0)}$ for each design variable l in the penalty vector ρ, while $c(l)$ is the corresponding cost parameter for the variable l. The benefit of the latter approach is to provide a systematic way to compute an effective ρ value without information on the problem, and therefore testing different ρ values is not necessary. Also, it has been shown that the ρ value will strongly influence the quality of the lower bound solution [67]. Usually, the larger the ρ value, the faster the convergence, and vice versa. As we seek a heuristic solution for the non-convex problem at hand, the primal solution obtained by PH should be sufficient; and, therefore, the variable specific ρ selection approach was chosen to eliminate the test searching for the best ρ values.

In this work, Pyomo, a Python-based optimization language, is used as the optimization platform [68] with its stochastic programming extension PySP [67]. PySP implements the PH algorithm framework and also includes several convergence acceleration heuristics [65]. At the same time, due to the non-convexity of the sub-problem, the sub-solver chosen is BARON [41, 69] as it is a global optimization solver capable of solving non-convex problems.

3.5 Results and discussion

In this section, we present the computational results obtained by directly applying the PH algorithm to the original non-convex MINLP problem. The pump parameters are

Table 3.1. Pump costs and parameters

Pump	Annualized cost($/yr)	a	b	c	α	β	γ
Type 1	2238.7	629	0.696	-0.0116	19.9	0.161	-0.000561
Type 2	882.8	215	2.95.	-0.115	1.21	0.0644	-0.000564
Type 3	1156.7	361	0.53.	-0.00946	6.52	0.102	-0.000232

based on the original study [59]. The pump costs were converted to U.S. dollars from the original currency and updated using equipment cost index between 1994 and 2016 [70].

3.5.1 Scenario generation for stochastic programming

In California, there are several electricity price structures that might be available to industrial customers, including time-of-use prices (TOU), the day-ahead market (DAM) and the real-time market (RTM). In this design problem, we considered each price structure separately. For the TOU electricity price scenarios, the electricity data were based on PG&E TOU rate for industrial consumers [71], where five different prices were considered including summer off-peak, summer partial peak, summer peak, winter off-peak and winter partial peak. The distribution for the electricity price data was obtained based on relative time throughout the year. The related prices and probabilities can be found in Table 3.2.

For both the DAM and the RTM markets, the price data were taken from a pricing node around Sacramento Valley for the year 2018, and the probability distribution for each price structure was generated using a simple k-means clustering technique. The resulting probability distributions are given in Table 3.3 and Table 3.4, respectively.

The pressure rise data were chosen randomly to show the difference between a low-pressure rise requirement, 100 kPa, and a high-pressure rise requirement, 400 kPa. Without loss of generality, both pressure rise probabilities were assumed to be 0.5 and, therefore, the expected value of pressure rise is 250 kPa. Five different flow rates were chosen, ranging from 50 m^3/h to 650 m^3/h, and the flow rates were assumed to be normally distributed, and the probability was then calculated, with a mean of 350 m^3/h and standard deviation of 150.0 m^3/h. The probability values of the realization h were then calculated

following the sampling rule described in [60]. The pressure and flow rate requirements were taken based on original data [58]. As all three different parameters are assumed to be independent, the total number of scenarios is 50, 40 and 60, for the TOU, DAM and RTM problems, respectively. The stochastic programming problem was solved on an Intel i7 machine with 16 GB memory, and it took 2208s (TOU), 1292s (DAM) and 2310s (RTM) for the PH algorithm to converge for each problem. We also attempted to use the global solver BARON to solve the deterministic equivalent problem, but after six hours the algorithm did not converge and the implementation was then terminated. After six hours, the optimality gap was still too large. For example, for the TOU problem the lower and upper bounds were 14881.6 and 483967, respectively; and for the RTM problem the lower and upper bounds were 24744 and 236298, respectively.

Table 3.2. TOU electricity price scenarios with their probabilities

Scenario	Price ($/kWh)	Probability
Summer off-peak	0.080	0.3384
Summer partial peak	0.107	0.0753
Summer peak	0.152	0.0904
Winter partial peak	0.101	0.1767
Winter off-peak	0.087	0.3192

Table 3.3. DAM electricity price scenarios with their probabilities

Scenario	Price ($/kWh)	Probability
Cluster 1	0.024	0.4668
Cluster 2	0.044	0.4367
Cluster 3	0.081	0.092
Cluster 4	0.392	0.003

Remark: The clustering technique implemented in this work is a relatively simple strategy which is used to showcase some of the extreme scenarios that can arise under the RTM pricing, which have interesting implications for the DR problem at hand (see the next section). However, it is well known that clustering algorithms usually exhibit a

Table 3.4. RTM electricity price scenarios with their probabilities

Scenario	Price ($/kWh)	Probability
Cluster 1	-0.003	0.067
Cluster 2	0.022	0.458
Cluster 3	0.036	0.331
Cluster 4	0.057	0.120
Cluster 5	0.103	0.017
Cluster 6	0.709	0.007

trade-off between the number of clusters and generality. In the current case, we aimed to strike a balance between the potential increase in the number of scenarios, on the one hand, and the increase in the complexity of the stochastic programming problem, on the other.

3.5.2 Results of stochastic programming

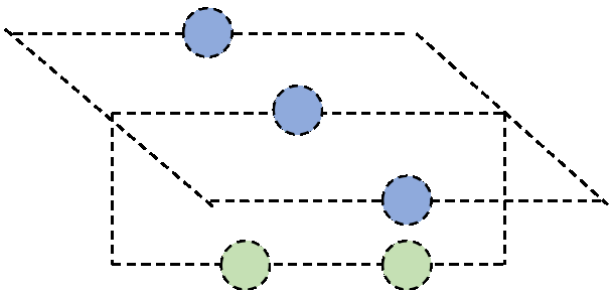

Figure 3.2. The pump network design for TOU, DAM and RTM scenarios. All cases have the same first-stage solution.

The reconfigurable design obtained after solving the stochastic optimization problem is shown in Figure 3.2, where the final first-stage design result is displayed. As can be observed, the final design includes only two pump types, types 1 and 3. Pump type 1 configuration includes 3 pumps connected in parallel, while pump type 3 has 2 pumps connected in series. The operating configurations for the TOU, DAM and RTM scenarios are shown in Figure 3.3, where configurations (a)-(c) are the configurations for the TOU case, configurations (d)-(f) are for the DAM case and configurations (g)-(n) are for the

Table 3.5. Operating configurations under different scenarios, where the configurations are labeled in Figure 3.3

Pressure Drop(kPa)	Vtot(m^3/h)	TOU		DAM		RTM	
		Price($/kWh)	Configuration	Price($/kWh)	Configuration	Price($/kWh)	Configuration
100	50	0.08	b	0.024	e	-0.003	g
		0.107		0.044		0.022	
		0.152		0.081		0.036	
		0.101		0.392		0.057	m
		0.087		-		0.103	
		-		-		0.709	
		Price($/kWh)	Configuration	Price($/kWh)	Configuration	Price($/kWh)	Configuration
400	50	0.08	b	0.024	e	-0.003	g
		0.107		0.044		0.022	
		0.152		0.081		0.036	
		0.101		0.392		0.057	m
		0.087		-		0.103	
		-		-		0.709	
		Price($/kWh)	Configuration	Price($/kWh)	Configuration	Price($/kWh)	Configuration
100	200	0.08	a	0.024	d	-0.003	g
		0.107		0.044		0.022	
		0.152		0.081		0.036	
		0.101		0.392		0.057	m
		0.087		-		0.103	
		-		-		0.709	
		Price($/kWh)	Configuration	Price($/kWh)	Configuration	Price($/kWh)	Configuration
400	200	0.08	a	0.024	d	-0.003	i
		0.107		0.044		0.022	
		0.152		0.081		0.036	
		0.101		0.392		0.057	l
		0.087		-		0.103	
		-		-		0.709	
		Price($/kWh)	Configuration	Price($/kWh)	Configuration	Price($/kWh)	Configuration
100	350	0.08	c	0.024	f	-0.003	h
		0.107		0.044		0.022	
		0.152		0.081		0.036	
		0.101		0.392		0.057	n
		0.087		-		0.103	
		-		-		0.709	
		Price($/kWh)	Configuration	Price($/kWh)	Configuration	Price($/kWh)	Configuration
400	350	0.08	a	0.024	d	-0.003	j
		0.107		0.044		0.022	
		0.152		0.081		0.036	
		0.101		0.392		0.057	l
		0.087		-		0.103	
		-		-		0.709	

Table 3.6. Operating configurations under different scenarios, where the configurations are labeled in Figure 3.3 Continued

Pressure Drop(kPa)	Vtot(m^3/h)	TOU		DAM		RTM	
		Price($/kWh)	Configuration	Price($/kWh)	Configuration	Price($/kWh)	Configuration
100	500	0.08	c	0.024	f	-0.003	k
		0.107		0.044		0.022	
		0.152		0.081		0.036	
		0.101		0.392		0.057	n
		0.087		-		0.103	
		-		-		0.709	
		Price($/kWh)	Configuration	Price($/kWh)	Configuration	Price($/kWh)	Configuration
400	500	0.08	a	0.024	d	-0.003	j
		0.107		0.044		0.022	
		0.152		0.081		0.036	
		0.101		0.392		0.057	l
		0.087		-		0.103	
		-		-		0.709	
		Price($/kWh)	Configuration	Price($/kWh)	Configuration	Price($/kWh)	Configuration
100	650	0.08	c	0.024	f	-0.003	k
		0.107		0.044		0.022	
		0.152		0.081		0.036	
		0.101		0.392		0.057	n
		0.087		-		0.103	
		-		-		0.709	
		Price($/kWh)	Configuration	Price($/kWh)	Configuration	Price($/kWh)	Configuration
400	650	0.08	c	0.024	f	-0.003	n
		0.107		0.044		0.022	
		0.152		0.081		0.036	
		0.101		0.392		0.057	
		0.087		-		0.103	
		-		-		0.709	

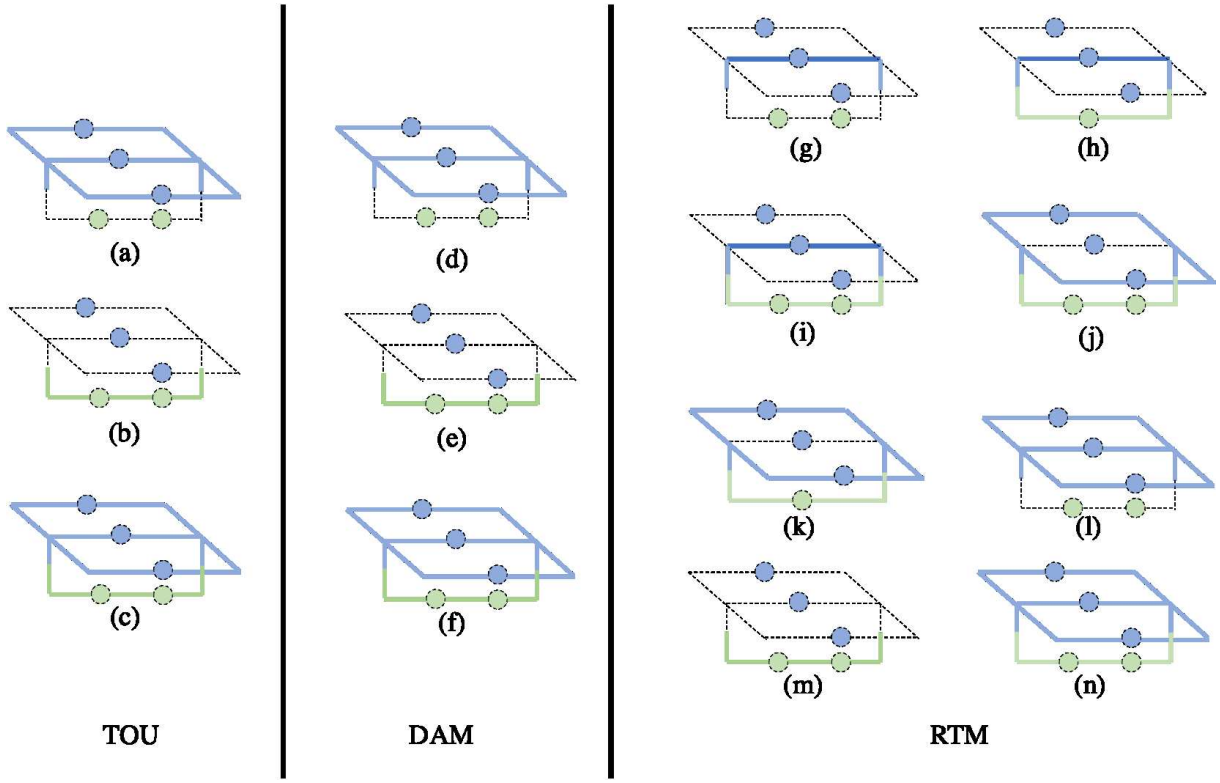

Figure 3.3. Operating configurations under different electricity price structures; the colored solid lines represent the pump being operated, while the black dash lines represent the pump not operating.

RTM case. It should be noted that there is some duplication in the configurations, where configurations (a), (d), and (l) represent the same configuration; configurations (b), (e) and (m) represent the same configuration; and configurations (c), (f) and (n) are considered identical. The results show that generally different network configurations exist under different scenarios. Configurations (a), (d) and (l), for example, indicate that only pump type 1 is being used, while configurations (b), (e) and (m) show only pump type 3. Notably, configurations (c), (f) and (n) contain both pump types. It is important to point out that, while some scenarios might have the same network configuration, the continuous variables under different scenarios (e.g., flow rate through different pump types) can be different. Also, one might notice that Configurations (c), (f), and (n) are actually the result using all the pumps in the first-stage design. It is also worth pointing out that for configurations (h) and (k), there is only one pump for pump type 3 (instead of 2 pumps like the other configurations). This result is consistent with the constraints in 3.6 and

3.7, where this possibility is not excluded.

The detailed results are summarized in Tables 3.5 and 3.6. As stated earlier, the design result does not use any pump type 2 and hence it is not included in the table. The results are presented in different groups, with each group having different electricity prices, while the same pressure rise and flow rate requirements are fixed. As shown in Tables 3.5 and 3.6, for all the TOU, DAM and RTM cases, changing the flow rate requirements and/or the pressure rise will usually trigger a reconfiguration, and even when the configuration is not changed, the continuous recourse variables usually will be different.

3.5.3 Effect of electricity prices and pressure rise on reconfiguration

The results show that for all the different groups in the TOU and DAM cases, for example, the group with a low-pressure rise and 50 m^3/h flow rate requirement, the change in electricity price does not change the physical configuration. The observation that the electricity price by itself does not trigger a configuration change seems to be consistent with the findings of Zhang et al. [19]. An interesting observation from the results is the fact that, for certain groups in Tables 3.5 and 3.6, when the electricity prices and the flow rate requirements remain the same, the increase in the demand for pressure rise actually results in using fewer pumps.

In the RTM cases, however, as there are scenarios having negative electricity prices, it can be seen that the configurations under the negative prices are different. Except for the case where $dP = 400kPa$ and $V_{tot} = 650m^3/h$, for the rest of the scenarios, negative electricity price triggers a reconfiguration. For the case where $dP = 400kPa$ and $V_{tot} = 650m^3/h$, the physical constraints might prevent the negative price from finding another configuration, as the configuration (n) is the only feasible configuration. Also, it can be seen that for different negative prices with different pressure drop and total flow rate requirements, there are multiple alternative configurations. Intuitively, when the electricity price becomes negative, which implies the least efficient configuration, more power consumption could potentially lead to a better economic outcome.

3.5.4 Value of stochastic solution

The stochastic solution is usually evaluated using the expected value of perfect information (EVPI) and/or value of stochastic solution (VSS) [61]. Generally speaking, EVPI indicates how sensitive the solution is to perfect information – the larger the value of EVPI the worse the solution, since a small deviation from the perfect information would result in a large regret. VSS is used as a measure for the benefit brought by the stochastic programming solution compared to its deterministic counterpart. For practical purposes, computing VSS is important because one needs to be clear about whether solving a stochastic programming problem, which is usually more computationally challenging, would be worthwhile.

To get the VSS of a specific problem, one first replaces all random variables by the corresponding expected values, and the resulting deterministic model, which is called the expected value problem (EV) is solved to obtain the expected value solution:

$$\mathrm{EV} = minimize_x f(x, \bar{\xi}), \tag{3.32}$$

where $\bar{\xi}$ is the expectation of the random variables ξ. Then the expected value solution, $\bar{x}(\bar{\xi})$, which is the solution of the EV problem, will be fixed for the original problem and resolved under different scenarios. The expected result of using the expected value solution is defined as:

$$\mathrm{EEV} = \mathbb{E}_\xi(f(\bar{x}(\bar{\xi})), \xi). \tag{3.33}$$

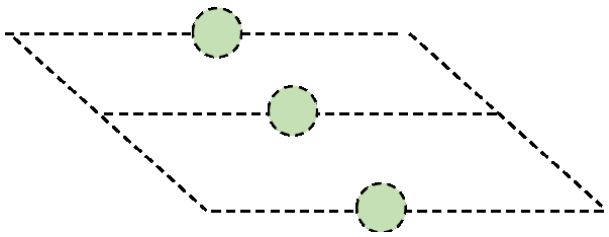

Figure 3.4. Configuration for the expected value deterministic problem.

The objective function value of the original stochastic programming problem, which is the first-stage design cost plus the expected second-stage cost, is denoted as RP (recourse

problem). Then, the VSS is defined as:

$$\text{VSS} = \text{EEV} - \text{RP}. \tag{3.34}$$

In this pump network design problem, the expected value of random variables for electricity prices is \$0.0944/kWh (TOU), \$0.0390/kWh (DAM), and \$0.0352kWh (RTM), respectively; for pressure rise we have 250 kPa and for the flow rate requirement the expected value is 350 m^3/h. The deterministic optimization configuration of the expected value problem is shown in Figure 3.4, where only type 3 pumps are used, and they are connected using three parallel lines with one pump in each line. The networks corresponding to all the electricity price scenarios are the same, as all three problems are only different in the expected value of the electricity price. To get the EEV of the problem, we fix this configuration for each situation and attempt to resolve the deterministic problem under each corresponding scenario. However, as one might expect, not all scenarios generate a feasible solution. In this case, the VSS is declared to be infinite since the EEV cannot be quantified for the TOU, DAM and RTM cases.

3.5.5 Comparison with the fixed design case

Next, we investigated the design problem without the reconfiguration constraints to show the potential benefit of a reconfigurable process network design. We formulated the problem in a similar fashion to the reconfigurable design problem using stochastic programming, but without the reconfiguration constraints as shown below:

minimize	*Objective* Eq. (3.30)
subject to	Pump performance, Eqs. (3.1) – (3.2)
	Design Constraints, Eqs. (3.3) – (3.5)
	Operating Constraints/bounds, Eqs. (3.13), (3.17) – (3.29)

The stochastic programming problem without reconfiguration is similar to the model developed in [60], and the problem is solved using the PH algorithm used in this work without further convexification of the original problem. Interestingly, the resulting first-stage design is the same as in Figure 3.2. However, the key difference is in the "fixed"

Table 3.7. The second-stage objective function value for the stochastic programming problem with and without reconfiguration constraints for different electricity price structures.

Problem	with reconfiguration ($/year)	without reconfiguration ($/year)
TOU	32105.33	34790.02
DAM	13277.58	14384.84
RTM	11926.20	12962.06

aspect of the design, where the switching to different configurations is prohibited, and thus the pump network is operated only under configuration (c), (f) and (n) all the time. The second-stage objective function values for the stochastic programming problem without reconfiguration constraints (which are shown in Table 3.7 for the TOU, DAM and RTM cases) are, anticipated, higher than those of the model with reconfiguration, since the reconfiguration allows the network structure to change in favor of a lower operating cost.

3.6 Conclusions

This work introduced a framework for process network design that enables process network reconfiguration under demand-side management. In the proposed framework, a steady-state stochastic programming model with mixed-integer recourse variables was developed. It was shown that a proactive reconfiguration can be triggered under different demand-side requirements and that the reconfigurable design might have potential economic benefits.

While this preliminary study shows promise, there are several issues that remain to be explored. First, the transition cost between different configurations was not considered. In fact, using a two-stage stochastic formulation, this feature might be difficult to capture as the solution of a two-stage stochastic programming problem only yields an operating decision under certain scenarios. To further explore the transition effect, a multi-scale, or even a multi-stage, optimization problem has to be developed and solved, where the transition cost in the model is explicitly accounted for, or a constraint to prevent frequent configuration changes is added. Second, in the context of pump network design problems, the assumption that electricity prices and flow rates are independent might not be realistic in some cases. As one might expect, the process operators may vary the operating flow

rate according to the electricity prices (e.g., using high flow rate when electricity price is low and vice versa). However, to remove this assumption one needs to change the flow rate requirements from random variables (parameters in the stochastic problem) to endogenous decision variables, and this will lead to having bilinear terms in the resulting model, which would cause further non-convexity. The problem will then become more challenging since further relaxation has to be performed to improve computational performance. Finally, while pressure changing equipment, such as pumps or compressors, are usually considered as fast-dynamics processes [15], in most applications, however, these equipments will not be used separately. For example, in an energy-intensive process flow sheet, the pump network might be connected to other slow dynamics processes such as distillation columns. Thus, considering a flow sheet design including the network with other processes needs to be further explored.

Chapter 4

Assessment of Demand Response Particibility Potential Through Load-Shifting Capacity

In this chapter, a model-based analytical framework is proposed to evaluate the cost-effectiveness of process design alternatives regarding their ability to participate (particibility) in Demand Response (DR) services (such as load shifting under the Day-Ahead market) through the use of supply curves. In Chapters 2 and 3, the discussion focused on the process network design and the process network reconfiguration to satisfy the demand response objective. However, we could only carry out the studies assuming the process is at steady-state, and therefore ignoring the process dynamics. This is mostly due to the complexity of the integration of process design and process control. Here, we present a bottom-up approach to analyze the relation between process design (in our case, the capital cost of the system) and load shifting potential, through the supply curves. In the sections that follow, we discuss the framework implemented in this work to analyze the cost-effectiveness of a certain process design. We define a new metric, namely *load-shifting capacity*, to quantify the DR capability of a given process in terms of load shifting. The *load-shifting capacity* metric is calculated using a scheduling-based model integrated with process dynamics. Through the proposed framework, we demonstrate the cost-benefits of considering DR aspects at the design stage. As a motivating example, the developed

framework is illustrated using a CSTR-storage model, for which supply curves are generated under different scenarios. A visualization is provided of the effect of the process design capacities on the DR capability, as well as the limitations on the load-shifting capacity of a given process design.

4.1 Motivation

Currently, studies incorporating the design with DSM are quite limited, even though the process design determines (establishes) how the plant could be operated and whether the process could be flexible enough during operation. As noted earlier in Chapter 1, two factors are important when considering the DR participation of a certain process: whether the process has enough intrinsic dynamics that could respond quickly to the market signal and whether the process has enough capacity to allow flexible operation. Due to these two factors, studies in DR are usually limited to specific process industries, such as aluminum, chlor-alkali or air separation and are also limited to operations rather than considering the process design. When considering the process design, one question to ask is whether overcapacity or certain control strategy can help increase the DR participation of a certain process. One simple way is to model the process operation under the varying electricity prices and optimize the lowest operating cost; however, through this way, it is difficult to compare two different designs on how much DR potential each could provide.

The load shift refers to a DR approach that involves moving electrical loads from one time to another to better match, either, the availability of low-cost power or to "valley fill" grid-level load requirements (i.e., peak-clipping), while providing equivalent energy service to the end user [72]. Naturally, a process can serve as a shift resource by adjusting its consumption pattern. The motivating question here is that can we compare different design by how much shifting load it could provide? If one could quantify the load-shifting potential, would it be worthwhile to perform the process design from this perspective?

4.2 Problem overview

The conceptual production system with the set of components considered in this study is shown in Figure 4.1. The system will be required to satisfy an hourly demand of the

product, and a storage unit is installed. The plant is also connected to the grid, so it can purchase electricity in different electricity markets. The key objective in this study is to evaluate the DR potential for various plant designs as well as for different storage capacities.

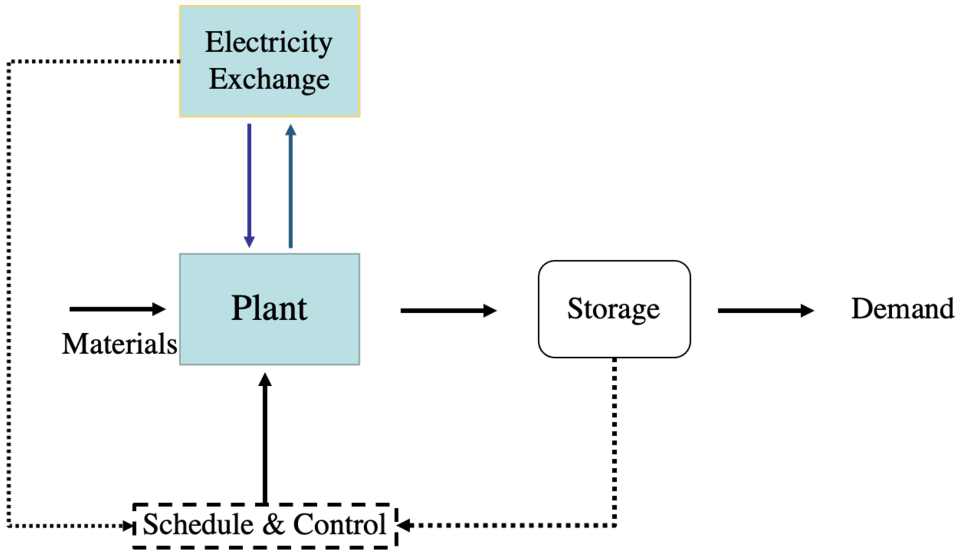

Figure 4.1. A schematic representation of the problem statement

4.2.1 Quantification of load-shifting

We define a metric, the load-shifting capacity, to quantify the DR capability. It is noted that this metric is used to evaluate the load-shifting capacity only under the RTM, such as the day-ahead market (DAM) and the five-minute market (FMM). As shown in Figure 4.2, the blue solid line represents the scheduled operating profile, while the orange dashed line represents the base load. Theoretically, if the total power consumption remains unchanged over a period of time, the total production over time should not change. Therefore, the area under the blue line and the area under the orange line should be nearly equal for a given period of time. We define the base load at the time t as E_t^b and the real scheduled load as E_t^s; thus we can quantify the *load-shifting capacity* as follows:

$$E^{shift} = \sum_t \frac{|E_t^b - E_t^s|}{2}. \tag{4.1}$$

As one might notice, this value is equal to the grey area in Figure 4.2. It basically describes the load that could be shifted to other time spots. Theoretically, over a certain period of time, if the production requirement does not change and the operation remains unchanged, the total energy consumption over this period should be unchanged. However, the load-shifting capacity can be different with a different control strategy.

4.3 Overview of analysis framework

The framework implemented in this study is a bottom-up approach, starting with a first-principles dynamic model to construct a high-fidelity process operating range and then to implement the scheduling model to analyze a metric defined as "load-shifting capacity".

The first step in the framework is to generate the feasible region for the operation-related decision variables. In Figure 4.1, we are referring to the plant part. This is performed using a first-principles dynamic model for the given process. The specific focus of this part is to provide the scheduling model with a feasible operating range as well as the transition profile information. The feasible region not only includes the operating range but also provides information on whether specific operating adjustments will violate the system constraints such as safety concerns or production requirements.

The second step is to develop a scheduling-oriented operating model to evaluate the potential of the load shifting under specific process design or capacity. We defined the base load of the process and then calculate the load-shifting capacity for each different design (e.g. with different inventory sizes or different capacity).

The last step in the proposed framework is to construct the supply curve to demonstrate the "cost-effectiveness" of various design alternatives. The scheduling model under different design parameters, such as reactor size or inventory capacity, is implemented repeatedly, and the results are used to construct the supply curve. The supply curve, which is widely used in the field of economics, is a graphical representation of the correlation between the cost of a good or service and the quantity supplied for a given period. Typically, the price will appear on the vertical axis of the plot and quantity supplied will appear on the horizontal axis. In the sections that follow, we discuss the framework

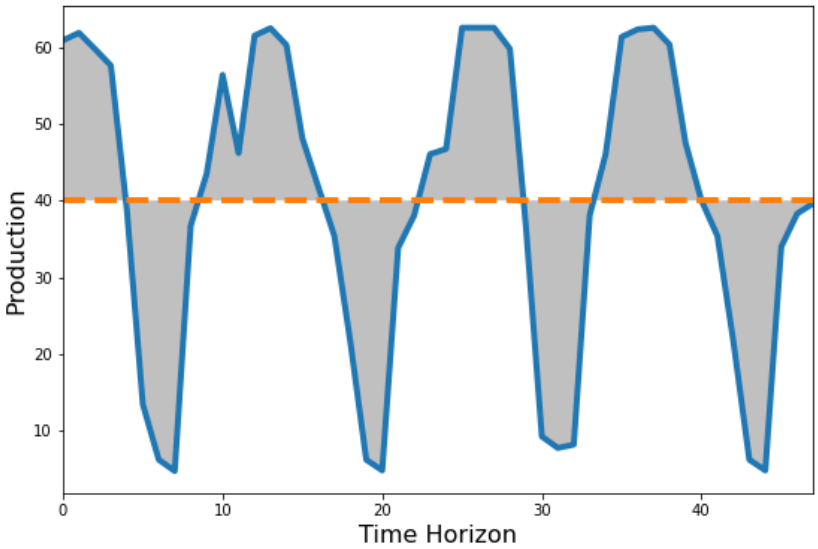

Figure 4.2. Demonstration of the *load-shifting capacity* concept, where the blue line shows the real scheduled production, and the orange dashed line shows the baseline.

implemented in this work to analyze the cost-effectiveness of a certain process design. We define a new metric, namely *load-shifting capacity*, to quantify the DR capability of a given process in terms of load shifting. The *load-shifting capacity* metric is calculated using a scheduling-based model integrated with process dynamics.

4.4 Scheduling model

The scheduling model presented herein extends the model proposed in [73]. The objective function for the operation is defined as follows:

$$J_{schedule} = \min(\Phi_1 + \Phi_2 + \Phi_3), \tag{4.2}$$

where

$$\Phi_1 = \gamma \sum^{T} (P_t \pi_t), \tag{4.3}$$

$$\Phi_2 = \sum^{T} \delta^{raw} F_t, \tag{4.4}$$

$$\Phi_3 = \sum^{T} \delta^{s} S_t. \tag{4.5}$$

The terms Φ_1, Φ_2, and Φ_3 represent the energy cost, the raw materials cost, and the inventory cost, respectively. The parameter γ is the scaling factor that links the production to the electricity consumption. The terms P_t, F_t, and S_t represent the production rate at the time t, the set-point for the production rate at the time t, and the storage capacity at the time t, respectively. π_t, δ^{raw} and δ^s represent the electricity price at the time t, the raw material cost and the inventory cost, respectively. We point out here that the energy cost in this model is assumed to be proportional to the production rate P_t, which is the same assumption implemented in Tong et al. [73, 74].

4.4.1 Production and transition

The production and transition model is provided as

$$P_t = F_t(1 - t_t^{trans}), \tag{4.6}$$

where the production rate at the time t, P_t, is set to the production rate set-point, F_t, times the production duration time, $1 - t_t^{trans}$, which implies that production over the transition time is treated as an off-spec product and is not counted towards production that satisfies the demand. The transition time is defined as:

$$t_t^{trans} = f(\mathbf{x_t}, \mathbf{\Delta x_t}). \tag{4.7}$$

and it is a function of the state variable $\mathbf{x_t}$, at the time t, and the step change $\mathbf{\Delta x_t}$. It should be noted that in [74], scheduling was considered between a discrete set of operating modes which were defined a priori. As a result, the transition time variables were treated as parameters. However, as the aim of the current scheduling formulation is to determine the optimal operating mode at any given time, a discretization strategy will not be practical as the range of possible operating modes could be considered infinite. This will result in a significant increase in the number of binary variables in the original model, thus making it intractable. In [75], however, the transition time was estimated using the log function transformation. But it is worth pointing out that a linearized feedback control scheme was implemented in that study, and therefore provided a good fit only using the log function transformation.

The production rate set-point, F_t should also satisfy the bounds and the ramping constraint given below

$$F_t \in [F_{min}, F_{max}] \tag{4.8}$$

$$F_t - F_{t-1} \leq \delta, \tag{4.9}$$

where F_{min} and F_{max} define the minimum and maximum production set-points, and δ defines the ramping limit.

4.4.2 Inventory constraint

The inventory constraint is expressed as:

$$S_t = S_{t-1} + P_t - D_t, \tag{4.10}$$

where D_t is the demand at time step t. The bounds of the inventory are given as $0 \leq S_t \leq S_{max}$. Satisfying the hourly demand is a hard constraint, and thus the inventory tank is initially charged with a certain amount of on-spec product S_0, which will be defined as $S_0 = aS_{max}$, and a and is the percentage of the inventory size to make the DR problem feasible. Also, to avoid depleting the product, the storage at the end of the time period is set equal to the initial storage (periodic terminal constraint): $S_T \geq S_0$. It is important to note that the complexity of the above problem will depend on the transition time profile [Eq. 4.7], which could be treated as a fixed parameter or as a function. As a natural extension of the formulation in [73], we remove the fixed parameter assumption and propose the use of a surrogate model for the transition time.

4.4.3 Definition of the capital cost

The capital cost is calculated as follows:

$$log_{10}C = K_1 + K_2 log_{10}(A) + K_3[log_{10}(A)]^2 \tag{4.11}$$

where C is the capital investment, A is the capacity or size parameter for the equipment, and K_1, K_2, K_3 are the cost coefficients. The equation and the values of the parameters are taken from [1].

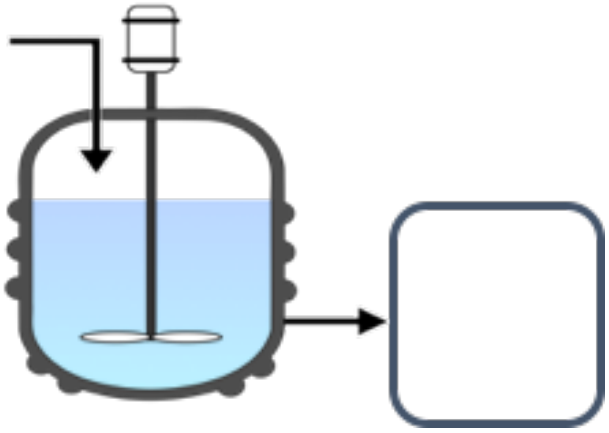

Figure 4.3. A non-isothermal CSTR connected to a storage system.

Table 4.1. Cost parameters for the equipment involved in the system from Turton et al. [1]

Equipment	K_1	K_2	K_3
CSTR	4.1052	0.3776	-0.0005
Storage	3.5565	0.3776	0.0905

4.5 Case study

We consider an illustrative case study inspired by earlier works ([74, 75]), where a non-isothermal CSTR is connected to a storage (inventory) system as shown in Figure 4.3. While the CSTR is usually not considered as an electricity-intensive process, the nonlinear dynamics of the system help to illustrate the proposed framework and analysis approach. The cost parameters of the CSTR system are taken from [1] and is given in the Table 4.1 and the cost plot is given in Figure 4.4. As shown in the figure, the non-isothermal CSTR will be more expensive than the inventory, and the rate of increase for CSTR is also faster than that of the inventory.

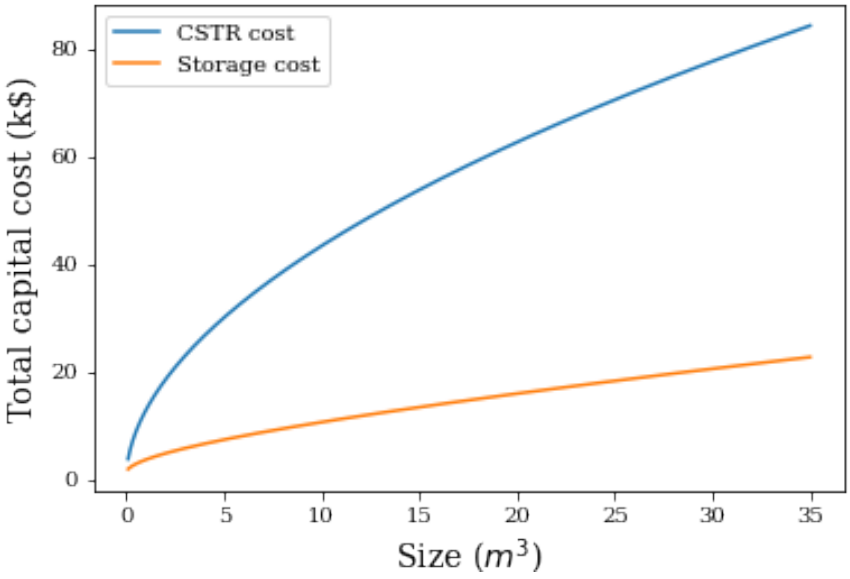

Figure 4.4. Capital cost for CSTR and storage

4.5.1 Dynamic process model

The dynamic model of the non-isothermal CSTR is derived from standard material and energy balances and expressed as:

$$V\frac{dc_R}{dt} = F(c_f - c_R(t)) - Vk_0e^{-\frac{E}{RT_R}}c_R(t), \tag{4.12}$$

$$\begin{aligned}\rho C_p V\frac{dT_R}{dt} &= F\rho C_p(T_f - T_R(t)) + \Delta HVk_0e^{-\frac{E}{RT_R}}c_R(t) \\ &\quad + UA_cF_c(T_c - T_R(t)),\end{aligned} \tag{4.13}$$

where $c_R(t)$ and $T_R(t)$ are the reactant concentration and the operating reactor temperature, respectively; V is the CSTR volume; F is the inlet flow rate; c_f is the reactant feed concentration; k_0 is the pre-exponential constant; E is the activation energy; ρ and C_p are the fluid density and heat capacity, respectively; T_f is the feed temperature; ΔH is the heat of reaction; U is the overall heat transfer coefficient; A_c is the heat transfer area; F_c and T_c are the coolant flow rate and temperature, respectively.

The model is then reformulated in the following dimensionless form:

$$\frac{dc}{dt} = \frac{1 - c(t)}{\theta} - k_0 e^{-\frac{n}{T}} c(t), \tag{4.14}$$

$$\frac{dT}{dt} = \frac{y_f - T(t)}{\theta} - k_0 e^{-\frac{n}{T}} c(t) + \alpha * u(t) * (y_c - T(t)), \tag{4.15}$$

where the below derivation are given:

$$\theta = \frac{V}{F}, \tag{4.16}$$

$$\alpha = \frac{UA_c}{\rho C_p V}, \tag{4.17}$$

$$y_f = \frac{\rho C_p T_f}{\Delta H}, \tag{4.18}$$

$$n = \frac{E\rho C_p}{R\Delta H}, \tag{4.19}$$

$$y_c = \frac{\rho C_p T_c}{\Delta H}, \tag{4.20}$$

$$c = \frac{c_R}{c_f}, \tag{4.21}$$

$$T = \frac{\rho C_p T_R}{\Delta H}. \tag{4.22}$$

Meanwhile, the dimensionless temperature, T, needs to satisfy the constraint:

$$0 \leq T(t) \leq 1, \ \forall t. \tag{4.23}$$

In this study, the cooling water flow rate $u(t)$ is used as the only manipulated variable to control the reactor temperature. The above CSTR model, together with the process parameters, are taken from [76] and shown in Table 4.2.

As mentioned earlier, the specific control scheme for the system could be designed differently. For example, in the earlier works ([73, 74]), a PID control scheme was implemented to execute the transitions between the different operating modes. For such a scheme, however, the transition dynamics are dependent on the choice of the PID tuning parameters. Given this, and the fact that the aim of the current study is to assess the DR potential for different design capacities, using a PID controller would require that the PID settings be adjusted each time the design capacity is varied to ensure that a meaningful comparison between the various design alternatives is made without the added influence

Table 4.2. Parameters in the case study

Variables	Values
k_0	300
α	1.95e-4
n	5
c_f	7.6
t_f	300
t_c	290
y_f	0.3947
y_c	0.3816

of the controller tuning. To eliminate the dependence on the controller settings, we use in this study a dynamic optimization-based control scheme that automatically accounts for the transition effects. An exploration of the influence of different control strategies on the potential of DR particibility is the subject of other research work.

The objective function for the optimal control problem is given by

$$obj = \Sigma_t[\beta(c(t) - c_s)^2 + \gamma(u(t) - u(t-1))^2], \tag{4.24}$$

where β and γ are the penalty weights, c_s is the target concentration of the desirable product. The objective function penalizes changes in the control action, as well as concentration set-point errors. The above dynamic optimization problem is solved using Pyomo [77] and using the differential-algebraic equation package [78]. The parameter β is 1e6 and γ is 1 in this case study. A sample transition profile is shown in Figure 4.5, where the transition occurs from the steady-state with $\theta = 60$ hr to the steady-state with $\theta = 30$ hr. As one should note, θ is defined as $\frac{V}{F}$.

4.5.2 Transition time space generation

To generate data points for the transition time profiles, the transition between two steady-states corresponding to different θ values, ranging from 8 to 80 hr, is simulated via dynamic optimization. The transition time value is then extracted from the resulting profile. Given that the time constant is defined as $\theta = \frac{V}{F}$, θ can be varied (for a given reactor volume

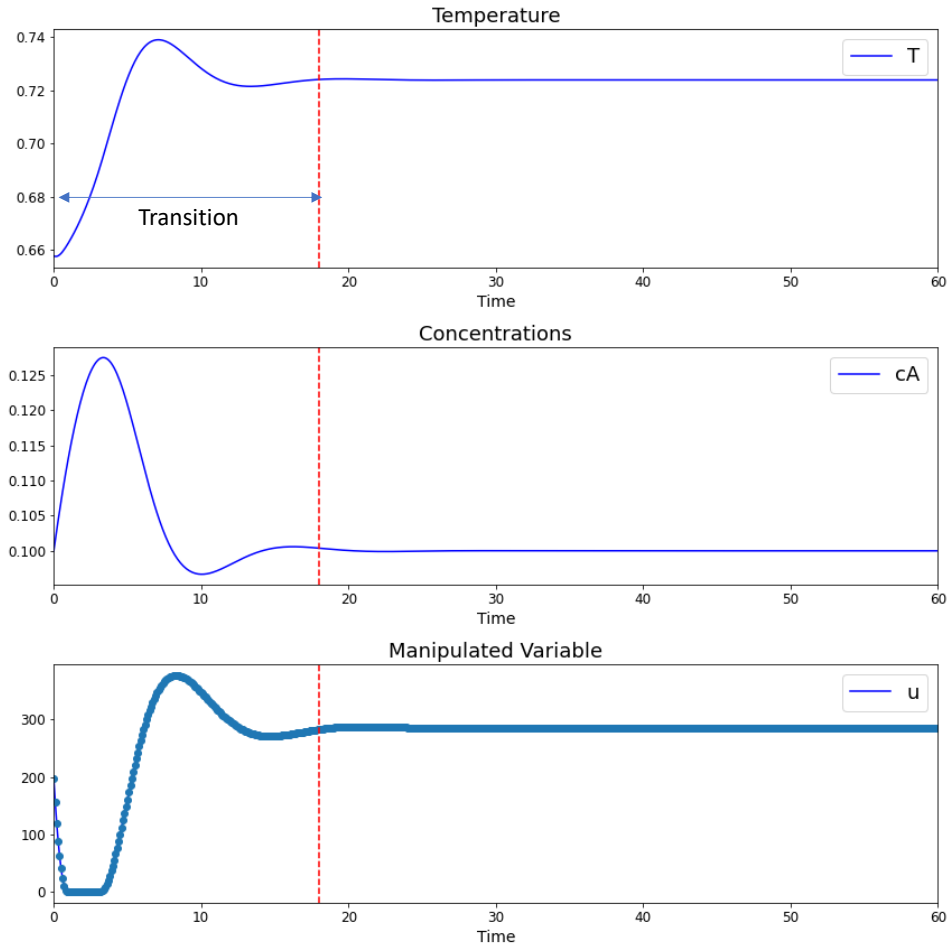

Figure 4.5. CSTR state and input transition profiles from $\theta = 60$ to $\theta = 30$ hr.

V) by varying the inlet flow rate F. For different θ values, there will be different steady-states. Therefore, we vary θ to generate different steady-states, and, thereafter, simulate the transition profiles from one steady-state to another. As shown in Eq. (4.7), the state variable would be θ_t and the step change would be $\Delta\theta_t$ correspondingly. The relation between F_t in Eq. (4.6) and θ_t would be given as $F_t = \frac{V}{\theta_t}$. Also, F_{min} and F_{max} could be replaced by: $F_{min} = \frac{V}{\theta_{max}}$ and $F_{max} = \frac{V}{\theta_{min}}$.

All the simulations then provide a transition time space to be used subsequently in the scheduling model. Figure 4.6 shows an example of the transition time space visualization for a CSTR with a volume of 400 L. To incorporate this information into the scheduling model, as the constraint in Eq. (4.7), a functional relationship needs to be constructed.

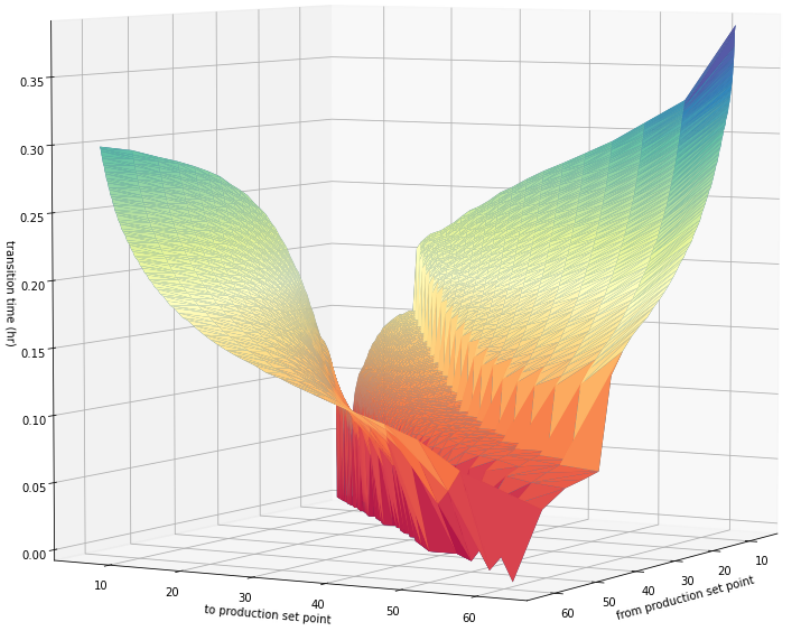

Figure 4.6. Visualization of the transition time between two steady-states (as a function of the starting and ending states) for a 400-L CSTR.

One way to construct a sample surrogate model is to utilize piecewise linear constraints. However, in general, this approach will significantly increase the size of the problem, since a significant number of binary variables is required to accurately represent the data. In this work, we formulate the transition time surface using the Big-M reformulation [79].It is worth to point out that in this work, an open-loop control of a non-linear dynamics system is implemented. This complicates the transition time space as shown in Figure 4.6. However, in a real application, a closed-loop strategy might be implemented and thus, linearization of the system is possible.

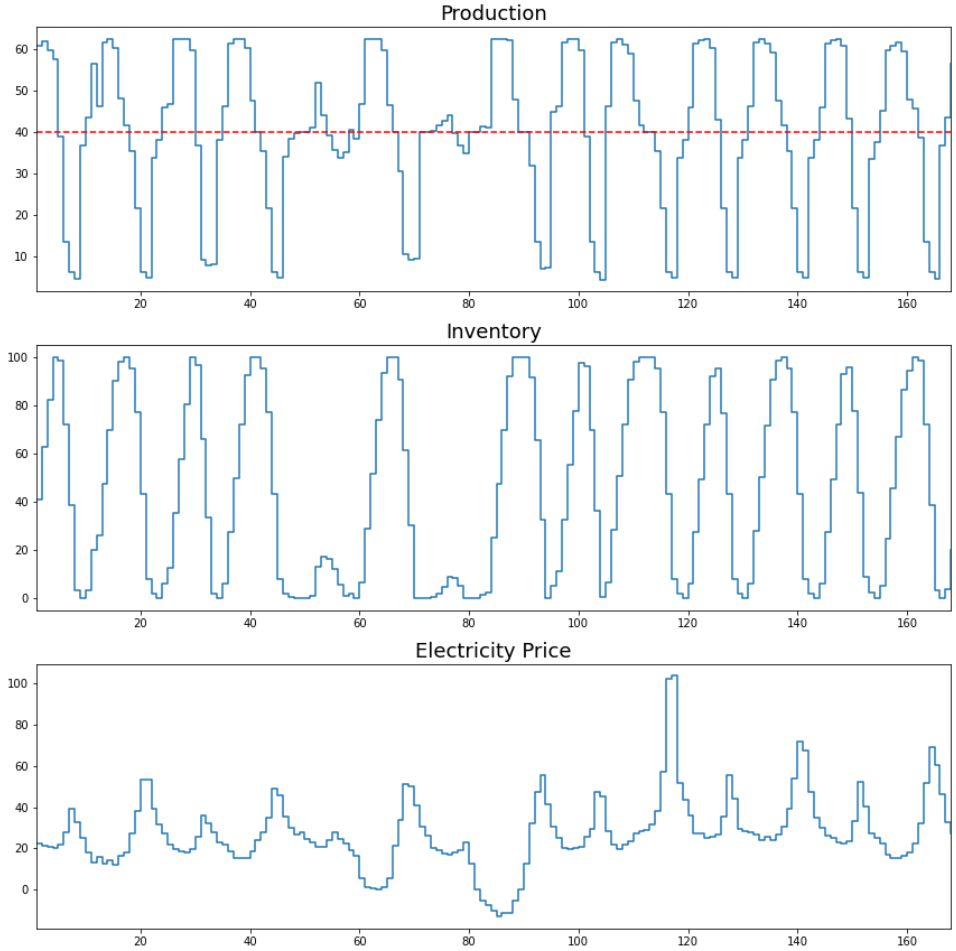

Figure 4.7. Visualization of the operating profiles for a 400-L CSTR.

4.6 Results

The scheduling problem with the Big-M transition time reformulation is solved in Pyomo [77] with the Gurobi solver [80]. In Figure 4.7, a sample scheduling result for the production (top plot) and inventory (middle plot) under a representative electricity price profile (bottom plot) is shown. The representative electricity price is taken from an aggregated node in California for the first week in 2019. The inventory and production profiles under the provided representative electricity prices are met as expected, i.e., as the price increases the production rate decreases and vice versa. To construct the supply curve for a given case, a range of parameters is used in the dynamic and scheduling models. For the design specifications, the CSTR size and the storage capacity will be considered as

the design variables. The CSTR size will range from 500 to 800 L, with an incremental increase of 50 L, while the storage size will range from 100 to 1000 L, with 50 L increments as well. Also, as described earlier, the power consumption for the process is assumed to be proportional to the production. Thus, the base power consumption in this study is proportional to the product demand.

4.6.1 Supply curves under different CSTR sizes

Figure 4.8 shows the supply curves, where the capital cost is plotted as a function of the daily shifted load, for different CSTR sizes (ranging from 500 to 800 L). The inventory cost parameter, δ^s, in this case is set to zero, while the hourly demand, D_t, is assumed to be constant and set to 50 L/hr. Therefore, for a given CSTR size, the cost in Figure 4.8 can be viewed as a function of the storage size as well.

The supply curve provides a visualization of the limitation of how much load a certain design choice could potentially shift for a given amount of capital investment. For example, for the CSTR size of 650 L, increasing the daily load-shifting capacity from 175 kWh to 350 kWh only requires a modest increase in capital investment; however, beyond 350 kWh the steep increase in the investment cost associated with the storage size suggests a limitation on the load-shifting capacity. It is intuitive to expect the range of daily load-shifting capacity to increase as the inventory size is increased. The supply curves, however, provide additional visual information regarding the limitation on the load-shifting capacity, implying that for a given CSTR design, while increasing the storage size could help increase the load-shifting capacity (and thus potentially yield profits from the DR load-shifting), there exists a limit beyond which the investment into additional storage capacity will no longer be cost-effective. As can be seen from the figure, this limit increases as the CSTR size increases, suggesting that a larger CSTR enjoys a wider range of “cost-effective" load-shifting capacities. Over this range, an increase in the load-shifting capacity requires only a modest increase in the storage investment cost.

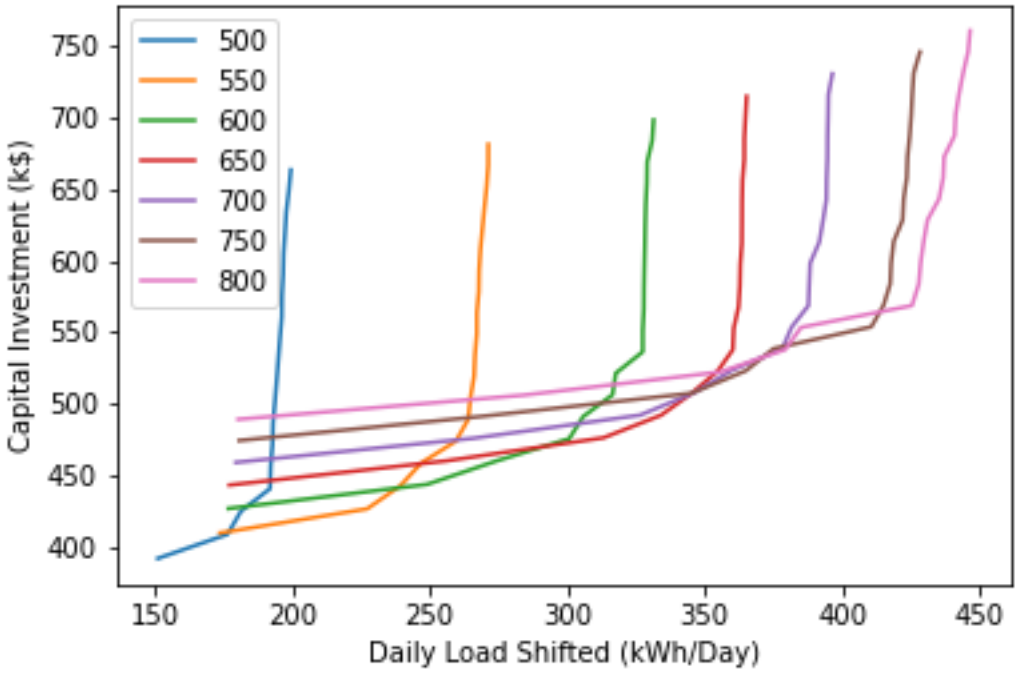

Figure 4.8. Supply curves for different CSTR sizes.

4.6.2 Supply curves under different storage sizes

Figure 4.9 depicts the supply curves for different storage sizes, with the inventory cost, δ^s, set to zero and the hourly demand, D_t, set to 50 L/hr. In this case, for a given storage size, the cost in Figure 4.9 can be viewed as a function of the CSTR size as well. It can be seen that when the storage size is small, i.e., in the range from 100 to 300 L, the increase in the CSTR investment exhibits a trend similar to that in the supply curves in Figure 4.3, where an increase in the CSTR size helps expand the range of load-shifting capacities, but only up to a limit beyond which further CSTR size increases become no longer cost-effective. However, for larger storage sizes, i.e., in the range from 400 to 1000 L, the supply curves become parallel to one another, which suggests that after the storage reaches a certain size limit, to reach the same load-shifting capacity, an increase in the storage size does not provide any benefit. This is consistent with the trend observed earlier in Figure 4.8.

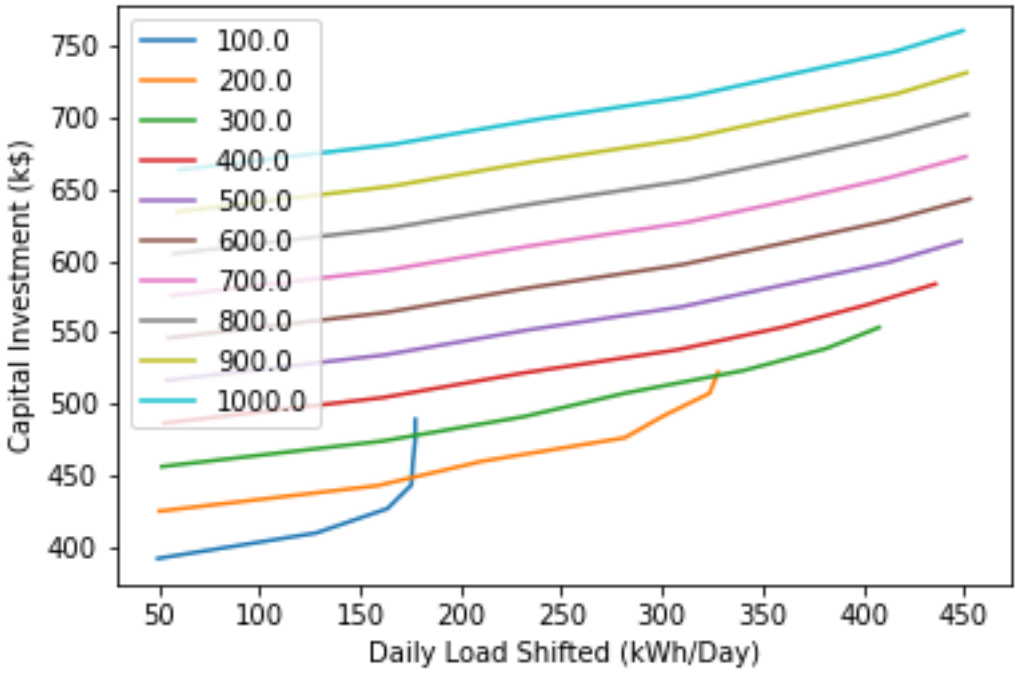

Figure 4.9. Supply curves for different storage sizes.

4.6.3 Supply curves under different inventory costs

So far in the analysis, we have assumed that no cost is associated with storing the product. To illustrate the limitations imposed by the cost of storing the product on the daily load-shifting capacity, we present in this part the supply curves for different values of the inventory cost parameter, δ_s. The supply curves for this scenario are presented in Figure 4.10. In this case, the hourly demand, D_t, is set to 50 L/hr and the CSTR size is set to 800 L. The results show that the daily load-shifting capacity is limited by the cost of storing the product. The case where $\delta^s = 0$ (i.e., no inventory cost) serves here as the base case. It can be seen that as the inventory cost increases, the supply curve shifts to the left, indicating a smaller range of cost-effective load-shifting capacities. The lower the inventory cost, the higher the capability of load shifting the system could reach. It is to be noted that when $\delta^s = 0$, the supply curve becomes almost vertical around a daily load-shifted value of 450 kWh/Day, which might also mean that the highest load-shifting

for this system will be capped at around this value.

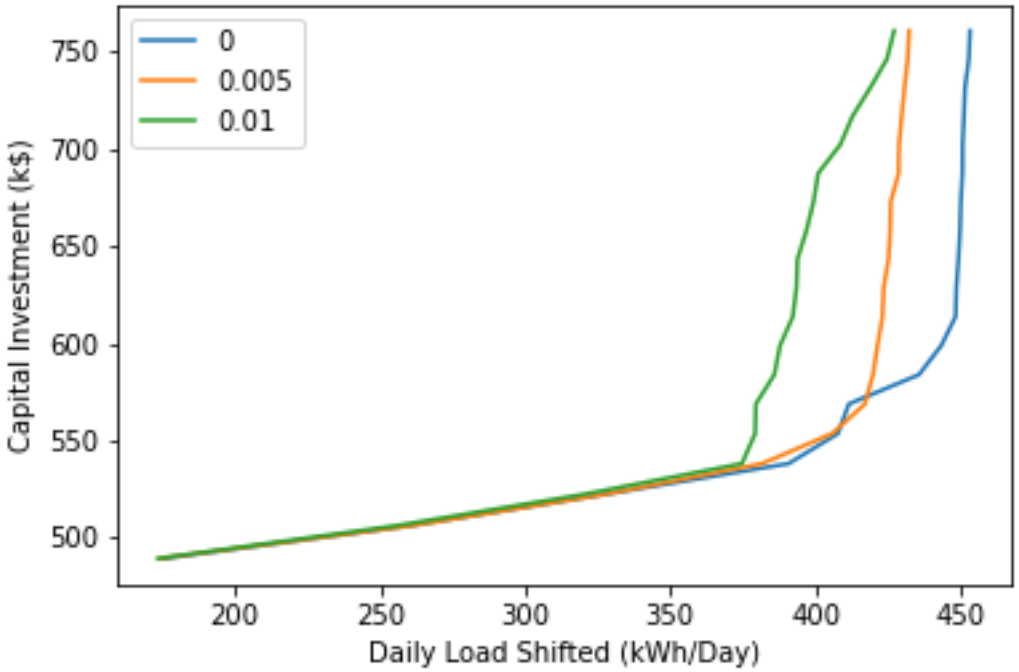

Figure 4.10. Supply curves for different inventory costs, δ^s.

4.6.4 Supply curves under different hourly demands

In Figure 4.11, the supply curves for different values of the demand, D_t, are presented. In this case, the CSTR size is set to 800 L, while the inventory cost parameter δ^s is set to zero. It can be seen that as the demand increases, the cost-effective range of load-shifting capacities increases, and so does the limiting load-shifting capacity. It is also interesting that with the increase in the demand parameter, the distance between the supply curves decreases. For example, the supply curve for $D_t = 50$ L/hr almost overlaps with the supply curve for the case with $D_t = 60$. This suggests that given a fixed CSTR size, the change in demand will no longer have an effect on the capability of load shifting.

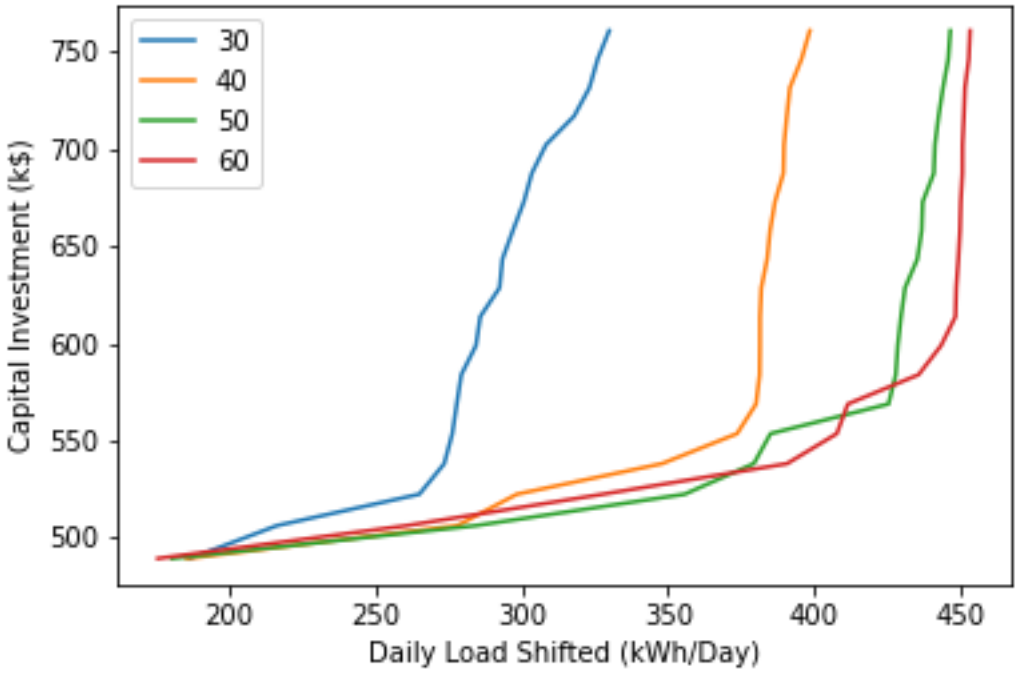

Figure 4.11. Supply curves under different hourly demand values.

4.7 Conclusions

In this chapter, we presented a sequential model-based analytical framework for assessing the potential of a process to participate in DR load-shifting services based on the cost-effectiveness of various design alternatives. The framework brings together tools from dynamic modeling, optimal control and operational scheduling, and culminates in the construction of the system supply curves which quantify the link between the capital investment of a given design and its DR load-shifting capability. For a conceptual demonstration of the approach, a non-isothermal CSTR combined with a simple inventory (storage) system was considered as a case study. Future research work will focus on applying the proposed framework to a more complex and realistic case study, as well as directly incorporating the load shifting metric into the system design.

Chapter 5

Evaluating the Benefits of Process Particibility using Levelized Cost

In Chapter 4, we developed the concept of the load-shifting capacity and the bottom-up approach to analyze the relationship between cost and load-shifting capacity, integrating design and operational objectives. In this chapter, we leverage the framework in the previous chapter to further define the concept of levelized cost of load-shifting capacity, which we could use to assess the overall cost of different design decisions when participating in the load-shifting DR services. We first briefly introduce the levelized cost of energy (LCOE), or levelized cost of electricity, followed by our adapted definition of the LCOE in terms of the levelized cost of load-shift (LCOL). Then we implement a similar bottom-up approach to calculate the load-shifting capacity and the levelized cost correspondingly. We illustrate the idea of LCOL by using a case study similar to the one in Chapter 4 with a discretized scheduling model. Two cases are explored in this study: we first investigate the difference of the load-shifting capacity between the participation in a day-ahead market and in a five-minute market; then we look into the effect of replacing the single reactor with smaller size reactors and compare the load-shifting capacity and levelized cost of this design decision.

5.1 Motivation

5.1.1 Levelized cost of energy

LCOE is a measure of the average net present cost of electricity generation for a generating plant over its lifetime. It is used for investment planning and to compare different methods of electricity generation on a consistent basis, and is calculated as the ratio between all the discounted costs over the lifetime of an electricity generating plant divided by a discounted sum of the actual energy amounts delivered. By definition, LCOE is generally applied to the electricity generation unit, such as different renewable generation resources. Compared to the normal cost metric, it has several characteristic features:

$$LCOE = \frac{\sum_{t=1}^{n} \frac{I_t + M_t + F_t}{(1+r)^t}}{\sum_{t=1}^{n} \frac{E_t}{(1+r)^t}}, \tag{5.1}$$

where n is the total life of the system, r is the discount rate, E_t is the electricity generated in year t, I_t, M_t and F_t stand for investment expenditure, operation and maintenance and fuel expenditures in year t, respectively.

While LCOE has been widely used in the energy system design, applying it to the chemical process design is, to the best of the authors' knowledge, not reported before. LCOE, by definition, will need one to provide the anticipated energy generation for a period of time although the majority of the chemical process, particularly the energy intensive processes such as chlor-alkali and air separation are actually energy consuming. Therefore, the term E^t in Eq. 5.1 cannot be given. However, if we utilize the load-shift capacity defined in Chapter 4, we then can use the LCOE as a metric to quantify the design of a chemical process and using such a metric to compare different process designs in terms of their DR particibility, or more specifically, load-shift capacity. In this sense, we can define the below metric levelized cost of load-shift (LCOL) as follows:

$$LCOL = \frac{I + \sum_{t=1}^{n} \frac{OM_t - Pro_t}{(1+r)^t}}{\sum_{t=1}^{n} \frac{E_t^{shift}}{(1+r)^t}}, \tag{5.2}$$

where I is the investment capital, OM_t is the total operation cost, Pro_t is the profit by selling the product and E_t^{shift} is the load-shift capacity defined in Chapter 4. The equation

incorporates all elements required to determine the full lifetime cost of a chemical process: investment, operation and maintenance (OM) as well as the profit of the process divided by electricity load shifted during the investment period. It assumes all investment costs are incurred in the first year and sums ongoing costs in each year (n) up to the system lifetime (N). By utilizing this metric, we can better compare the design and operation of different processes while having a better understanding of how much DR potential could a chemical process provide to the grid as a "grid-level" battery. The explanation to the LCOE could be how much it costs for the generation system to provide 1 MWh electricity to the system. Thus, if electricity price is higher than that value, it is profitable. As for the LCOL, a similar explanation could be used that how much it costs for the chemical process to provide 1 MWh load-shift capacity to the grid system, while currently the grid does not directly provide payment for such service, one could still compare this metric to the battery cost. As for the battery, the levelized cost usually suggest how much it costs to store 1 MWh electricity. Thus, the chemical process can then be compared with the true battery in terms of the load shifting.

5.2 Problem statement

We assume the capacity of a plant will be determined by two factors, the capacity of the process, such as reactor volume and distillation column size for the process and the inventory (storage) capacity. Apparently, the capacity of the process will still be the dominant factor, but the inventory can still have a big impact on the choice of the operational level. As shown in Figure 4.1, assuming the process will participate in the wholesale electricity market, with a required hourly demand D_t, one would like to determine the capacity of the process $\bar{V}$ and inventory size $\bar{S}$. A similar bottom-up framework adopted in Chapter 4 will be followed: different process capacity and inventory sizes will be evaluated and corresponding LCOL will be calculated and compared.

To assess the LCOL under different market conditions, we first define two different time sets, $t \in T$ and $st \in ST$. $T := \{1, 2, ..., N\}$ denotes the day-ahead market layer, where the Δt is 1 hour and $ST := \{1, 2, ..., N^{ST}\}$ specifies the 5-min market layer, where

Δst is an interval of 5 min. Thus, the overall time set T^* can be defined as $T^* := T \times ST$ $= \{(1,1),(2,1),...,(N^{ST},N)\}$.

5.3 Model formulation

A model similar to the one presented in Chapter 4 will be implemented, but a MILP version will be developed to model different market structures. Thus, we define the production mode $m \in M$ and equipment $e \in E$.

5.3.1 Scheduling model

Different from the continuous model in Chapter 4, the operating mode $m \in M$ is predefined in the discrete model, thus, once the dynamic model is solved, the transient profile of the system, including the transition time will be defined among different operating modes. Such an approach that utilizes the offline fixed transition times is common for capturing process dynamics in the scheduling of the process [81, 82]. The discrete model is extended based on [74]. Tong et al. [74] claim that the resulting model is a MINLP problem; yet, with simple convexification of the bilinear term, the problem could be then converted into a mixed-integer linear programming (MILP) problem.

5.3.1.1 Transition and mode constraints

We define $e \in E$ as different equipment sizes, $t \in T$ as the discrete time. Then, we have

$$\sum_{m \in M} y_m^{e,t} = 1, m \in M, \tag{5.3}$$

where, $y_m^{e,t}$ denotes the binary variable of whether reactor e is operating with the mode m at the time t. This constraint specifies that, at the time t, only 1 mode could be selected. Additionally, we have

$$\sum_{m_1 \in M} z_{m_1,m_2}^{e,t} = y_{m_2}^{e,t}, m_1 \in M, e \in E, t \in T, \tag{5.4}$$

$$\sum_{m_2 \in M} z_{m_1,m_2}^{e,t} = y_{m_1}^{e,0}, m_1 \in M, e \in E, t = T, \tag{5.5}$$

$$\sum_{m_2 \in M} z_{m_1,m_2}^{e,t} = y_{m_1}^{e,t-1}, m_1 \in M, e \in E, t > 0, \tag{5.6}$$

where $z^{e,t}_{m_1,m_2}$ denotes the binary variable that whether there is a transition occurring from operating mode m_1 to m_2. Equations 5.4 to 5.6 are a group of transition constraints that specify the whether there is a transition occurring between mode 1 and mode 2 for equipment e at the time t. $z^{e,t}_{m_1,m_2} = 1$ is true if and only if a transition from mode m_1 to mode m_2 occurs from time step $t-1$ to t.

5.3.1.2 Production constraint

The production rate for the plant at the time t is given as follows:

$$Q^t = \sum_{e\in E}\sum_{m_1\in M}(y^{e,t}\frac{V^e}{\theta^e_{m_1}})\left[1 - \sum_{m_2,m_1\in M}(z^{e,t}_{m_2,m_1}\cdot tt^e_{m_2,m_1})\right], \tag{5.7}$$

where Q^t is the total production rate at the time t and $y^{e,t}\frac{V^e}{\theta^e_{m_1}}$ defines the production rate of equipment e at mode m_1. The terms in the bracket define the total production time which will be 1 minus the transition time $tt^e_{m_2,m_1}$ times the transition binary variable $z^{e,t}_{m_2,m_1}$, with units of hour. It is noted that, when expanding the equation, one may have a bilinear term that involves two binary variables, $y^{e,t}$ and $z^{e,t}_{m_2,m_1}$. Thus, we perform convexification as:

$$yz^{e,t}_{m_1,m_2} \leq y_{m_2}, m_1, m_2 \in M, e \in E, t \in T, \tag{5.8}$$

$$yz^{e,t}_{m_1,m_2} \leq z^{e,t}_{m_1,m_2}, m_1, m_2 \in M, e \in E, t \in T, \tag{5.9}$$

$$yz^{e,t}_{m_1,m_2} \geq y^{e,t}_{m_2} + z^{e,t}_{m_1,m_2} - 1, m_1, m_2 \in M, e \in E, t \in T, \tag{5.10}$$

where $yz^{e,t}_{m_1,m_2}$ is the convexified term that will replace the $y^{e,t}\cdot z^{e,t}_{m_2,m_1}$. Then we define

$$F^{e,t} = \sum_{m\in M}\frac{y^{e,t}_m \cdot V^e}{\theta^e_m}. \tag{5.11}$$

With the above definition and convexification, Eq. 5.7 can be replaced by the following convex linear constraint:

$$Q^t = \sum_{e\in E}[F^{e,t} - \sum_{m_2\in M}(\sum_{m_1\in M} yz^{e,t}_{m_1,m_2}\cdot tt^e_{m_1,m_2}\cdot\frac{V^e}{\theta^e_{m_2}})]. \tag{5.12}$$

5.3.1.3 Inventory constraint

The inventory constraint includes the storage S^t, production Q^t and the hourly demand D^t and is defined as

$$S^t = S^{t-1} + Q^t - D^t, t > 0, \tag{5.13}$$

The storage will be limited by the design size:

$$S^t \leq S^{max}. \tag{5.14}$$

5.3.1.4 Objective function

The objective function of the scheduling problem is similar to the one in Chapter 4, however, the power function will be adapted to satisfy the new assumption as well as the time interval difference.

$$J_{schedule} = \min(\Phi_1 + \Phi_2 + \Phi_3), \tag{5.15}$$

where

$$\Phi_1 = \sum_{e \in E} \sum_{t \in T} \sum_{st \in ST} \cdot \pi_{st}^t \cdot P_{st}^{e,t}, \tag{5.16}$$

$$\Phi_2 = \sum^{T} \delta^{raw} F_t, \tag{5.17}$$

$$\Phi_3 = \sum^{T} \delta^{s} S_t. \tag{5.18}$$

$P_{st}^{e,t}$ is the power consumption for equipment e at time interval (t, st), as this variable should be related to the detailed process, it will be given in Eq. 5.24 below. Also, π_{st}^t is the electricity price for the interval (t, st). For the DAM case, the price should be the same within the interval $t \in T$; thus, we could have $\pi_{st}^{t^*} = \pi^{t^*}$, where $st \in ST$. However, this is not true for the FMM case.

5.4 Case study

5.4.1 Dynamic model & power consumption

In Chapter 4, one key assumption in the power consumption is that the power is proportional to the production rate. However, this assumption, while has been used in literature [73, 74] is no longer valid when considering different markets. Assuming that the power

consumption is proportional to the production rate suggests that either in a DAM or an FMM, as long as the production mode is set at the beginning of the time step, the power consumption will be fixed for the time step. Apparently, under this assumption, when there is a mode switch, overshooting in the cost will not be captured by the DAM. Thus, we modified the assumption, similar to the work in Beal et al. [75] that the cooling power is used instead of the power consumption.

Next we provide the derivation of the power expression used in this chapter. We have a cooling flow temperature dynamics as follows for the case study:

$$\frac{dT_c}{dt} = \frac{F_c}{V_j}(T_{c,in} - T_c) + \frac{UA_c}{\rho_c V_j C_{p,c}}(T - T_c), \tag{5.19}$$

where, T_c is still the cooling temperature, F_c is the cooling flow rate, V_j is the jacket volume, $T_{c,in}$ is the cooling inlet temperature, ρ_c and $C_{p,c}$ are cooling flow density and heat capacity, respectively. Now, given the system's power consumption is indeed the cooling power:

$$\Delta H_{cooling} = \rho_c C_{p,c} F_c (T_c - T_{c,in}). \tag{5.20}$$

According to the dynamic model, there are few important implicit assumptions. First, T_c is a parameter and therefore does not change. Thus, we could then assume $\frac{dT_c}{dt}$ is 0 at a given steady-state. This might suggest the $T_{c,in}$ is changing. Therefore,

$$\frac{F_c}{V_j}(T_c - T_{c,in}) = \frac{UA_c}{\rho_c V_j C_{p,c}}(T - T_c). \tag{5.21}$$

Combining Eqs. (5.20) and (5.21), we can see:

$$\Delta H_{cooling} = UA_c(T - T_c). \tag{5.22}$$

Therefore, Eq. 5.22 could be rewritten as

$$\Delta H_{cooling} = \alpha \Delta H V u(T - y_c). \tag{5.23}$$

Apparently, as α and ΔH are parameters, the cooling load will scale with the CSTR volume.

Based on the assumption, we can then derive the power consumption as

$$P_{st}^{e,t} = \gamma(V) \sum_{m_2 \in M} \sum_{m_1 \in M} y z_{m_1,m_2}^{e,t} \cdot u_{m_1,m_2,st}^{e} \cdot (T_{m_1,m_2,st}^{e} - T^*), \tag{5.24}$$

where $P_{st}^{e,t}$ is the power consumption at interval st, $yz_{m_1,m_2}^{e,t}$ is the relaxed binary variable and $u_{m_1,m_2,st}^{e}$ specifies the power related variable. $\gamma(V)$ is the scaling factor where $\gamma(V) = \alpha\Delta HV$.

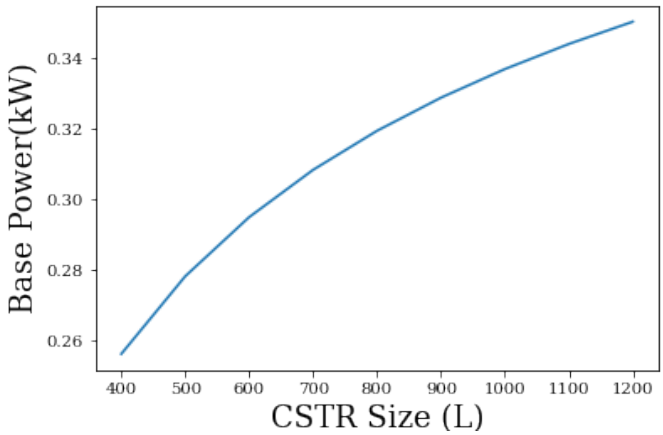

Figure 5.1. Base power consumption for different sizes of the CSTR for production demand at 50 L/h

Then, to calculate the base power of the process, we first specify the base θ under a specific product demand for the CSTR size V. For example, for the CSTR size $500L$, to satisfy the hourly demand of $50L/hr$, θ is $10hr$. This θ will then be used to calculate the power values, which will be used as the base power for a CSTR size of $500L$. Based on the methodology, a sample base power consumption for different sizes of the CSTR for production demand at $50L/h$ is shown in Figure 5.1, where the base power consumption increases with the increase in the reactor size.

5.4.2 Transition profiles

The feasible operating modes for the CSTR process are specified in Table 5.1. Similar to the case study in Chapter 4, the minimum of the parameter θ is 8 and its maximum is 80. The transition times, tt, from different operating modes, are given in Table 5.2. The selection of the modes can be arbitrary. As the scheduling model is an MILP model depending on the number of operating modes, the increase in the number of modes will increase the complexity of the model. Also, since we want to use the same transition profile for all the CSTR sizes, we choose to fix the range of the θ values. With different

sizes of the CSTR, since θ values are fixed for different modes, the operating flow rate or the production rate F^t will be different. However, the θ will define the transition profiles and thus, we have different feasible operating ranges under different designs. One could also consider varying the operating flow rate from F to F instead of from θ to θ, and in such a scenario, the dynamic profiles will be different as the volume V changes and θ is varied for different designs, increasing the number of dynamic optimization results. In this study, we assume the fixed θ for all different CSTR sizes. The selection of the θ values for different modes are based on a reactor size of $400L$, then from flow rate $\frac{400}{80}$ to $\frac{400}{8}$, flow rates are equally sampled and then converted back to the θ values. Therefore, varying θ can definitely be realized under this framework. Similar to Chapter 4, the dynamic profiles are generated through Pyomo [77] and the differential-algebraic equation package ([78]).

Table 5.1. Feasible operating modes for the CSTR

mode	0	1	2	3	4	5	6	7	8	9
θ	8.	8.889	10.	11.4286	13.3333	16.	20.	26.6667	40.	80.

Table 5.2. Transition times for the open-loop CSTR from θ_{m_1} to θ_{m_2}

θ mode	0	1	2	3	4	5	6	7	8	9
0	0.0000	0.0000	0.0383	0.0550	0.0700	0.0833	0.1000	0.1217	0.1600	0.3383
1	0.0000	0.0000	0.0000	0.0400	0.0583	0.0750	0.0933	0.1167	0.1550	0.3300
2	0.0150	0.0000	0.0000	0.0000	0.0433	0.0633	0.0833	0.1083	0.1483	0.2450
3	0.0267	0.0183	0.0000	0.0000	0.0000	0.0467	0.0717	0.0983	0.1383	0.2367
4	0.0383	0.0317	0.0217	0.0000	0.0000	0.0000	0.0533	0.0833	0.1267	0.2250
5	0.0500	0.0450	0.0383	0.0283	0.0000	0.0000	0.0000	0.0617	0.1083	0.2067
6	0.0633	0.0600	0.0550	0.0483	0.0367	0.0000	0.0000	0.0250	0.0817	0.1800
7	0.1117	0.1050	0.0750	0.0700	0.0633	0.0517	0.0267	0.0000	0.0383	0.1383
8	0.1533	0.1483	0.1400	0.1317	0.0967	0.0900	0.0783	0.0517	0.0000	0.0700
9	0.2433	0.2383	0.2283	0.2200	0.2100	0.1967	0.1817	0.1433	0.1183	0.0000

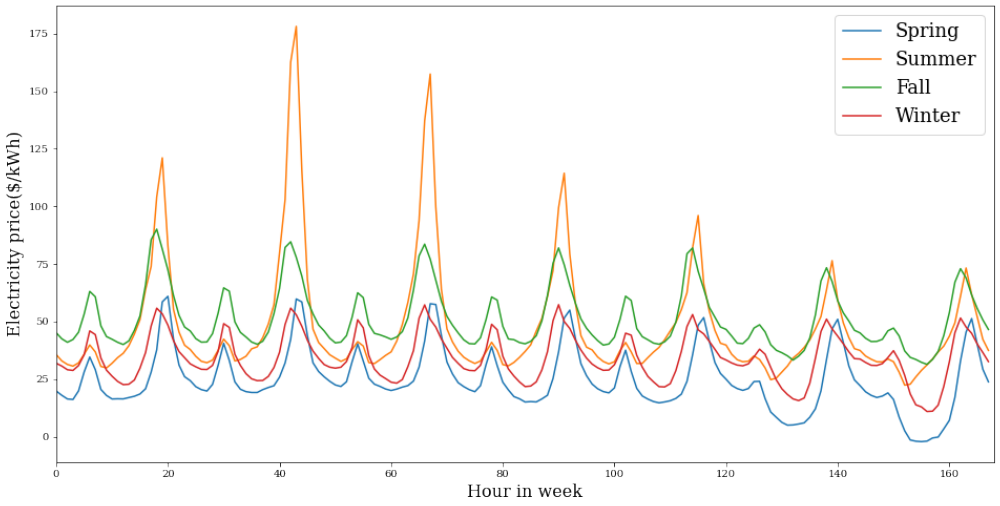

Figure 5.2. DAM electricity price at a CAISO Node in 2018

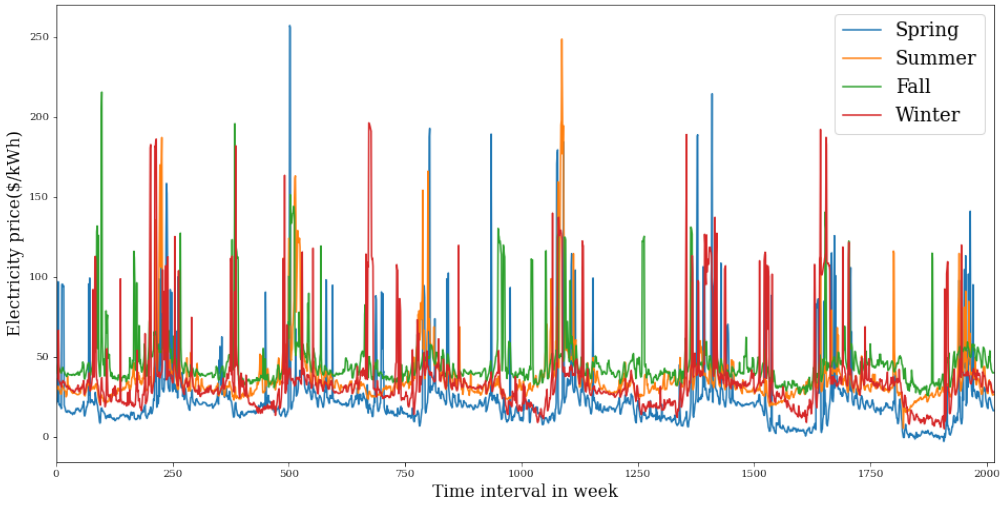

Figure 5.3. RTM electricity price at a CAISO Node in 2018

5.4.3 Seasonal representation

The LCOL calculation intrinsically considers a long-term design and operation up to years, yet the electricity prices are at the level of 1 hour and 5-min intervals. To adapt to

this multi-scale problem, we instead leverage a seasonality of the electricity price [83, 84]. Electricity prices for both DAM and FMM are separated into four different seasons, and then averaged over the period of that season. Sample seasonal electricity price profiles for both DAM and FMM in 2018 of a node in the CAISO market are shown in Figures 5.2 and 5.3. As one might notice in the DAM, the summer season has high average prices while the spring usually has lower prices, and even negative prices. While in the FMM, it is more difficult to tell whether the patterns are different from season to season. The scheduling and operation problem will then be solved for each market under each season, and the operating cost and the shifted load will then be calculated correspondingly.

5.5 Results and discussion

The scheduling model is solved using the Gurobi solver [80]. We explored two cases using the above-mentioned model:

- Single CSTR under different markets
- Two CSTRs with different sizes under different markets

We also have two assumptions:

- We assume an extreme case where the material cost and the inventory cost are 0.
- We assume a period of 2 years in calculating the LCOL and a discount rate of 5%.

Indeed, while the assumption with 0 material and inventory cost could be extreme, under such a scenario, a process could be treated exactly like a battery with only the electricity involved in the LCOL calculation. We also ignore the profit of selling the potential product here, so LCOL will only involve the electricity consumption cost as well as the load-shifting capacity.

5.5.1 Optimization results for a single CSTR

To verify the optimization result, the results for the CSTR size of $500L$ and storage size of $250L$ and the CSTR size of $700L$ and storage size of $250L$ under FMM are shown in Figures 5.4 and 5.5, respectively. In both figures, the upper row shows the production

levels in different seasons, while the lower rows show the power consumption. The red dotted lines specify the base power consumption for the corresponding CSTR size. As one can see, for the $700L$ CSTR, the load-shifting activity is indeed more frequent than that of the $500L$ CSTR. The loads shifted are also shown in Table 5.3. Also, for both cases, it is worth pointing out that the power consumption tends to fluctuate between the system minimum and maximum, as one might expect, the load-shift capacity, by definition will be maximized.

Table 5.3. Weekly power shifted for CSTR = 500 L and 700 L under different seasons

Weekly power shifted (MW)	CSTR = $500L$	CSTR = $700L$
Spring	79.5974	166.1959
Summer	80.3108	172.0224
Fall	78.0487	175.3420
Winter	79.1334	175.3995

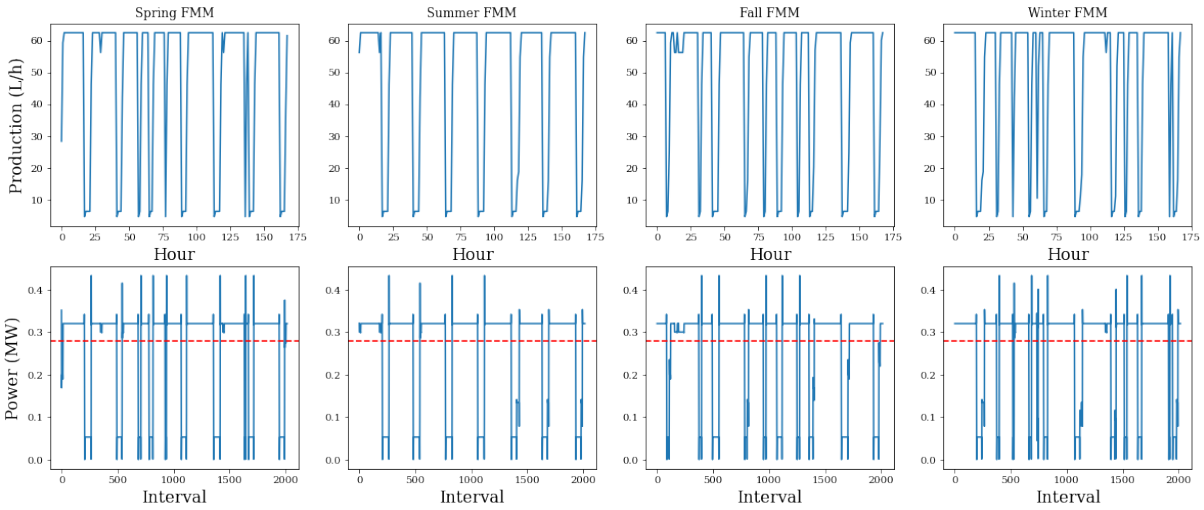

Figure 5.4. Production level and power consumption for CSTR size $500L$ and storage size $250L$

5.5.2 Comparing DAM and FMM for a single CSTR

One of the key observations when comparing the LCOL of the same design under DAM and RTM is provided in Figure 5.6, where the LCOLs are plotted against the discounted

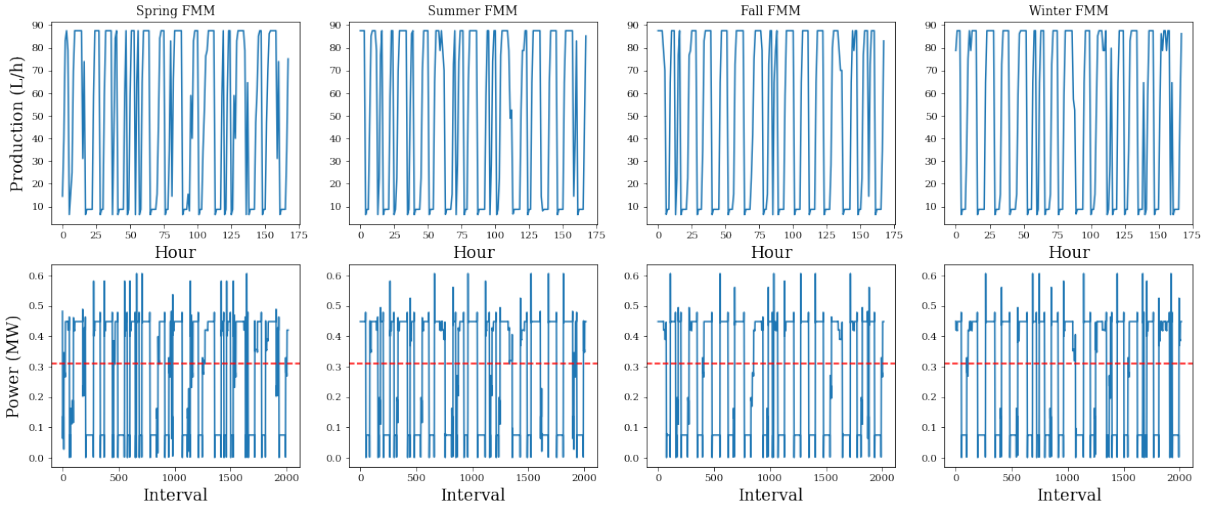

Figure 5.5. Production level and power consumption for CSTR size at 500 L and storage size at 250 L

shifted energy over the year. The dotted lines specify the FMM, while the normal lines specify the DAM. As can be seen, the dotted lines are below the normal lines, suggesting that the LCOL when scheduling under the FMM are lower than that of the DAM. Using the FMM for scheduling can lower the LCOL. Meanwhile, one notes that the LCOL, with the increasing of the shift power, will first decrease and then increase. This increase is also extremely steep. This has two implications: firstly, there exists a limitation for a CSTR capacity in both markets, even with the different storage sizes. The limitation of the load-shift capacity is determined by the reactor capacity. Secondly, one could lower the LCOL while maximizing the load-shift capacity per year as well. Besides, when the CSTR size is increased from 500 to 600 L, we notice a significant drop in the LCOL cost as well as a right shift in the shift power in the plot. This trend, however, starts to fade away with increasing CSTR sizes.

5.6 Optimization results for multiple CSTRs

Instead of using one single CSTR, in this case study, we assume one can split the single CSTR into two smaller CSTRs. In general, this will increase the capital cost; however, different sizes might potentially increase the operating flexibility. In this case, we set the base case to be the single CSTR with the size of 1000 L, with an hourly demand for

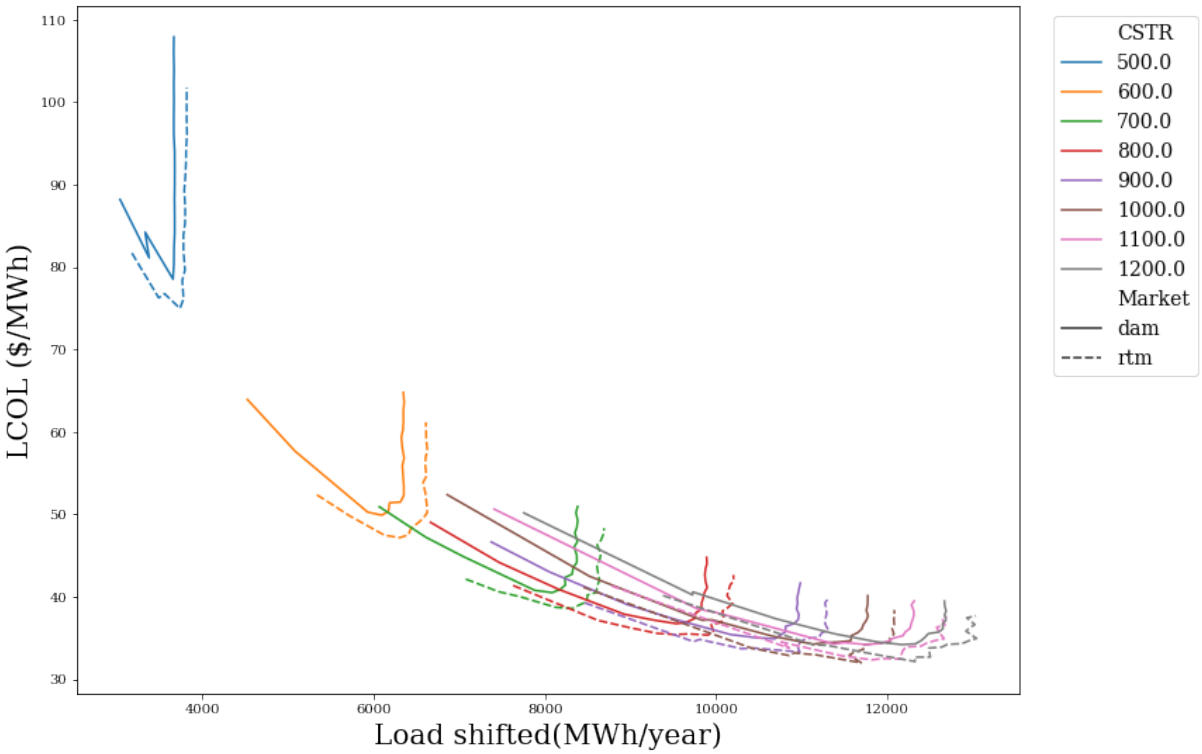

Figure 5.6. LCOL for different sizes of CSTR under different markets

$100L/h$. The scheduling optimization results are shown in Figures 5.7, 5.8, 5.9 and 5.10, corresponding to spring, summer, fall and winter seasons. A sample daily operation for different seasons are shown in these figures. The first row of the figures specifies the CSTR operation level; the second row denotes the inventory for different setups and the last row indicates the power consumption with the dotted line as the base power consumption. It is interesting to see that whatever setup is used, the large CSTR (red line) is always kept at very high operation levels.

Average weekly load-shift capacity and the LCOL cost for different CSTR sizes, set up with 100, 300 and 500 L storage capacities under the FMM are shown in Table 5.4. One might notice the single CSTR setup across all the designs have the lowest LCOL, and also the LCOL is much smaller compared to other dual setup. This suggests in this case study, that the CSTR capital cost might be dominant and thus one will not see any potential benefits from operating multiple equipment. For the dual CSTR setup, when the storage size is small, the equal size setup (500, 500) has the lowest LCOL, with a

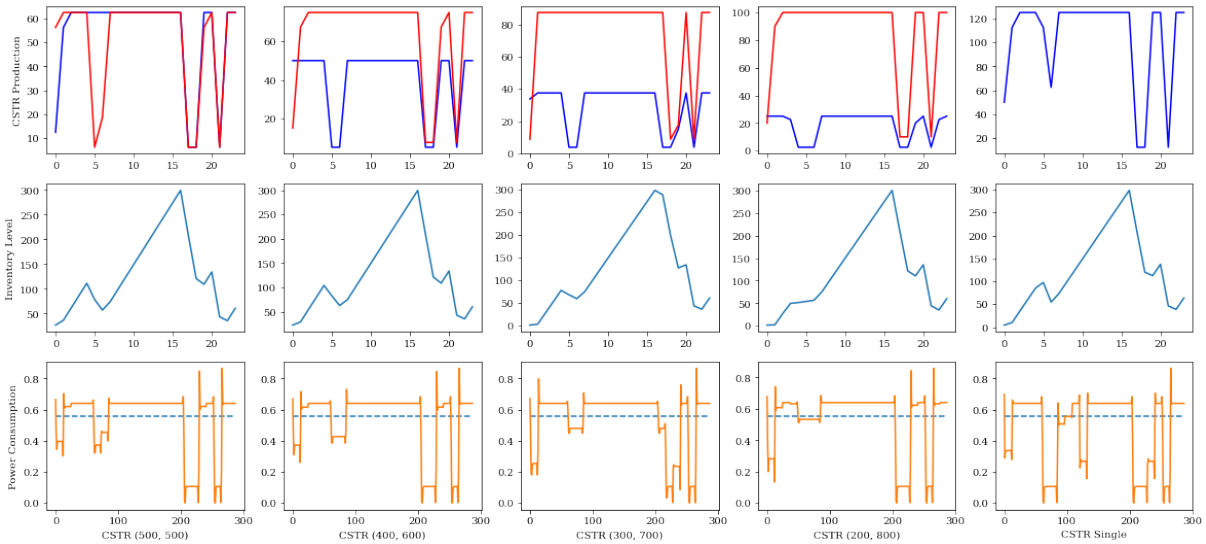

Figure 5.7. Sample daily CSTRs operation under FMM, inventory and power consumption in spring for different CSTR setup with storage of 300 L

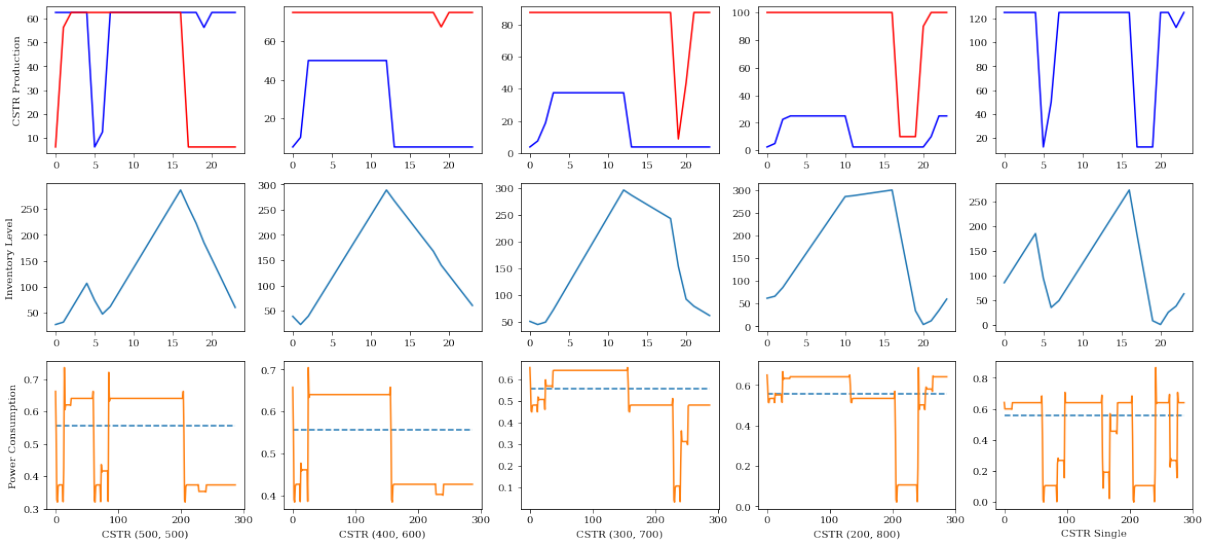

Figure 5.8. Sample daily CSTRs operation under FMM, inventory and power consumption in summer for different CSTR setup with storage of 300 L

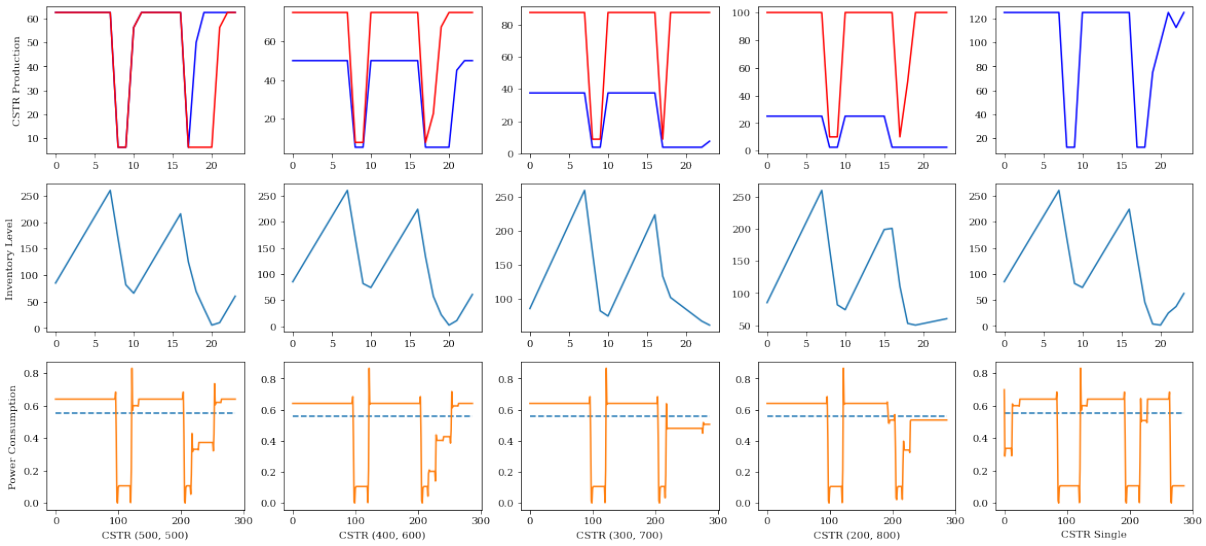

Figure 5.9. Sample daily CSTRs operation under FMM, inventory and power consumption in fall for different CSTR setup with storage of 300 L

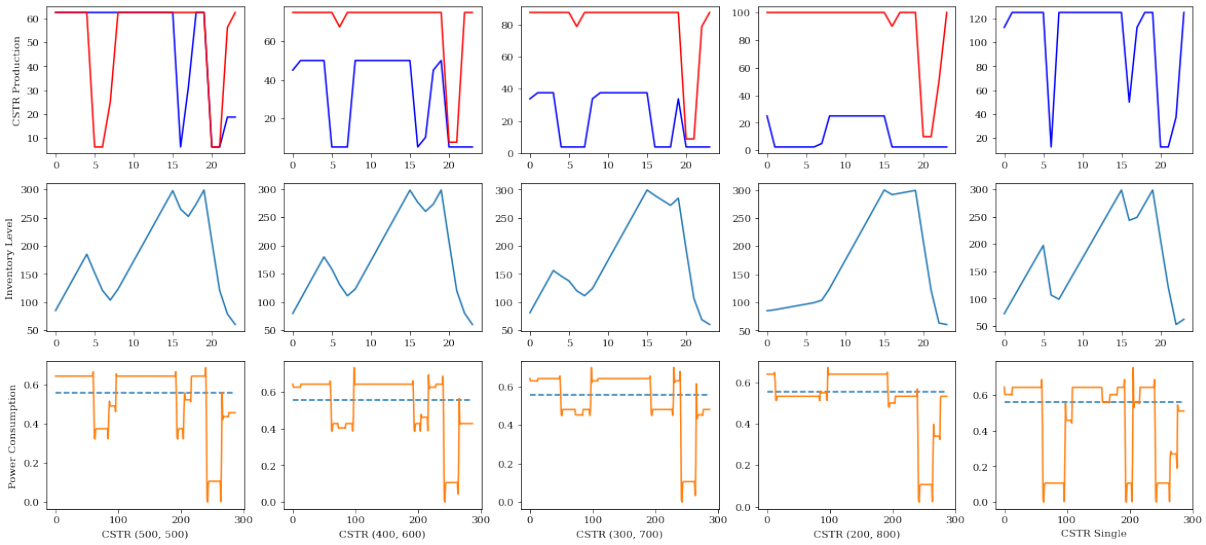

Figure 5.10. Sample daily CSTRs operation under FMM, inventory and power consumption in winter for different CSTR setup with storage of 300 L

value of \$97.8707/MWh at the storage size of $100L$.

Table 5.4. Different sizes CSTR setup with 100, 300, 500 L storage under FMM

CSTR setup (L)	Storage size (L)	Average Weekly load-shift (MWh)	LCOL (\$/MWh)
Single CSTR	100	305.1605	30.7808
Dual(500, 500)	100	108.5747	97.8707
Dual(400, 600)	100	104.4295	101.2443
Dual(300, 700)	100	88.0899	118.5822
Dual(200, 800)	100	67.9027	150.5959
Single CSTR	300	332.6213	29.2561
Dual(500, 500)	300	138.7289	80.0287
Dual(400, 600)	300	137.6324	80.3697
Dual(300, 700)	300	133.0519	82.2696
Dual(200, 800)	300	126.5644	84.7929
Single CSTR	500	344.3666	29.7029
Dual(500, 500)	500	153.2955	76.1950
Dual(400, 600)	500	152.0802	76.5572
Dual(300, 700)	500	150.9928	76.3449
Dual(200, 800)	500	151.2491	74.8051

Apparently, in this case study, a single CSTR setup favors the lower LCOL cost and, in general, a higher load-shift capacity. This could be due to a few factors. First, the capital cost of the single CSTR is much cheaper than the dual setup and this could contribute significantly to the LCOL calculation. Meanwhile, the case study use a fixed θ mode and thus the transition profiles are also fixed. Whether small equipment can have faster dynamics and therefore make up the capital lost also could be better investigated with selecting a proper control scheme.

5.7 Conclusions

In this work, an optimization-based analytical framework is proposed to assess the potential of a chemical process to participate in load shifting. While the approach is a

bottom-up sequential approach, it is successfully implemented to evaluate the levelized cost of load-shift capacity, namely LCOL. Utilizing the metric, a chemical process could be viewed as a grid battery and compared with the energy generation unit or the battery to see how valuable the load-shifting process can provide. The designs under two different cases: (i) comparing different markets while the LCOL is showing the benefits of participating in the FMM in the scheduling and (ii) comparing different size CSTRs in terms of particibility. The case study in this work favors using a single CSTR for the DR-participation. One potential direction would be to utilize the LCOL metric to compare the true battery connected system to the chemical process system. Indeed, one implication from the LCOL could be expressed as the chemical process, and how much it costs for the process to provide 1 MWh energy shift services. Such metrics could also be helpful for the grid operator to design better electricity market products to incentivize customer participation. A key feature of the proposed assessment approach is that it provides the flexibility to address other different factors, such as same equipment but different control paradigms in closed-loop manner. Also, besides the participation in the wholesale market, other incentive-based DR services could also be compared. Meanwhile, process design problem could also be targeted using the LCOL as the objective function to favor a process design that could provide better load-shift capacity with a lower cost to the grid.

Chapter 6

Conclusions and Recommendations for Future Work

In this chapter, the conclusions and limitations of this dissertation are addressed. Potential future research directions are also discussed.

6.1 Conclusions and Limitations

The primary focus of the dissertation has been divided into two parts. The first part focused on the development of the optimization framework for the flexible design that allows for process network reconfiguration when meeting the demand side management constraints. Both heuristic and systematic approaches are attempted and applied to two different energy-intensive processes. The second part focused on developing a bottom-up approach to integrate the process design, operation, and control levels and to define a novel metric to evaluate the process particibility in the electricity markets. The key contributions of the dissertation are summarized below.

(1) Addressed the topic of incorporating the demand-side management into the process design, which still remains as a topic that requires further research.

(2) The proposed flexible framework for the process design integrating the process network reconfiguration under demand-side management has shown that a proactive reconfiguration can be triggered under different demand-side requirements and that the reconfigurable design might have potential economic benefits under certain scenarios.

(3) Proposed a model-based analytical framework for evaluating the cost-effectiveness of process design alternatives with respect to their ability to participate (particibility) in Demand Response (DR) services. A new metric, namely the load-shifting capacity is defined to quantify the process shift capacity. A novel approach in modeling the chemical process as a "grid-level" battery and evaluate the economics value by using the levelized cost is developed.

However, although such research is beneficial in moving forward in incorporating the demand-side management and process design, many shortcomings and challenges still remain. The contributions of this work are mostly theoretical innovations such as the concept of reconfiguration and levelized cost in load-shifting. In the reconfiguration study, the reconfiguration is mostly between different steady-states and thus the dynamics involved in this transition are not considered. However, accounting for the process dynamics in the reconfiguration can be computationally demanding. In the levelized cost study, on the other hand, the integrated approach is sequential and might not be optimized and therefore would also need a better integrated approach. Moreover, the application in the study is quite illustrative, while enough for a conceptual study, a realistic energy-extensive process might be needed to better justify this approach. These limitations will be the subject of future research work.

6.2 Future research

With the increasing penetration of renewable resources into the power grids, the power grid will witness significant changes in the next decades. With the energy system changing, the field of chemical process design might witness a paradigm shift as well. In this work process network reconfiguration and the LCOL approach are offered as two methods that are considered to better adaptation to the smart grid. Yet, in both approaches presented in this dissertation, the simultaneous process design, operation, and control are not addressed as this is considered non-trivial due to the nature of the resulting Mixed-Integer Dynamics Optimization (MIDO) problem. Future development in the area of computational methods might be desired thereafter to address these issues. Moreover,

the LCOL approach provided a new perspective to evaluate the process design, where chemical processes are treated as a "grid-level" battery. However, besides the load-shift capacity, one could look into other metrics that could better capture the shorter-term performance such as the frequency control market. Also, the dynamics of the process can be explored using this metric to evaluate the best control paradigm to benefit the load-shifting operation.

References

[1] R. Turton, J. Shaeiwitz, D. Bhattacharyya, and W. Whiting, *Analysis, Synthesis, and Design of Chemical Processes: Analy Synth Desig Chemi Pr_5*, ser. International Series in the Physical and Chemical Engineering Sciences. Pearson Education, 2018. [Online]. Available: https://books.google.com/books?id=eV5gDwAAQBAJ

[2] "SB-100 California Renewables Portfolio Standard Program: emissions of greenhouse gases," 2018. [Online]. Available: https://leginfo.legislature.ca.gov/faces/billNavClient.xhtml?bill_id=201720180SB100

[3] P. Denholm, M. O'Connell, G. Brinkman, and J. Jorgenson, "Overgeneration from Solar Energy in California. A Field Guide to the Duck Chart," Tech. Rep. November, 2015. [Online]. Available: http://www.osti.gov/servlets/purl/1226167/

[4] "Utility-scale battery storage costs decreased nearly 70% between 2015 and 2018," 10 2020. [Online]. Available: https://www.eia.gov/todayinenergy/detail.php?id=45596

[5] F. E. R. Commission, "Assessment of demand response and advanced metering," Tech. Rep., 2006.

[6] M. Soroush and D. J. Chmielewski, "Process systems opportunities in power generation, storage and distribution," *Computers & Chemical Engineering*, vol. 51, pp. 86–95, 2013.

[7] B. F. Gerke, G. Gallo, S. J. Smith, J. Liu, S. V. Raghavan, P. Schwartz, M. A. Piette, R. Yin, and S. Stensson, "The California Demand Response Potential Study, Phase 3: Final Report on the Shift Resource through 2030," Tech. Rep., 2020.

[8] M. Baldea, "Employing Chemical Processes as Grid-Level Energy Storage Devices," in *Advances in Energy Systems Engineering*, G. M. Kopanos, P. Liu, and M. C. Georgiadis, Eds. Cham: Springer International Publishing, 2017, pp. 247—271. [Online]. Available: https://doi.org/10.1007/978-3-319-42803-1_9

[9] Q. Zhang and I. E. Grossmann, "Enterprise-wide optimization for industrial demand side management: Fundamentals, advances, and perspectives," *Chemical Engineering Research and Design*, vol. 116, pp. 114–131, 2016.

[10] F. E. R. Commision, "National Action Plan on Demand Response," Tech. Rep., 6 2010. [Online]. Available: https://www.energy.gov/sites/prod/files/oeprod/DocumentsandMedia/FERC_NAPDR_-_final.pdf

[11] U. D. o. Energy, "Benefits of Demand Response in Electricity Markets and Recommendations for Achieving Them," Tech. Rep. [Online]. Available: http://citeseerx.ist.psu.edu/viewdoc/download?doi=10.1.1.476.730&rep=rep1&type=pdf

[12] D. J. Chmielewski, "Smart grid: The basics -What? Why? Who? How?" *Chemical Engineering Progress*, vol. 110, no. August, pp. 28–34, 2014.

[13] S. Mitra, I. E. Grossmann, J. M. Pinto, and N. Arora, "Optimal production planning under time-sensitive electricity prices for continuous power-intensive processes," *Computers and Chemical Engineering*, vol. 38, pp. 171–184, 2012.

[14] R. C. Pattison, C. R. Touretzky, T. Johansson, I. Harjunkoski, and M. Baldea, "Optimal Process Operations in Fast-Changing Electricity Markets: Framework for Scheduling with Low-Order Dynamic Models and an Air Separation Application," *Industrial & Engineering Chemistry Research*, vol. 55, no. 16, pp. 4562–4584, apr 2016.

[15] M. T. Kelley, R. C. Pattison, R. Baldick, and M. Baldea, "An MILP framework for optimizing demand response operation of air separation units," *Applied Energy*, vol. 222, no. October 2017, pp. 951–966, 2018.

[16] X. Wang, N. H. El-Farra, and A. Palazoglu, "Optimal scheduling of demand responsive industrial production with hybrid renewable energy systems," *Renewable Energy*, vol. 100, pp. 53–64, jan 2017.

[17] L. C. Brée, K. Perrey, A. Bulan, and A. Mitsos, "Demand side management and operational mode switching in chlorine production," *AIChE Journal*, vol. 00, no. 0, pp. 1–14, 2018.

[18] H. Hadera, P. Wide, I. Harjunkoski, J. Mäntysaari, J. Ekström, G. Sand, and S. Engell, "A Mean Value Cross Decomposition Strategy for Demand-side Management of a Pulping Process," *Computer Aided Chemical Engineering*, vol. 37, pp. 1931–1936, jan 2015.

[19] X. Zhang and G. Hug, "Bidding strategy in energy and spinning reserve markets for aluminum smelters' demand response," in *2015 IEEE Power and Energy Society Innovative Smart Grid Technologies Conference, ISGT 2015*, 2015, pp. 1–5.

[20] A. Gholian, H. Mohsenian-Rad, Y. Hua, and J. Qin, "Optimal industrial load control in smart grid: A case study for oil refineries," in *IEEE Power and Energy Society General Meeting*. IEEE, 2013, pp. 1–5.

[21] S. Mitra, L. Sun, and I. E. Grossmann, "Optimal scheduling of industrial combined heat and power plants under time-sensitive electricity prices," *Energy*, vol. 54, pp. 194–211, 2013.

[22] R. Dominguez, L. Baringo, and A. J. Conejo, "Optimal offering strategy for a concentrating solar power plant," *Applied Energy*, vol. 98, pp. 316–325, oct 2012.

[23] E. Lizarraga-Garcia, A. Ghobeity, M. Totten, and A. Mitsos, "Optimal operation of a solar-thermal power plant with energy storage and electricity buy-back from grid," *Energy*, vol. 51, pp. 61–70, mar 2013.

[24] A. W. Dowling, T. Zheng, and V. M. Zavala, "A decomposition algorithm for simultaneous scheduling and control of CSP systems," *AIChE Journal*, vol. 64, no. 7, pp. 2408–2417, 2018.

[25] C. Tong, A. Palazoglu, and N. H. El-Farra, "A Decomposition Scheme for Integration of Production Scheduling and Control: Demand Response to Varying Electricity Prices," *Industrial and Engineering Chemistry Research*, vol. 56, no. 31, pp. 8917–8926, 2017.

[26] Q. Zhang, J. L. Cremer, I. E. Grossmann, A. Sundaramoorthy, and J. M. Pinto, "Risk-based integrated production scheduling and electricity procurement for continuous power-intensive processes," *Computers and Chemical Engineering*, vol. 86, pp. 90–105, 2016.

[27] Q. Zhang, I. E. Grossmann, C. F. Heuberger, A. Sundaramoorthy, and J. M. Pinto, "Air separation with cryogenic energy storage: Optimal scheduling considering electric energy and reserve markets," *AIChE Journal*, vol. 61, no. 5, pp. 1547–1558, may 2015.

[28] Q. Zhang, M. F. Morari, I. E. Grossmann, A. Sundaramoorthy, and J. M. Pinto, "An adjustable robust optimization approach to scheduling of continuous industrial processes providing interruptible load," *Computers and Chemical Engineering*, vol. 86, pp. 106–119, 2016.

[29] R. C. Pattison and M. Baldea, "Optimal Design of Air Separation Plants with Variable Electricity Pricing," *Computer Aided Chemical Engineering*, vol. 34, pp. 393–398, 2014.

[30] Y. Cao, C. L. Swartz, M. Baldea, and S. Blouin, "Optimization-based assessment of design limitations to air separation plant agility in demand response scenarios," *Journal of Process Control*, vol. 33, pp. 37–48, sep 2015.

[31] A. W. Dowling, R. Kumar, and V. M. Zavala, "A multi-scale optimization framework for electricity market participation," *Applied Energy*, vol. 190, pp. 147–164, 2017.

[32] A. W. Dowling and V. M. Zavala, "Economic opportunities for industrial systems from frequency regulation markets," *Computers and Chemical Engineering*, vol. 114, pp. 254–264, 2018.

[33] J. I. Otashu and M. Baldea, "Scheduling chemical processes for frequency regulation," *Applied Energy*, vol. 260, p. 114125, 2020.

[34] P. Schäfer, H. G. Westerholt, A. M. Schweidtmann, S. Ilieva, and A. Mitsos, "Model-based bidding strategies on the primary balancing market for energy-intense processes," *Computers and Chemical Engineering*, no. xxxx, 2018.

[35] H. Teichgraeber and A. R. Brandt, "Optimal design of an electricity-intensive industrial facility subject to electricity price uncertainty: stochastic optimization and scenario reduction," *Chemical Engineering Research and Design*, vol. 163, pp. 204–216, 2020.

[36] X. Wang, N. H. El-Farra, and A. Palazoglu, "Proactive Reconfiguration of Heat-Exchanger Supernetworks," *Industrial and Engineering Chemistry Research*, vol. 54, no. 37, pp. 9178–9190, 2015.

[37] M. Rademacher, Y. Liu, N. H. El-Farra, and A. Palazoglu, "Optimal Configuration of Work-Heat Exchanger Networks (WHEN) in the Presence of Demand Response Objectives," *Computer Aided Chemical Engineering*, vol. 44, no. Energy 113 2015, pp. 1813–1818, 2018.

[38] Q. Chen and I. E. Grossmann, *Recent Developments and Challenges in Optimization-Based Process Synthesis*, 2017, vol. 8, no. 1. [Online]. Available: http://www.annualreviews.org/doi/10.1146/annurev-chembioeng-080615-033546

[39] J. Douglas and M. Douglas, *Conceptual Design of Chemical Processes*, ser. Chemical engineering series. McGraw-Hill, 1988.

[40] J. Viswanathan and I. Grossmann, "A combined penalty function and outer-approximation method for MINLP optimization," *Computers & Chemical Engineering*, vol. 14, no. 7, pp. 769–782, 1990.

[41] M. Tawarmalani and N. V. Sahinidis, "A polyhedral branch-and-cut approach to global optimization," *Mathematical Programming*, vol. 103, pp. 225–249, 2005.

[42] R. Misener and C. A. Floudas, "ANTIGONE: Algorithms for coNTinuous / Integer Global Optimization of Nonlinear Equations," *Journal of Global Optimization*, vol. 59, no. 2-3, pp. 503–526, 2014.

[43] B. Linnhoff and E. Hindmarsh, "The pinch design method for heat exchanger networks," *Chemical Engineering Science*, vol. 38, no. 5, pp. 745–763, 1983.

[44] T. Yee and I. Grossmann, "Simultaneous optimization models for heat integration—II. Heat exchanger network synthesis," *Computers & Chemical Engineering*, vol. 14, no. 10, pp. 1165–1184, 1990.

[45] K. C. Furman and N. V. Sahinidis, "A Critical Review and Annotated Bibliography for Heat Exchanger Network Synthesis in the 20th Century," *Industrial & Engineering Chemistry Research*, vol. 41, no. 10, pp. 2335–2370, 2002.

[46] A. Wechsung, A. Aspelund, T. Gundersen, and P. I. Barton, "Synthesis of heat exchanger networks at subambient conditions with compression and expansion of process streams," *AIChE Journal*, vol. 57, no. 8, pp. 2090–2108, 2011.

[47] M. Razib, M. Hasan, and I. Karimi, "Preliminary synthesis of work exchange networks," *Computers & Chemical Engineering*, vol. 37, pp. 262–277, 2012.

[48] V. C. Onishi, M. A. Ravagnani, and J. A. Caballero, "Simultaneous synthesis of work exchange networks with heat integration," *Chemical Engineering Science*, vol. 112, pp. 87–107, 2014.

[49] K. Huang and I. Karimi, "Work-heat exchanger network synthesis (WHENS)," *Energy*, vol. 113, pp. 1006–1017, 2016.

[50] J. R. Roebuck and H. Osterberg, "The Joule-Thomson Effect in Nitrogen," *Physical Review*, vol. 48, no. 5, pp. 450–457, 1935.

[51] J. Chen, "Comments on improvements on a replacement for the logarithmic mean," *Chemical Engineering Science*, vol. 42, no. 10, pp. 2488–2489, 1987.

[52] R. T. Rockafellar and R. J. B. Wets, "Scenarios and Policy Agregation in Optimization under Uncertainty," *Mathematics of Operations Research*, vol. 16, no. 1, pp. 119–147, feb 1991.

[53] Y. Liu, Y. Fan, A. Palazoglu, and N. H. El-Farra, "A flexible design framework for process systems under demand-side management," *AIChE Journal*, vol. 66, no. 7, 2020.

[54] "Pump life cycle costs: A guide to lcc analysis for pumping systems - executive summary," U.S. Department of Energy, Office of Industrial Technologies,Energy Efficiency and Renewable Energy, Tech. Rep., 2001. [Online]. Available: https://www.energy.gov/eere/amo/downloads/pump-life-cycle-costs-guide-lcc-analysis-pumping-systems-executive-summary

[55] G. Marks, E. Wilcox, D. Olsen, and S. Goli, "Opportunities for Demand Response in California Agricultural Irrigation: A Scoping Study," no. January, p. 82, 2013. [Online]. Available: https://esdr.lbl.gov/sites/all/files/LBNL-6108E.pdf

[56] D. Olsen, A. Aghajanzadeh, and A. T. McKane, "Opportunities for Automated Demand Response in California Agricultural Irrigation," Tech. Rep., 2015.

[57] A. Aghajanzadeh, C. P. Wray, and A. T. McKane, "Opportunities for Automated Demand Response in California Wastewater Treatment Facilities," Tech. Rep., 2015.

[58] T. Westerlund, F. Pettersson, and I. E. Grossmann, "Optimization of pump configurations as a MINLP problem," *Computers & Chemical Engineering*, vol. 18, no. 9, pp. 845–858, sep 1994.

[59] C. S. Adjiman, I. P. Androulakis, and C. A. Floudas, "Global optimization of mixed-integer nonlinear problems," *AIChE Journal*, vol. 46, no. 9, pp. 1769–1797, sep 2000.

[60] X. Li, Y. Chen, and P. I. Barton, "Nonconvex generalized benders decomposition with piecewise convex relaxations for global optimization of integrated process design and operation problems," *Industrial and Engineering Chemistry Research*, vol. 51, no. 21, pp. 7287–7299, 2012.

[61] J. R. Birge and F. Louveaux, "Introduction to Stochastic Programming," 2011.

[62] A. Ben-Tal and A. Nemirovski, "Robust optimization – methodology and applications," *Mathematical Programming*, vol. 92, no. 3, pp. 453–480, 2002.

[63] C. Li and I. E. Grossmann, "convergence algorithm for two-stage convex 0-1 mixed-integer nonlinear stochastic programs with mixed-integer first and second stage variables," *Computers and Chemical Engineering*, vol. 112, pp. 165–179, apr 2018.

[64] D. Gade, G. Hackebeil, S. M. Ryan, J. P. Watson, R. J. Wets, and D. L. Woodruff, "Obtaining lower bounds from the progressive hedging algorithm for stochastic mixed-integer programs," *Mathematical Programming*, vol. 157, no. 1, pp. 47–67, 2016.

[65] J. P. Watson and D. L. Woodruff, "Progressive hedging innovations for a class of stochastic mixed-integer resource allocation problems," *Computational Management Science*, vol. 8, no. 4, pp. 355–370, 2011.

[66] Y. Fan and C. Liu, "Solving stochastic transportation network protection problems using the progressive hedging-based method," *Networks and Spatial Economics*, vol. 10, no. 2, pp. 193–208, jun 2010.

[67] J.-P. Watson, D. L. Woodruff, and W. E. Hart, "PySP: modeling and solving stochastic programs in Python," *Mathematical Programming Computation*, vol. 4, no. 2, pp. 109–149, jun 2012.

[68] W. E. Hart, C. D. Laird, J.-P. Watson, D. L. Woodruff, G. A. Hackebeil, B. L. Nicholson, and J. D. Siirola, *Pyomo — Optimization Modeling in Python*, 2017, vol. 67.

[69] N. V. Sahinidis, *BARON 21.1.13: Global Optimization of Mixed-Integer Nonlinear Programs,* User's Manual, 2017.

[70] R. Turton, J. A. Shaeiwitz, D. Bhattacharyya, and W. B. Whiting, *Analysis, Synthesis and Design of Chemical Processes 5th Edition*, ser. Prentice Hall International Series in the Physical and Chemical Engineering Sciences. Pearson Education, 2018.

[71] "Pacific Gas & Electric - Tariffs." [Online]. Available: https://www.pge.com/tariffs/electric.shtml

[72] P. Alstone, J. Potter, M. A. Piette, P. Schwartz, M. A. Berger, L. N. Dunn, S. J. Smith, M. D. Sohn, A. Aghajanzadeh, S. Stensson, J. Szinai, T. Walter, L. McKenzie, L. Lavin, B. Schneiderman, A. Mileva, E. Cutter, A. Olson, J. L. Bode, A. Ciccone,

and A. Jain, "2025 California Demand Response Potential Study - Charting Californiaextquoterights Demand Response Future: Final Report on Phase 2 Results," Tech. Rep., 2017.

[73] C. Tong, A. Palazoglu, and N. H. El-Farra, "A Decomposition Scheme for Integration of Production Scheduling and Control: Demand Response to Varying Electricity Prices," *Industrial and Engineering Chemistry Research*, vol. 56, no. 31, pp. 8917–8926, 2017.

[74] R. C. Pattison and M. Baldea, "Equation-oriented flowsheet simulation and optimization using pseudo-transient models," *AIChE Journal*, vol. 60, no. 12, pp. 4104–4123, dec 2014.

[75] L. D. Beal, D. Petersen, D. Grimsman, S. Warnick, and J. D. Hedengren, "Integrated Scheduling and Control in Discrete-time with Dynamic Parameters and Constraints," *Computers & Chemical Engineering*, vol. 115, pp. 361–376, 2018.

[76] A. Flores-Tlacuahuac, S. T. Moreno, and L. T. Biegler, "Global Optimization of Highly Nonlinear Dynamic Systems," *Industrial & Engineering Chemistry Research*, vol. 47, no. 8, pp. 2643–2655, 2008.

[77] W. E. Hart, C. Laird, J.-P. Watson, and D. L. Woodruff, *Pyomo – Optimization Modeling in Python*, 2012.

[78] B. Nicholson, J. D. Siirola, J.-P. Watson, V. M. Zavala, and L. T. Biegler, "pyomo.dae: a modeling and automatic discretization framework for optimization with differential and algebraic equations," *Mathematical Programming Computation*, vol. 10, no. 2, pp. 187–223, 2018.

[79] I. E. Grossmann and F. Trespalacios, "Systematic modeling of discrete-continuous optimization models through generalized disjunctive programming," *AIChE Journal*, vol. 59, no. 9, pp. 3276–3295, 2013.

[80] Gurobi Optimization, LLC, "Gurobi Optimizer Reference Manual," 2021. [Online]. Available: https://www.gurobi.com

[81] M. Baldea and I. Harjunkoski, "Integrated production scheduling and process control: A systematic review," *Computers & Chemical Engineering*, vol. 71, pp. 377–390, 2014.

[82] Y. Chu and F. You, "Integration of scheduling and control with online closed-loop implementation: Fast computational strategy and large-scale global optimization algorithm," *Computers & Chemical Engineering*, vol. 47, pp. 248–268, 2012.

[83] Q. Zhang, A. M. Bremen, I. E. Grossmann, and J. M. Pinto, "Long-Term Electricity Procurement for Large Industrial Consumers under Uncertainty," *Industrial and Engineering Chemistry Research*, vol. 57, no. 9, pp. 3333–3347, 2018.

[84] S. Mitra, J. M. Pinto, and I. E. Grossmann, "Optimal multi-scale capacity planning for power-intensive continuous processes under time-sensitive electricity prices and demand uncertainty. Part I: Modeling," *Computers & Chemical Engineering*, vol. 65, pp. 89–101, 2014.